CYCLONES

551.510
F636
TR-14

STATE WATER SURVEY DIVISION
LIBRARY COPY
AIRPORT

FLORIDA STATE UNIVERSITY

DEPARTMENT OF METEOROLOGY

FAM
RGS
KW

TECHNICAL REPORT NO. 14

A Numerical Experiment in Deduction of the Divergence Associated with a Model of a Steady Cold Cyclone

By Stanley E. Asplund

PREPARED UNDER PROJECT NR-082-071, CONTRACT NONR-1600(00)

WITH THE OFFICE OF NAVAL RESEARCH

31 JANUARY 1959

Department of Meteorology
Florida State University
Tallahassee, Florida

Technical Report No. 14
Contract No. Nonr-1600(00)

551.510
F636
TR-14

A NUMERICAL EXPERIMENT IN DEDUCTION OF THE DIVERGENCE ASSOCIATED WITH A MODEL OF A STEADY COLD CYCLONE

By Stanley E. Asplund

The research reported in this document has been made possible through partial support by the Geophysics Branch, Office of Naval Research, under Contract No. Nonr-1600(00), Project NR-082-071. Reproduction of this document in whole or in part, is permitted for any purpose of the United States Government.

Publication approved: Seymour L. Hess
Seymour L. Hess
Principal Investigator

ACKNOWLEDGEMENTS

The investigation reported herein carries out an idea suggested by Professor Seymour L. Hess. Credit for unexhausted patience and optimism in contending with many obstacles is accorded to him. His aid in both scientific and administrative respects is gratefully acknowledged.

Thanks are also extended to Professor Werner A. Baum, former Head of the Department of Meteorology, who as Department Head and Director of University Research has efficiently supported the departmental objectives by provision of facilities. His help in making possible the use of the FSU IBM 650 computer is greatly appreciated. The contributions of Mr. Robert B. Desjardins, manager of the FSU Computing Center, are deserving of special mention and thanks.

Faculty members of the Department of Meteorology have given generously of time whenever requested. Several workers have cooperated in the long program of computations. Special mention for jobs well done is deserved by Messrs. W. J. Koss, Harold Orville, and C. C. Shen. All have worked diligently and enthusiastically. Thanks are extended also to Martin Hershkowitz for aid in computations and programming of the IBM 650, to Mrs. Pat Ashton for typing of the manuscript, and Mr. Dave Balanky for drafting of figures.

TABLE OF CONTENTS

Page

ACKNOWLEDGEMENTS ii

TABLE OF CONTENTS. iii

LIST OF TABLES v

LIST OF ILLUSTRATIONS. vi

ABSTRACT 1

Section

1. INTRODUCTION 3

2. GENERAL PLAN OF INVESTIGATION. 7

3. PRELIMINARY STEPS IN PRESCRIBING THE MODEL WIND FIELD. . . . 14

General remarks
Background on the choice of functional form
Restriction of the functional form
Implications of the functional form
Observational basis for the model

4. DESCRIPTION OF THE MODEL 23

The vortex at the reference surface
Zonal current at the reference surface
Vertical variation functions
Implied vorticity in the model
Possibilities for obtaining implied height distributions
Approximation of contour distributions implied by the vortex wind field
Other criteria for interpretation of the vortex contour field
Approximation of contour distributions implied by the zonal wind field
Implied height distributions

5. BOUNDARY CONDITIONS. 54

Vertical motion at the lower boundary
Lateral boundaries

Section Page

6. PROGRAM OF NUMERICAL SOLUTION FOR STRUCTURE 59

Cartographic considerations
Component parts of iterative procedure
The divergent part of the wind field
Divergence required by divergent-wind advection
Divergence required by vertical-motion effects
Development of iterative solution
Final scheme of iterative solution
Accuracy of approximative procedures
Empirical information on propagated error
Reliability of results

7. RESULTS 95

Observed convergence of successive approximations
Scheme of presentation of computed structural elements
Divergence and vertical motion on isobaric surface
Vertical cross sections of divergence and vertical motion
Tabular summaries of structural elements at selected grid points
Divergent wind contributions to total wind of system

8. GENERAL DISCUSSION OF RESULTS 157

9. CONCLUSION. 170

REFERENCES. 176

LIST OF TABLES

Table — Page

1. Vertical variation functions for zonal wind (F) and vortex wind (G), and their derivatives F' and G'. 28

2. Successive approximate increments of divergence on 60 centibar pressure surface, in units of 10^{-5} per second 96

3. Successive approximate increments of divergence on 50 centibar pressure surface, in units of 10^{-5} per second 97

4. Vorticity advection contributions of zonal and vortex winds . .109

5. Summary of divergence contributions and vertical motion at selected grid points. 135

6. Comparison of vertical advection of vorticity term (A) and tipping term (T) evaluated as divergence contributions. 145

7. Comparison of divergent and nondivergent wind 153

LIST OF ILLUSTRATIONS

Figure		Page
1.	(a) Above: Radial profile of vortex part of model wind field. (b) Below: North-south profile of zonal part of model wind field	25
2.	Vertical variation functions F(p) and G(p).	29
3.	Vertical profiles of maximum wind speed in vortex and maximum zonal wind speed	29
4.	Vertical variations of position of neutral points in model wind field and of center and col points on constant pressure topography at 0300 GCT 10 January 1953.	31
5.	Radial profile of relative vorticity of vortex at reference level.	33
6.	North-south profile of relative vorticity of model wind field at reference level (zonal current and vortex combined)	33
7.	Distribution of absolute vorticity on 500 mb surface	35
8.	Distribution of absolute vorticity on 900 mb surface	35
9.	Height profiles of constant pressure surfaces.	39
10.	500 mb contour chart corresponding to model wind field	46
11.	700 mb contour chart corresponding to model wind field	47
12.	850 mb contour chart corresponding to model wind field	48
13.	500 mb contour chart for cold low case of 0300 GCT 10 January 1953.	49
14.	Thickness charts derived from fig. 10-12	53
15.	Finite difference grid	68

Figure Page

16. Key to selection of grid points in tables 5 and 7. 106

17. Divergence approximation $D_{90}^{(0)}$ 112

18. Divergence approximation $D_{90}^{(4)}$ 112

19. Highest approximation to ω at 90 centibars. 114

20. Divergence approximation $D_{80}^{(0)}$ 114

21. Net change of divergence approximations on 80 centibar surface. 115

22. Divergence approximation $D_{80}^{(4)}$ 115

23. Divergence approximation $D_{70}^{(0)}$ 117

24. Net change of divergence approximations on 70 centibar surface. 117

25. Divergence approximation $D_{70}^{(4)}$ 118

26. Highest approximation to ω at 70 centibars. 118

27. Divergence approximation $D_{60}^{(0)}$ 120

28. Net change of divergence approximations on 60 centibar surface. 120

29. Divergence approximation $D_{60}^{(4)}$ 121

30. Highest approximation to ω at 60 centibars. 121

31. Divergence approximation $D_{50}^{(0)}$ 123

32. Net change of divergence approximations on 50 centibar surface. 123

33. Divergence approximation $D_{50}^{(4)}$ 125

34. Highest approximation to ω at 50 centibars. 125

35. West-east cross section of final approximate divergence and vertical motion. 129

36. South-north cross section of final approximate divergence and vertical motion. 130

Figure Page

37. Northwest-southeast cross section of final approximate divergence and vertical motion. 132

38. Southwest-northeast cross section of final approximate divergence and vertical motion. 133

39. Computed divergent wind at 90 centibars 149

40. Computed divergent wind at 70 centibars 150

41. Computed divergent wind at 50 centibars 151

ABSTRACT

The tropospheric wind structure in a sub-class of cut-off cold-core cyclones is idealized in a model. This model is a hypothetical case in which velocity divergence is present in exactly the right amount to maintain a zero local rate of change of vorticity. The rotational nondivergent part of the total wind field is prescribed. The divergent irrotational part is obtained by an iterative numerical process based upon evaluation of divergence from the vorticity equation. Beginning with the lower-boundary assumption of vertical velocity, the divergence required to balance all other contributions to vorticity tendency is computed at 100 mb intervals. Successive pressure surfaces are linked by numerical integration of the continuity equation. Computations and results through 500 mb are reported and discussed.

The model wind field is prescribed by mathematical expressions for zonal wind superimposed on a vortex at a reference surface of 565 mb. Each part of the wind field varies with height. At each pressure a given part has a fixed ratio to its value at the corresponding point of the reference surface. The observational basis and other considerations leading to selection of this model are discussed. The chosen model wind field is described by profiles of zonal and vortex wind speed on the reference surface, graphs of vertical variation functions, and plan views of the implied vorticity distribution on the 500 mb and 900 mb pressure surfaces. Profiles and plan-view mappings of an approximation to the implied height field are also shown.

Vertical motion at the 900 mb lower boundary is obtained as the result of convergence in the friction layer, using Ekman-spiral theory. Zero lateral boundary values are assumed for the divergent wind field.

The vorticity and continuity equations in the (x, y, p, t) coordinate system are adapted to a finite-difference lattice established upon a selected Lambert Projection. The first approximation to divergence balances the advection of vorticity by the model wind field. "Divergence-linked" effects are evaluated by a method of successive approximations devised for the purpose. Values of vertical motion obtained by numerical integration of the continuity equation are used in computation of vertical-motion effects. The irrotational divergent wind field corresponding to approximated divergence is obtained by relaxation solution of Poisson-type equations.

The results presented are the divergence required to balance advection of vorticity by the nondivergent wind, additional contributions by vertical-motion effects and divergent-wind advection of vorticity, vertical motion, and divergent wind. These are given by tables and scalar analyses of plan-view and vertical cross-section distributions. The empirical evidence of the experiment in regard to the over-all iterative procedure is examined.

Results are interpreted in terms of success of the numerical process, indications of what is important in a model, and meteorological significance. It is concluded that further case studies and deductions of structure by numerical process, built upon this exploration, will be profitable.

1. INTRODUCTION

The main stream of development of numerical experimentation in dynamic meteorology has been channeled toward improvement of prediction of the future states of atmospheric systems from their observed initial states. A large number of investigators, working at some half-dozen centers during the last twelve years, have built up an extensive amount of information on the use of methods of discrete mathematical analysis for dynamic weather prediction.

While the present state of this vigorous area of meteorological science contains several additions which are crucial to the success of the approach, its essential basis is the point of view taken by L. F. Richardson [1] in a now-famous pioneering attack on the mathematical problem contained in the governing equations. In brief, Richardson's formulation is forward extrapolation of the instantaneous local rate of change of a quantity. Among the more fundamental contributions of recent thinking are the use of vorticity as the extrapolated quantity, and the suppression of possible solutions which are meteorologically unimportant and mathematically impracticable. The use of "filtering approximations" to accomplish the latter has led to improved understanding of quasi-geostrophic and balance-equation winds. It has also been convenient to deal with the horizontal motion field as the sum of a nondivergent part and an irrotational part.

In addition to the above fundamental refinements of Richardson's efforts at numerical integration, the recent years have seen numerous improvements in techniques of numerical solution and more effective use of high-speed computing devices. It is unquestionable that the availability of electronic computers was a prerequisite to development of numerical prediction as it exists today. Even so, the existing limitations on further increases in quality are in part due to limitations of machine capacity.

As a matter of method, a not inconsiderable part of the potential usefulness of dynamic prediction methods lies in the avowed philosophy of step-by-step development [2]. The idea has been to work up through a "hierarchy" of increasingly general representations of the atmosphere and the governing equations, gaining knowledge in digestible increments.

From time to time it is pointed out that the existence of high-speed computing devices of large memory capacity opens new avenues of scientific investigation. Applied to meteorology, this point has been made in regard to the possibilities of using machines to compare the consequences of varying sets of controlled circumstances constrained by the appropriate mathematical relationships. For full exploitation of these possibilities, theoretical meteorologists interested in problems of the large-scale behavior of atmospheric motion systems ought not to be dedicated to the proposition of importance of time dependence above all other considerations. Although provision for prediction does not preclude the treatment of vertical structure, the limitations of machine memory and operational priorities have had the effect of

limiting the production of information about distributions along the vertical.

The purpose of this study is to take a first step in systematic investigation of the structure of atmospheric systems by mathematical modeling and the use of discrete mathematical analysis. In contrast with the philosophy of numerical prediction investigations, the treatment is founded on the premise that it is fruitful to consider the circumstances in which the vorticity tendency is not free to be determined by the interplay of the fields of motion and mass. Instead, the vorticity tendency is required to be zero. The loss of generality inherent in this steady-state assumption is compensated by the possibility of paying more attention to details of distribution of vertical motion.

The approach of this structure investigation further is directed toward realization of the potential value of controlled experimentation by using, instead of observations, a physical model of an atmospheric motion system. This model is prescribed as a continuous function of the space coordinates. The particular type of system modeled is the high-level cyclone cut off from the maximum westerlies, or cold low.

It is thus assumed that there exists a distribution of horizontal motion compatible with the existence of a steady state of vorticity in this prominent synoptic model. One then ventures to prescribe the distribution of the nondivergent part of the wind field and of the substantial derivative of pressure at the lower boundary. These prescriptions give sufficient restriction that the vorticity and continuity equations comprise a complete system. This system is solved by successive approximations and discrete analysis to yield the distributions

of horizontal divergence and vertical motion. A three-dimensional lattice of points is used for the framework of finite-difference approximations. The third dimension of the lattice consists of surfaces of constant pressure spaced at 100 mb intervals, beginning at 900 mb. The lower boundary distribution of vertical motion is crudely prescribed as that found at the top of a friction layer through which the wind follows the Ekman spiral [3].

The use of a generalizing continuous function instead of wind observations from a particular case is in part a matter of preferred methodology in the area of deduction of structure by numerical experimentation on motion systems. On this basis alone, however, one has the drawback that in generalizing without extensive preliminary case studies there is risk of removing crucial physical properties. A further reason for performing the analysis on a functionally prescribed model is that testing of the proposed numerical methods is part of the experiment. By making the fundamental model wind field essentially regular and smooth, there is a better chance for detection of mathematical aberrations due to method of solution, merely by inspection of the results. This assumes that the correct solution itself is not so irregular as to look like a computational distortion.

As will be seen, the deduced structure is quite smooth, and the numerical results are far from being results of delicate balances which could be easily upset. These facts indicate that the correct solution would be smooth. They are also <u>a posteriori</u> justification for judging success of the approximative procedure by smoothness of the computed results.

2. GENERAL PLAN OF INVESTIGATION

All attempts at analysis of the state of motion of the atmosphere are necessarily based upon simplifications. In the study undertaken here, the introduction of most of the physical assumptions takes place in the choice of a model wind field.

The formulation of the requirements upon the model wind field is based upon the scalar vorticity equation (1) and the continuity equation (2), written in the (x, y, p, t) [4] coordinate system:

$$\begin{aligned} \partial\zeta_T/\partial t = &- \underline{V}_T \cdot \nabla (\zeta_T + f) - \omega\, \partial\zeta_T/\partial p \\ &- \underline{k} \cdot \nabla\omega \times \partial\underline{V}_T/\partial p - (\zeta_T + f)\, \nabla \cdot \underline{V}_T \,, \end{aligned} \tag{1}$$

$$\nabla \cdot \underline{V}_T = - \partial\omega/\partial p \,. \tag{2}$$

Here the symbol $\underline{V}_T$ is used to denote the horizontal component of the total velocity field, ζ_T is the vertical component of vorticity, and ω is the substantial derivative of pressure. The operator ∇ is the horizontal operator $\underline{i}\,(\partial/\partial x')_p + \underline{j}\,(\partial/\partial y')_p$ in a curvilinear orthogonal coordinate system (x', y', p). The indicated differentiation operations are directional derivatives along the coordinate directions x' and y' of the meteorological coordinate system [5]. The unit vectors $\underline{i}$ and $\underline{j}$ are tangent to the x' and y' coordinate curves in level surfaces.

The introduction of the assumption $\partial\zeta_T/\partial t = 0$ in equation (1) is a severe limitation upon the atmospheric systems for which the ensuing analysis can be meaningful. A cut-off high-level cyclone is one motion system which has often been regarded as comforming to essentially this very condition. The usual occurrence of a steady-state assumption for these systems is in connection with interpretation of observed precipitation [6]. The use of this simplification in the mathematics of the present model is more restrictive, however, in that it is applied to the entire volume of atmosphere within the model. This investigation is an exploration of the requirements on horizontal and vertical structure of the divergence field and vertical motion when the steady-state assumption is made for the vorticity field in the tropospheric portion of a particular field of motion. The further step of close identification of the model wind field with observed systems is not essential. Such identification is desirable, however. It would seem to be acceptable in a first approximation to the final stage in the development of a cut-off high-level cyclone south of the maximum westerlies [7, 8].

The vorticity method of determination of vertical motion is based on solving equation (1) for the horizontal divergence, substituting into equation (2), and integrating with respect to pressure. In the application of this procedure to observations it is common to neglect the effects of vertical motion in (1). The possibility of retention of these terms is part of the reason for performing the present experiment. The use of the vorticity and continuity equations contemplated here is an application of the vorticity method in a framework of mathematical modeling which provides more detail, some additional information,

and is free of some of the shortcomings of the vorticity method in its applications to observations.

It is useful to regard the wind field $\underline{V}_T$ as a combination of a nondivergent field $\underline{V}$ and an irrotational field $\underline{W}$. Thus

$$\underline{V}_T = \underline{V} + \underline{W} , \tag{3}$$

where

$$\begin{aligned} \underline{k} \cdot \nabla \times \underline{V} &= \zeta = \zeta_T , \\ \nabla \cdot \underline{V} &= 0, \end{aligned} \tag{4}$$

and

$$\begin{aligned} \underline{k} \cdot \nabla \times \underline{W} &= 0 \\ \nabla \cdot \underline{W} &= D = \nabla \cdot \underline{V}_T . \end{aligned} \tag{5}$$

This separation of the wind field is a convenient device in connection with the use of the vorticity method for obtaining divergence. It is related to the theorem of vector analysis which states [9] that a vector field with uniformly continuous derivatives in a finite region can be expressed as the sum of two vectors, one irrotational and one solenoidal. This theorem as stated does not say that the horizontal component of a three-dimensional vector field can be so decomposed. However, as pointed out by Sherman [10], a knowledge of the (scalar) vorticity ζ and the horizontal divergence of the wind, together with appropriate boundary conditions, is sufficient to determine the wind field.

Assuming the general representation (3) for the total wind field of the system under investigation, we obtain upon substitution of it into the vorticity equation (1) (written for zero local vorticity change)

$$\nabla\cdot \underline{V} + \nabla\cdot \underline{W} = -(\zeta_T + f)^{-1}\,[\underline{V}\cdot\nabla(\zeta_T + f) + \underline{W}\cdot\nabla(\zeta_T + f) + \omega(\partial\zeta_T/\partial p) + \underline{k}\cdot\nabla\omega \times (\partial\underline{V}/\partial p) + \underline{k}\cdot\nabla\omega \times (\partial\underline{W}/\partial p)\,] .$$

In view of (3) and (4), this becomes

$$D = -(\zeta + f)^{-1}\,[\underline{V}\cdot\nabla(\zeta + f) + \underline{W}\cdot\nabla(\zeta + f) + \omega(\partial\zeta/\partial p) + \underline{k}\cdot\nabla\omega \times (\partial\underline{V}/\partial p) + \underline{k}\cdot\nabla\omega \times (\partial\underline{W}/\partial p)\,] . \qquad (6)$$

The continuity equation (2) becomes

$$D = -(\partial\omega/\partial p). \qquad (7)$$

These equations are a complete set for determination of $\underline{W}$ and ω, if $\underline{V}$ is known. The assumption that there exists a time in the life cycles of some synoptic entities when the relative vorticity is not changing with time anywhere within the system has already been pointed out to be a crucial point in the development. The usefulness of this approach also depends upon having confidence in the assumed knowledge of $\underline{V}$, the nondivergent part of the wind field. In this experiment, it is proposed to model a $\underline{V}$ field for a particular clear-cut synoptic entity. This entity, the cold low south of the maximum westerlies, has typical simplicity and symmetry which encourages its use for this trial.

The overall symmetry of the wind distribution is quite pronounced in many examples of cut-off cold lows. This characteristic is shown quite clearly in several published cross sections [8, fig. 8], [11, fig. 8], [7, fig. 10]. The lack of a systematic study of wind fields characterizing the general class of synoptic entities in question made the generalizations essential to the pursuit of the experiment somewhat risky. However, in order to proceed with the experimentation it was assumed that a typical tropospheric wind field for a cut-off cyclone does indeed exist, and that its essential features can be captured in a relatively simple distribution prescribed as a continuous function of the space coordinates. The functions providing the model $\underline{V}$ field are chosen to have the general appearance needed to produce a model cold-low wind field as qualitatively envisioned from inspection of selected cases. Specific values of available arbitrary constants in these functions are assigned so as to make certain quantitative parameters of the system be in reasonable accord with observation.

The considerations which favor the foregoing approach to prescription of the model are as follows. First, the representation of $\underline{V}$ by functions on the continuum of space coordinates has the great advantage that its use alleviates a difficulty encountered in observational studies of computed vorticity. This difficulty enters with the use of finite difference approximations [12, 13]. In this study, the correctness of the determination of vorticity and vorticity advection is dependent only upon the acceptability of the functional representation. The need for use of finite difference approximations

to derivatives is put off to a stage later than if a discrete representation of the wind field had been used.

Second, the considerable smoothing which is entailed by the use of subjective curve fitting has recommendations other than expediency. The subjectivity is in accordance with the aim of making broad generalization without exhaustive dissection of numerous cases, in order to expedite the trial of the numerical experimentation aspects of the study. Moreover, the fewer the subtleties of the model the clearer will be the implications of the main features.

Further details on the prescription of $\underline{V}$ are given in section 3.

The procedure for deduction of the divergent part of the wind field and the vertical motion from equations (6) and (7) is one of successive approximations to the divergence by alternate use of (6) and (7), with ω obtained by integration of (7). Upward integration from prescribed lower boundary values of ω is carried out in steps of 100 millibars by use of simple forms of numerical integration. The procedure of solution for the divergence and divergent wind is applied successively at the pressure surfaces 900 mb, 800 mb, 700 mb, 600 mb, and 500 mb. To get started, it is necessary to have lower boundary values of ω. These are obtained as the values to be expected at the top of the friction layer due to frictional convergence over a level ground surface, assuming the Ekman spiral analysis to be valid. Section 5 gives further details of this boundary value prescription.

The development of a program for solving the differential equation system (6) and (7) to yield divergence and divergent wind at successive pressure surfaces is presented in section 6.

3. PRELIMINARY STEPS IN PRESCRIBING THE MODEL WIND FIELD.

General remarks.-The plan of attack which has been outlined in the foregoing section requires that the model wind field have the following attributes:

(a) It is given as a function of the coordinates in closed mathematical form. The functional expression is as simple as possible within the bounds imposed by the wish for reasonable verisimilitude.

(b) It is nondivergent, and has an associated vorticity distribution which is representative of a cut-off cold low at maximum development. For the contemplated situation, one in which a well-developed cold low is stationary, the assumption of simultaneous occurrence of a vorticity maximum in time amounts to having a steady state of vorticity.

Background on the choice of functional form.-In the consideration of possibilities for a mathematical expression of the large-scale wind field in a cut-off high level cyclone, as described for example by Palmen [8], it is natural to start with a radially symmetric set of streamlines and isotachs. A structure of this type is often used as a basis for qualitative inferences about the configuration of the fields of vorticity and divergence. The inferences for a wind field of pure radial symmetry are indicated by Deardorff [14], who uses the vorticity and continuity equations with inclusion of vertical

advection of vorticity but not of the tipping term.[1] In his model the streamlines, isotachs, and vorticity isopleths are all concentric circles. Under the assumption that the vorticity pattern is relatively steady, the eastward translation of the system requires upward motion ahead of and downward motion behind the system. One could interpret this model as a steady-state vorticity pattern imbedded in a constant easterly flow.

Another study which accepts circular symmetry as an important component of a mature vortex wind field has been made by Tojo [15]. The purpose of that investigation was to determine by analytic methods the form of the radial variation of wind speed and speed of propagation in a barotropic, nondivergent and frictionless field of horizontal motion. In the Tojo model the symmetric vortex is specified to be propagating eastward at some speed less than that of a constant zonal current in which it is imbedded. Terms arising from the sphericity of the earth are neglected. The requirement of conservation of absolute vorticity in the model is shown to imply radial variation of the cyclonic component of the wind according to a first-order Bessel function of the first kind. It is found that the speed of propagation depends upon the speed of the zonal current and a characteristic dimension of the vortex. For the vortex which conserves the absolute vorticity of horizontally moving fluid elements this characteristic dimension may be either the radius at which tangential

---

[1] Otherwise known as the differential vertical advection term, twisting term, turning of vortex tubes into the vertical, etc.

speed is greatest, or the radial distance at which the tangential vortex wind is zero.

Restriction of the functional form.-The functional form chosen for the representation of the nondivergent wind in a cold low for the purposes of this experiment is the following:

$$\underline{V}\,(x, y, p) = G(p)\,\underline{c}\,(r) + F(p)\,\underline{U}\,(Y). \qquad (8)$$

The vector $\underline{V}$ is the nondivergent part of the horizontal field of motion. It will be henceforth called the model wind field. The independent variables (x, y) pertain to a rectangular coordinate system established on a particular mapping of the figure of the earth. The horizontal coordinates (x, y) are related to the radial coordinate r by $x^2 + y^2 = r^2$. The coordinate Y represents north-south distance on the map, measured positive northward from the latitude of the center of the vortex part $\underline{c}$ of the model wind field. The relationship between Y and the rectangular coordinates (x, y) is derived from cartographic considerations, discussed in section 6.

Implications of the functional form.-It is seen in Equation (8) that the wind field under examination is a combination of a radially symmetric wind field and a westerly flow varying with latitude. Each of these configurations has its most convenient analytic expression in a particular coordinate framework. In this connection it is pointed out that the radial symmetry of the vortex part of the wind model is assumed to exist in its purest form on the particular map base which is used in this study. This approach to the mapping of the model gives an uncomplicated functional expression for the vortex

part of the wind field as it appears on the map. It has the advantage of being amenable to future refinement by use of functions of successively greater degree of complexity, still tied to the idea of essentially circular symmetry.

A second benefit of the representation of $\underline{V}$ as separate vortex and zonal parts is the automatic separation of advective effects. In addition to being a mathematical convenience, this separation is in keeping with the meteorologist's accumtomed view of middle-latitude tropospheric flow patterns. Since the present model is the first to be analyzed for structure of horizontal divergence and vertical motion by this particular procedure, the possibilities for evaluation of effects of changes in structure of the model are limited. Separation makes it easier to observe the relative importance of the two parts of the model wind and their derived properties as a function of location within this single model. These observations can aid in evaluation of the usefulness of the general plan of attack and help to single out the more promising directions of improvements upon it.

In regard to the dependence of $\underline{V}$ upon the vertical coordinate p, the assumed form is a considerable restriction. However, this choice of form effects a great simplification in computing derived properties of the wind field. The basic prescription of the horizontal wind field is done once and for all at a midtropospheric pressure surface called the "reference level" or "reference surface". Certain required quantities which involve considerable computation for the reference level are easily computed for other values of

pressure, simply by multiplication of their reference surface values by $F(p)$ and/or $G(p)$, or derivatives of these vertical variation functions.

Reduction of computation is thus the main reason for separation of the horizontal and vertical parts of the wind model expressions. Separate representation is also desirable from the point of view of future usefulness of this investigation as a venture in mathematical modeling. A similar justification has been mentioned in regard to separation of the reference-level wind field into vortex and zonal parts. Both of these separations reflect accustomed habits of synoptic thinking.

The use of separate functions of pressure to provide for the vertical variation of the component parts of the model wind means that the wind direction for each of these parts remains constant with height. The total wind can change with height from the one extreme of pure vortex to the other of pure zonal flow, by appropriate assignments of values to the respective vertical variation functions. Because there is only one value of $F(p)$ and $G(p)$ for all points on a given pressure surface, there is no provision for reproducing the vertical variation of wind through a nonisobaric tropopause. This restriction is of no consequence as far as the scope of this particular experiment is concerned. A typical system of the class under consideration has of course an exceptionally low tropopause, but hardly lower than the 400 mb surface. The high-level cyclone over Albuquerque, New Mexico at 0300 GCT 4 November 1949, presented by Palmen [8] as a typical case, shows

the tropopause just above the 400 mb surface. In another case, 0300 GCT 10 January 1953, the lowest point of the tropopause was above 300 mb. For the purpose of a first experiment, the requirements of similarity to a typical high-level cyclone did not include modeling of its extension into the stratosphere.

Observational basis for the model.-A few observed occurrences of high-level cyclones cut off from the maximum westerlies are present in meteorological literature [7, 8, 11, 16]. Several others were examined in the Northern Hemisphere Historical Map Series [17, 18]. Consideration was given to the characteristics of these observed systems from the point of view of symmetry, speed of change and movement, nature of low level structure, and availability of data. One result of this was a conclusion which is inimical to ready attainment of the goals of the investigation. This conclusion is that the study of the structure of even such restricted systems by mathematical modeling is a formidable task, when one sets the goal of reasonable conformity of the model and its implications to the evidence of the weather map.

However, since a start must be made somewhere, it was decided that the modeling functions would be required to reproduce as many of the features of a selected prototype as possible within the chosen framework. The smoothing inherent in the framework is in some respects an advantage in that it connotes a greater generality than would a more exacting function-fitting. The dangers are that the generalization is toward a structure which the atmosphere cannot sustain, or that the framework precludes essential structural

features. Rather than being deterrents, the rationale of this investigation as a meteorological research problem is that these risks are part of a cut-and-try procedure. It also bears on the question that the operations used in the performance of the trying of a single cut are also experimental. There is no a priori assurance that the mathematical procedure is feasible, and there are many details to be worked out in carrying out that procedure. Viewed as necessary apparatus for the mathematical experimentation one might consider the chosen model as unduly detailed. Consideration of observations was a guide in arriving at the required compromises.

A number of cases of high-level cyclones were reviewed. The general type sought is exemplified by the cases of 0300 GCT 4 November 1946 [8], 0300 GCT 6 March 1948 [7], 1500 GCT 19 November 1948 [11], and 1500 GCT 13 March 1951 [16]. Other cases of sufficient preliminary promise were found on the Northern Hemisphere maps for 1500 GCT 14 February 1951 and 0300 GCT 10 January 1953. The latter two cases and that of November 1946 were selected for further investigation. The analyses made by the U. S. Weather Bureau for the standard constant pressure surfaces 1000 mb to 100 mb were obtained from the Synoptic Reports and Forecast Division. Additional analyses of 300 mb, 500 mb, 700 mb, 850 mb and 1000 mb were made on plotted charts for 0300 GCT 10 January 1953.

The observed situation which was chosen to be the principal guide in adjusting the model prescription is that of 0300 GCT 10 January 1953. At this time a cut-off high-level cyclone had reached a stage and configuration which seem amenable to

mathematical representation. Some use was also made of the cases of 4 November 1946 and 6 March 1948 as controls against prescribing extreme values which might be exhibited by an individual case, but which would be unrepresentative of the broader class.

The main prototype system was centered at latitude 33°N on the Alabama-Georgia border. There was cyclonic circulation throughout the troposphere, and the line of centers was nearly vertical. The intensity of the cyclone, by any reasonable definition, also was greatest in the upper troposphere. The observed system was very slow moving, particularly in the twelve hour period beginning at 0300 GCT on 10 January 1953. The synoptic situation is marred as a prototype of the ultimate model by low-level frontal structure. No other requirement was placed on the model in the 900-800 mb layer than the presence of a cyclonic circulation (rather than the anticyclonic or indifferent pressure patterns which are also observed below upper cyclones [19]), with reasonable characteristics of contour configuration and wind speed.

The observational basis for assignment of the mode of vertical variation of the vortex and zonal components of the model wind field was to a very considerable extent one of subjective evaluation of successive trials. Reference was made to the vertical profiles shown by Hsieh [7] and Palmen [8], and to mandatory pressure level maps for the case of 10 January 1953. The considerable diversities from one case to another make objective generalization a difficult thing to do. All that can be said in justification of the lower levels

of the model as reflection of synoptic reality is that the patterns obtainable within the framework of (8) are acceptable smoothed versions of possible atmospheric motion states. It seems that low-level effects which can be included within the present modeling framework do not have an important bearing on the implied upper-level structure. Hence the primary concern for synoptic reality of the mode of vertical variation is with regard to the levels above 800 mb.

4. DESCRIPTION OF THE MODEL

The vortex at the reference surface.-The prescription of the vortex part $\underline{c}(r)$ of the nondivergent model wind field (8) was found by a series of trials of functions of the form

$$c(r) = C_o \left[\phi \left([r-a]/b \right) - \phi \left([r + c]/d \right) \right] , \tag{9}$$

where $\phi(x)$ is the error function $\exp(-x^2/2)$. After much experimentation the following values were settled upon:

$$\begin{aligned} C_o &= 85 \text{ m/sec} , \\ a &= 7 , \\ b &= 8 , \\ c &= 6.125 , \\ d &= 7 . \end{aligned} \tag{9a}$$

The coordinate r is radial distance from the origin of the coordinate system, which is placed at 34°N, 95°W. The latitude of the origin is appropriate for the class of system considered. The choice of longitude is irrelevant, since effects of topographical relief are not considered. The radial coordinate r and the other quantities with dimensions of length are measured in centimeters on the Lambert Conformal Conic Projection with 1 map centimeter equal to 7.5×10^4 m at the standard parallels 25°N and $48\frac{1}{2}$°N. The vectors $\underline{c}(r)$ are tangential to circles of radius r on this map, centered at 34°N and 95°W.

The vortex wind profile for the reference level is shown in fig. 1(a). The profile has a peak of 29.6 m/sec at a radial distance of approximately 6 1/4 latitude degrees from the center. The course of the curve near the center is not exactly in accordance with the values of the function (9). It has been modified arbitrarily in such a way as to make the curve horizontal at $r = 0$. This modification is required in order not to have a discontinuity of the vorticity gradient at the origin. The question of the need to avoid such a discontinuity is interesting, but is academic as far as the model is concerned because the origin is not one of the grid points (section 6). In the representation of the wind and its derived quantities by discretely spaced values, there is infinite freedom between points. The view that these values are samples of functions continuous over the whole region avoids conceptual complications.

The wind speeds in the profile are small at the boundaries and approach zero asymptotically. It is intended that there should be so little vortex effect at the boundary as not to matter. The object of study is thus by implication the structure associated with a vortex imbedded in a general zonal flow, without contiguous influences.

The shape and the size of the profile and the value and location of maximum wind in fig. 1 are a subjective composite of the cold low cases of 10 January 1953 and 4 November 1946. The resulting vortex wind model seems an acceptable representation of the principal characteristics common to east-west wind cross sections in systems of the kind considered.

Figure 1. (a) Above: Radial profile of vortex part of model wind field.

(b) Below: North-south profile of zonal part of model wind field.

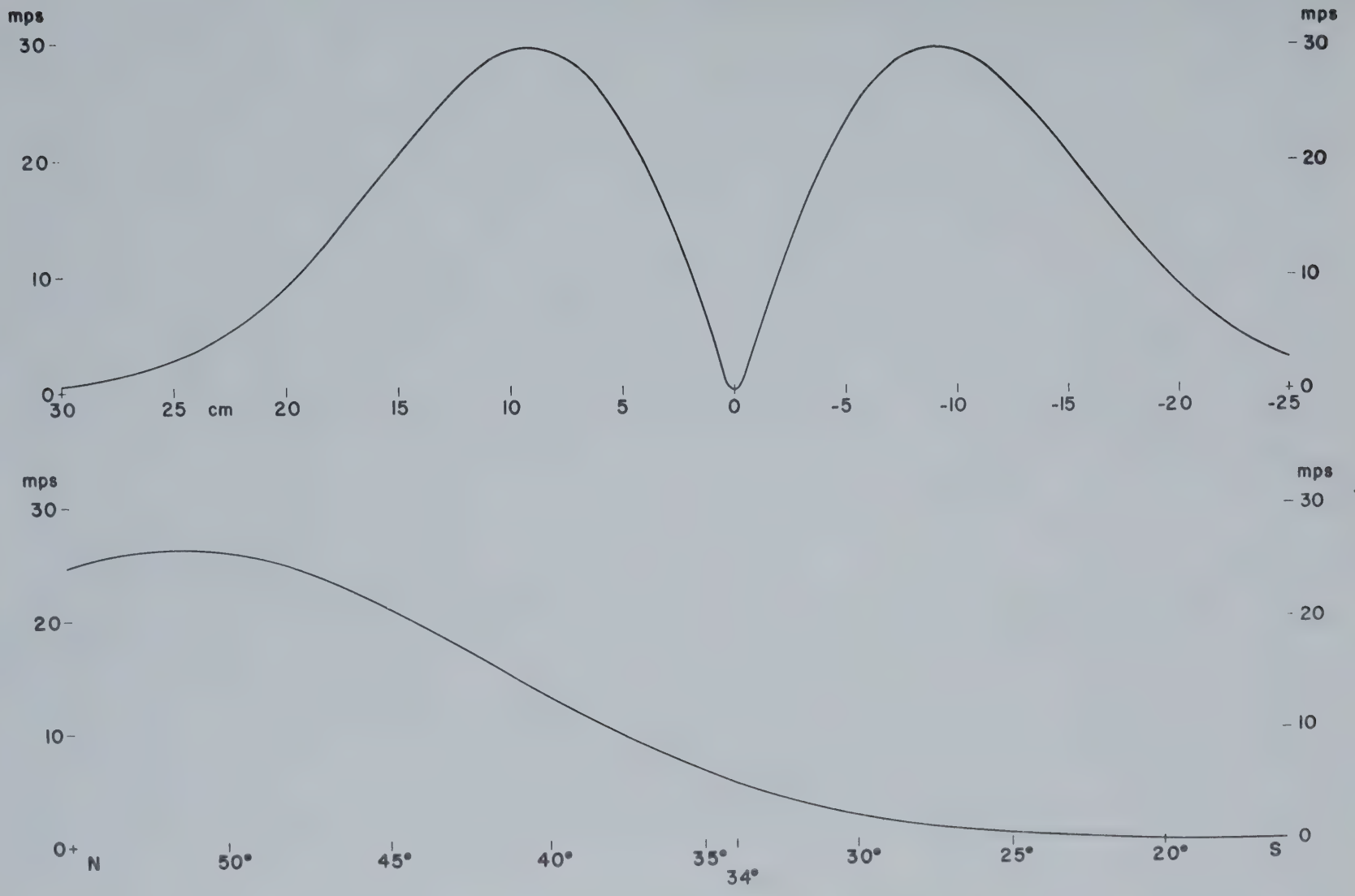
mps
30
20
10
0
mps
30
20
10
0
30 25 cm 20 15 10 5 0 -5 -10 -15 -20 -25
mps
30
20
10
0
mps
30
20
10
0
N 50° 45° 40° 35° 34° 30° 25° 20° S

25.

Fig. 1

Zonal current at the reference surface.-The zonal wind $\underline{U}(Y)$ in the nondivergent part of the model cold low (8) is represented by the function

$$\underline{U}(Y) = U(Y)\,\underline{I}\,,$$
$$U(Y) = 66\,\phi\,[(Y - 25)/14], \tag{10}$$

where Y is distance in centimeters from the parallel 34°N, measured along meridians on Air Transport Association Chart 11, and $\underline{I}$ is the unit vector directed eastward.

The suitability of the error function $\phi(x)$ is not as obvious for representation of the zonal wind profile as for a symmetric vortex. It was found to be as good as any for the latitudes under consideration. Guides to prescription of a basic westerly current in the hypothetical decomposition of a generalized prototype cold low are not easily come by without preliminary case studies. The modeling in this case was guided in a general way by graphs of North American sector zonal index data for 0300 GCT 10 January 1953. Profiles for 1500 GCT on 9 and 10 January were also examined for background, along with profiles derived from published cold low case studies.

Within the limitations of a basic westerly flow without longitudinal variation, the considerations mentioned above indicated that a suitable profile for the reference level should have a maximum speed of something like 20 to 30 m/sec at a latitude approximately 20 degrees north of the cyclone center, and small speed at the latitude of the center. The parameters which determined the shape and amplitude of a function having the general form of (10) were set in part

by the foregoing considerations. Use was made also of the requirement that the combination of zonal wind with vortex wind, when interpreted in terms of contour patterns by a method described later in this section, should give a height field that is not foreign to synoptic experience.

The final choice of a zonal wind profile at the reference level is shown in fig. 1(b). The maximum speed of westerly current is 26 1/3 m/sec at latitude 52°N, and the speed drops off southward in a very flattened error curve. At the latitude of the vortex center the zonal wind speed is just over 5 m/sec.

Vertical variation functions.-Vertical variation of the component parts of the model wind field is given by values of the functions $F(p)$ and $G(p)$ in equation (8). Since the reference level of 565 mb sets the pattern for the streamline and isotach fields at all levels modeled, $F(p)$ and $G(p)$ are given values relative to unity at the reference level. The values used are shown in table 1. This table shows values at 100 mb intervals through 300 mb, although the computations reported here go only through 500 mb. Table 1 also gives the values of the derivatives dF/dp and dG/dp which enter into the computation of terms in the vorticity equation arising from the effects of vertical advection and differential vertical motion. The functions $F(p)$ and $G(p)$ are shown graphed against pressure in fig. 2. These functions are defined by values at the pressure steps. The necessary derivatives were obtained by measurement on graphs similar to those of fig. 2. The accuracy obtainable by such measurement is not as great as indicated by the number of significant

figures given. By averaging measurements made by several people the random error was reduced enough to justify the number of figures given. Since it is true that given any finite number of values of a function and its derivatives there is a continuous function that fits, one may certainly take the values given in Table 1 to describe the vertical variation.

TABLE 1.-Vertical variation functions for zonal wind (F) and vortex wind (G) and their derivatives F' and G'

p cb	F(p)	G(p)	F'(p) cb^{-1}	G'(p) cb^{-1}
90	0.320	0.500	-.0158	-.0120
80	0.490	0.625	-.0178	-.0128
70	0.680	0.760	-.0204	-.0153
60	0.910	0.930	-.0250	-.0180
50	1.180	1.140	-.0280	-.0210
40	1.470	1.360	-.0300	-.0230
30	1.770	1.480	-.0300	-.0280

The graphs of F(p) and G(p) are shown again in fig. 3, in the form of profiles of the maximum wind in the vortex and in the zonal current. The graphs in the latter figure are on a vertical scale of the natural logarithm of pressure, i.e. height. To give some orientation, the magnitudes of the maximum shears at 500 mb are 4.6 m sec^{-1} per km in the vortex, and 5.0 m sec^{-1} per km in the zonal current. These values apply along the isotachs of maximum wind for the vortex and zonal wind fields respectively.

Figure 2. Vertical variation functions $F(p)$ and $G(p)$. Ordinate is linear scale of pressure, abscissa is value of function relative to reference level.

Figure 3. Vertical profiles of maximum wind speed in vortex (c_{max}) and maximum zonal wind speed (U_{max}) . Ordinate is ln p.

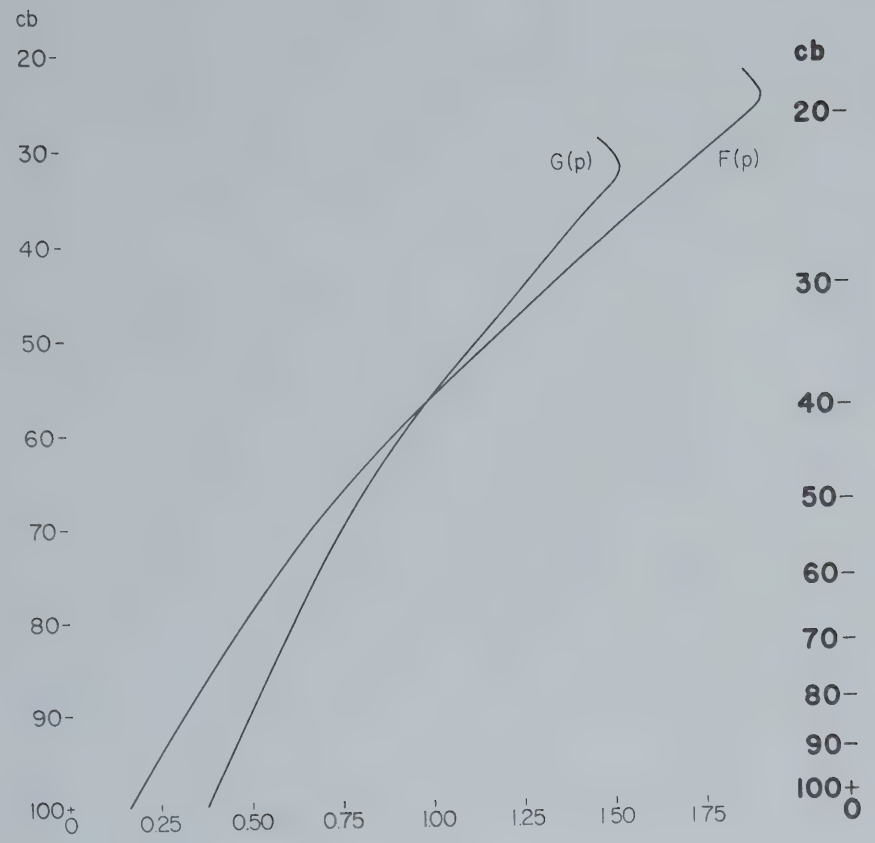
cb
20-
30-
40-
50-
60-
70-
80-
90-
100+
0
0.25
0.50
0.75
1.00
1.25
1.50
1.75
G(p)
F(p)

Fig. 2

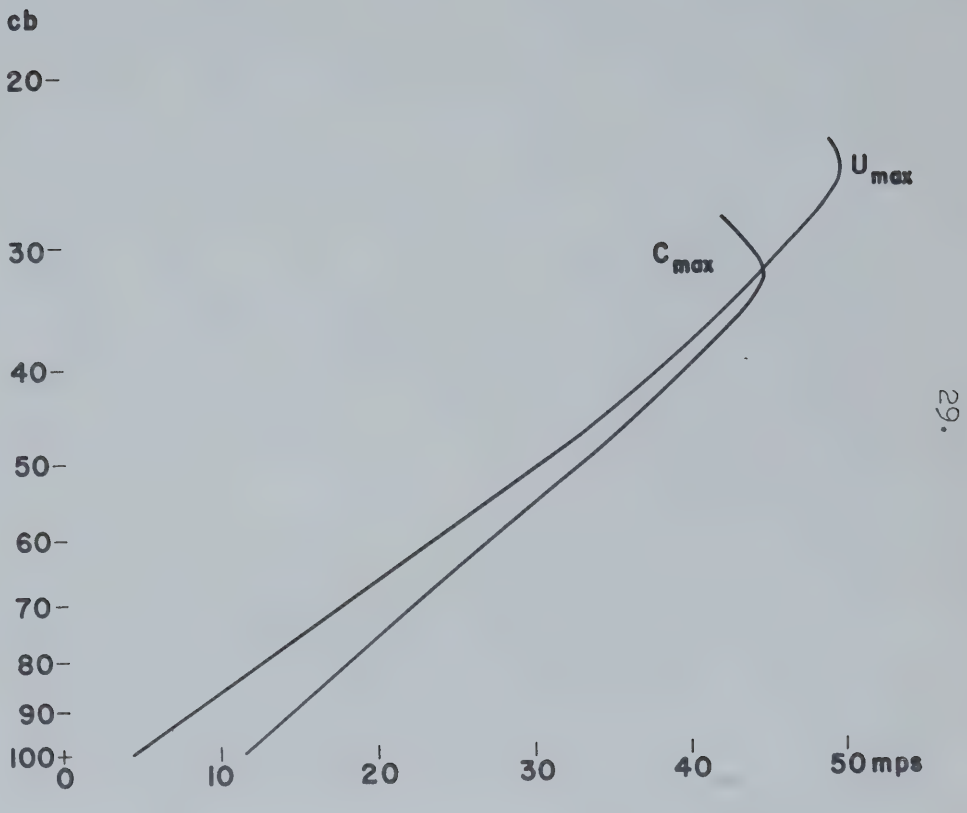
cb
20-
30-
40-
50-
60-
70-
80-
90-
100+
0
10
20
30
40
50 mps
U_{max}
C_{max}

Fig. 3

A great deal of adjusting and cross-referencing was necessary in order to find satisfactory combinations of F and G with the wind field prescriptions. Seven sets of values of F and G were tried and discarded for one reason or another. As a subsidiary control on the manipulations, the neutral points of the model wind field were obtained from graphs of the zonal and contour profiles in the regions of occurence of cancellation of the westerly zonal wind by easterly vortex wind. The loci of these points are shown for the final model in fig. 4. For comparison the loci of the positions of the cyclone center and col on the mandatory pressure surfaces at 0300 GCT 10 January 1953 are also shown in fig. 4, with the latitude scale shifted two degrees northward to facilitate comparison.

Implied vorticity of the model.-The basic requirement in this plan for deduction of horizontal divergence and vertical motion is an appropriate model of the field of relative vorticity. However, the wind field has been taken as the starting point. There are two reasons for this substitution: (1) lack of ready knowledge of the configuration of a characteristic vorticity field; (2) if one begins with the vorticity field, the nondivergent wind corresponding to it must be determined by integration. The latter can be done in the same way as used herein for getting $\underline{W}$. Because of the lack of information at this stage it would not be profitable to get $\underline{V}$ in this manner. The vorticity field remains the essential element of the problem of modeling, however, and should be described.

Figure 4. Vertical variations of position of neutral points (solid lines) in model wind field and of center and col points (dashed lines) on constant pressure topography at 0300 GCT 10 January 1953.

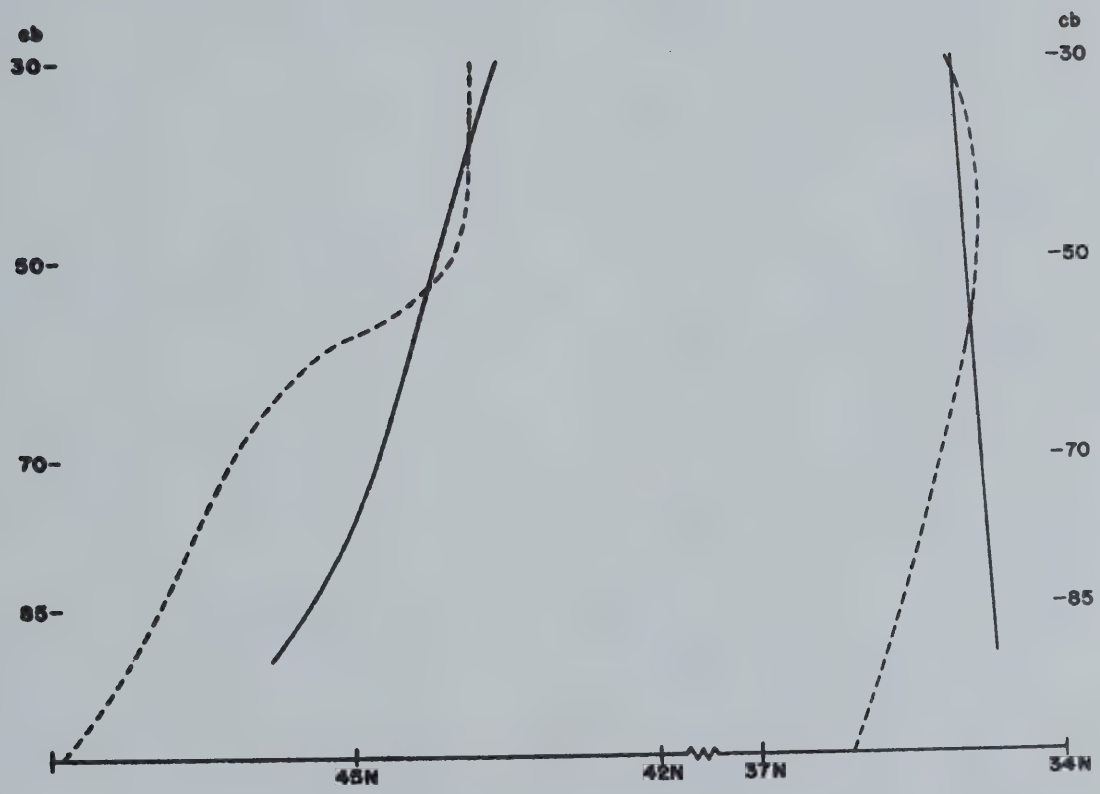

Fig. 4

The vorticity of the zonal wind alone is very small, and is not shown. It is negative over most of the system. For the reference surface, the extreme value is 1.3×10^{-5} sec^{-1} of anticyclonic vorticity at 41°N. The vorticity of the zonal wind is zero at 50°N and cyclonic northward of that point. This change to cyclonic vorticity just south of the peak zonal speed is due to the inclusion of the effect of curvature of parallels of latitude (section 6). At the latitude of the vortex center the zonal wind contributes only -0.9×10^{-5} sec^{-1} to the vorticity of the system.

Figure 5 shows the profile of relative vorticity of the vortex along any radial line on the reference surface, and fig. 6 shows relative vorticity of the complete model along the meridian through the center of the system. The vorticity of the vortex wind field is computed by equation (21) in section 6. As indicated above, and as is apparent from comparison of fig. 5 and 6, most of the relative vorticity is contributed by the model vortex. Near the center the curvature term dominates, accounting for an annular ring of maximum vorticity at approximately 2 map cm (150 km) from the center. The shear and curvature terms are of the same sign from the center to the peak vortex wind at 9 map cm (about 700 km) from the center. Beyond this point the shear is anticyclonic, and is responsible for anticyclonic relative vorticity outside of 12.5 map cm (950 km) at the latitude of the center.

The vorticity pattern of the zonal wind produces a small amount of asymmetry in the total relative vorticity pattern, since it is symmetric across the north-south axis but not symmetric along

Figure 5. Radial profile of relative vorticity of vortex at reference level. Units of vorticity are 10^{-5} sec^{-1}.

Figure 6. North-south profile of relative vorticity of model wind field at reference level (zonal current and vortex combined). North is at left. Units of vorticity are 10^{-5} sec^{-1}.

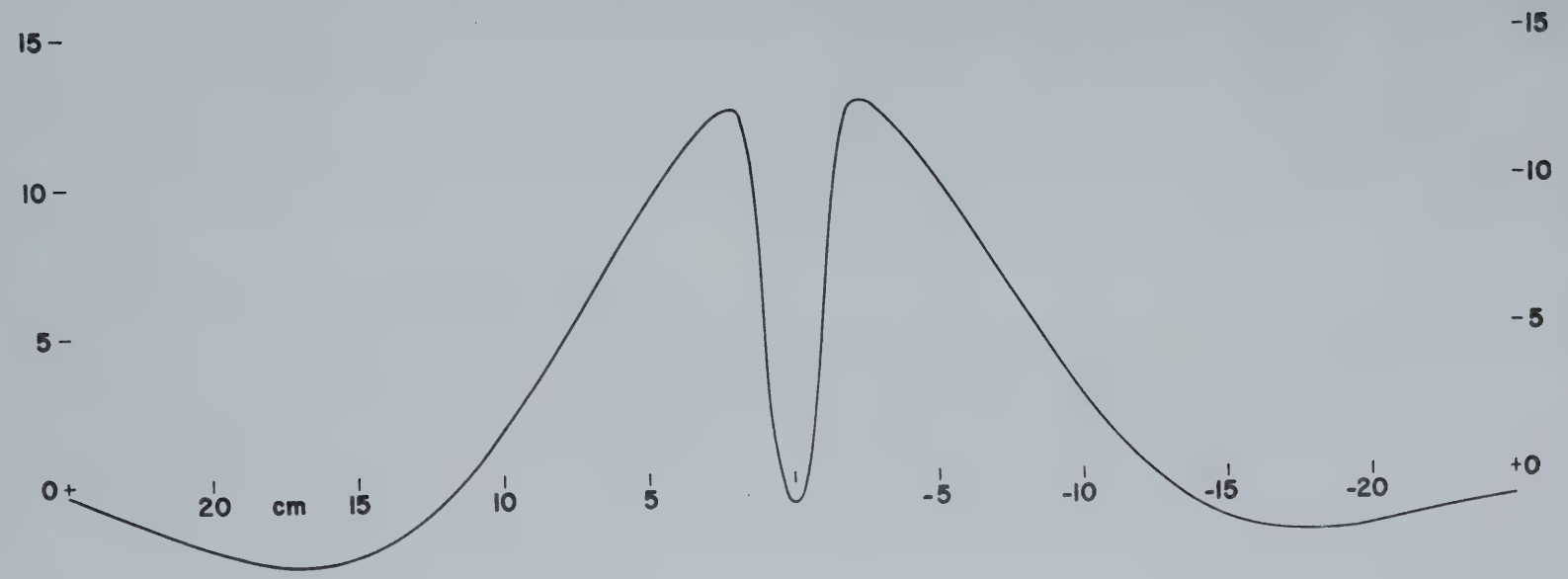
15 -
10 -
5 -
0 +
20
cm
15
10
5
-5
-10
-15
-20
-15
-10
-5
+0

Fig. 5

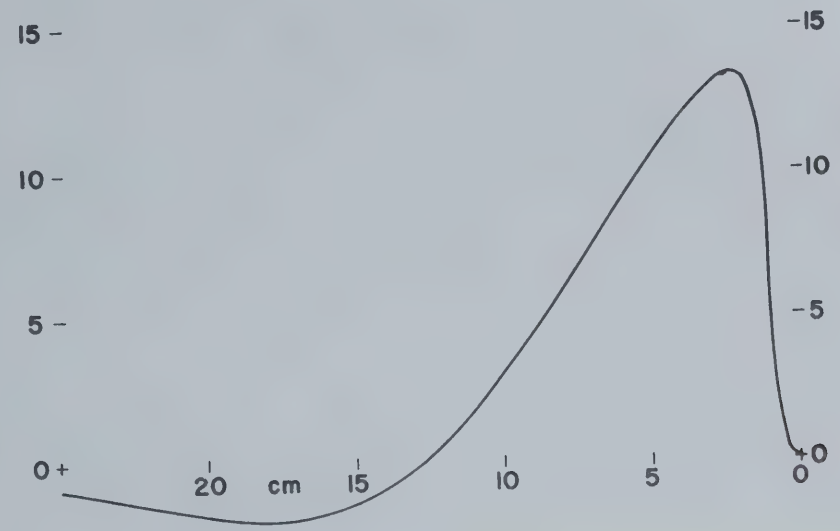
15 -
10 -
5 -
0 +
20
cm
15
10
5
0
-15
-10
-5
+0

Fig. 6

any other line through the center of the vortex. This effect is shown in plan view in fig. 7 and fig 8. These figures show the distribution of the 500 mb and 900 mb absolute vorticity $\zeta_a = \zeta + f$. The effect of variations of the Coriolis parameter is therefore also included.

At the 500 mb level the maximum of absolute vorticity is 22×10^{-5} sec^{-1}, distributed in an annular ring which is not quite circular. The relatively greater effect of the vortex at lower levels and constancy of the Coriolis parameter with height makes the pattern at 900 mb somewhat different, but the similarities of the two patterns are clearly seen. The effect of such height variation as does exist will bear investigation. Cressman [20] assumes complete conservation of shape of absolute vorticity patterns in the troposphere to derive an approximate equation for the horizontal divergence at 850 mb. His basis for this assumption is synoptic experience [21].

Implied height distributions.-The consequences of the wind model in terms of the topography of the constant pressure surfaces are undoubtedly the most familiar basis for interpretation of the model in the light of meteorological experience. I venture to say that few meteorologists can readily summon to mind a Gestalt of the wind field typical of a given type of synoptic system, except in generalities and/or for a few special situations. Most, however, will feel that a presentation of the topography of constant pressure surfaces is readily judged, at least in regard to broad features.

Given only the nondivergent part of the wind field, one cannot derive height fields for exact comparison with those seen on synoptic maps. Given the end results of this investigation, one could use the

Figure 7. Distribution of absolute vorticity on 500 mb surface. Units are 10^{-5} sec^{-1}.

Figure 8. Distribution of absolute vorticity on 900 mb surface. Units are 10^{-5} sec^{-1}.

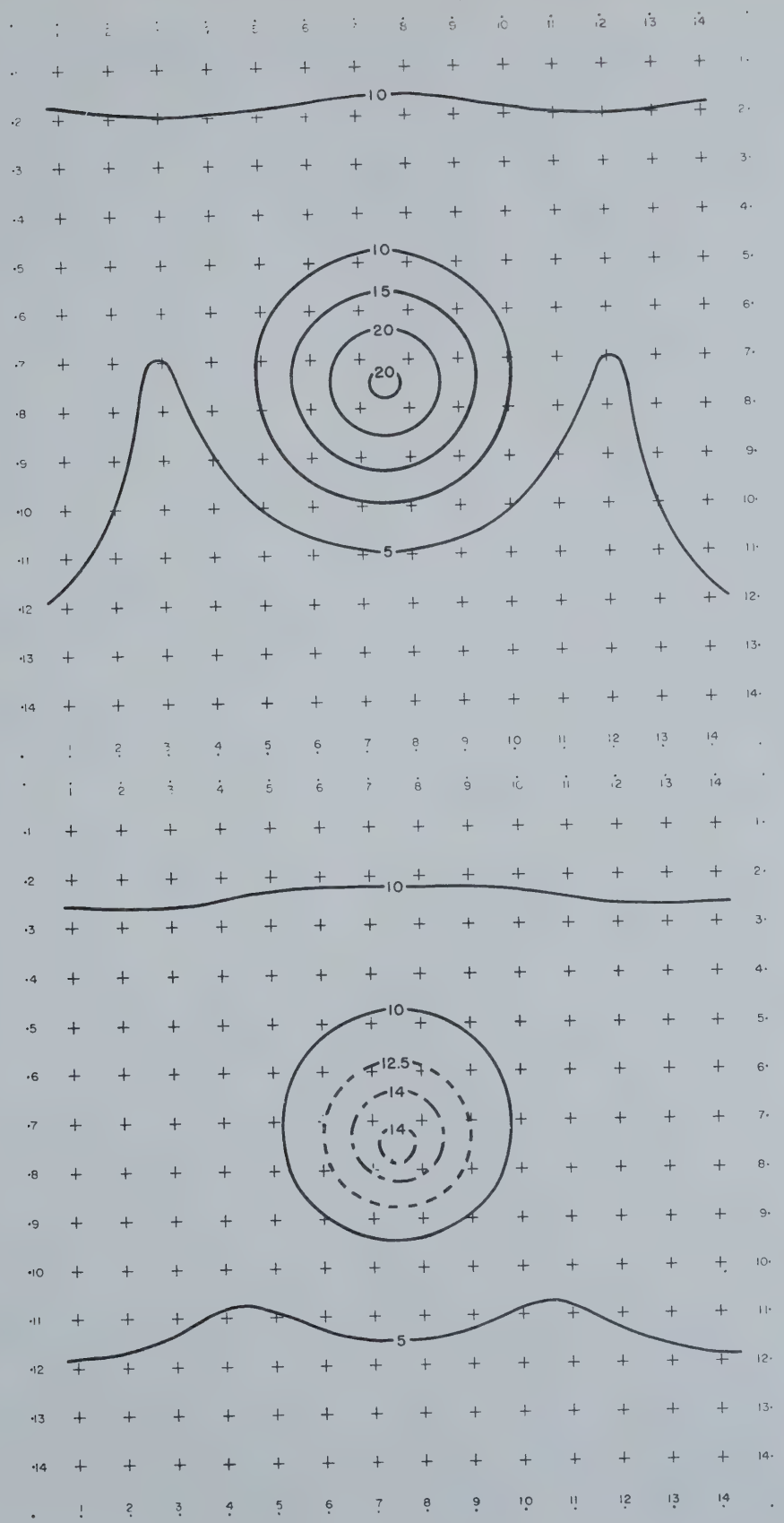

Fig. 7

Fig. 8

divergence equation [10, 22] to derive the height field associated with the total wind field of the system. The mathematical problem is not difficult, since it involves the solution of a Poisson equation similar to that which is dealt with as a part of this investigation. However, the extensive computation required to obtain the known function prohibits the inclusion of such an investigation in the present study.

The information available at the modeling stage is precisely that which is needed if the balance equation [22, 23, 24] is considered as a means for obtaining the height distribution corresponding to the nondivergent part of a wind field on a constant pressure surface. The solutions for geopotential thus obtained would be expected to be very close to the geopotential which satisfies the equation of motion for the total wind field. This way of getting contour patterns to show what is being taken as a model has interesting possibilities. Taken together with the results obtained with the divergence equation, the results of solution of the balance equation for geopotential can supplement the reasoning and evidence which are used in the design of filtering approximations in nongeostrophic numerical prediction models. The references to the bases and implications of the use of the balance equation are very numerous; the early justifications, as brought out by Pettersen [22], Kuo [23], Bolin [24], Charney [25], and others, have been subjected to a good deal of critical evaluation. The principal bases of evaluation have been the performance of experiments in numerical prediction and theoretical analyses of questions raised

by such experiments. The use of the present treatment and similar modeling experiments to obtain direct information on the assumptions in the balance equation appears to be an appropriate avenue of investigation.

For the purpose of getting a contour field representing the model, the above possibility of using the balance equation is out of the question. The computations required in the testing of various possible wind models by rigorously derived height field are unconscionable. An expedient substitute was devised. This alternative, described below, has the advantage of being feasible for repeated applications. It has the disadvantage that it cannot give the desired contour patterns exactly, and could conceivably give a very wrong picture. The extent to which it is a dependable basis for evaluation of implied height distributions is thought to be enough to justify its cautious use for interpretation of trial wind fields.

Approximation of contour distributions implied by the vortex wind field.-The normal-component equation of motion is [26]

$$K_H v^2 + fv + g\, \partial z/\partial n = 0 \ . \qquad (11)$$

Here v is wind speed, K_H is horizontal curvature of the path, g is the acceleration due to gravity and z is contour height. Contour profiles for the zonal and vortex components separately were obtained by numerical integration of (11) along special curves of the normal coordinate n .

The integration of the vortex wind prescription to obtain vortex height h_c was done along radial lines lying along and perpendicular to the north-south axis of the system. It is convenient to use a polar coordinate system for this integration. Equation (11) is written

$$dh_c/dr = g^{-1} [(G(p)c)^2/r + f\, G(p)c]. \qquad (12)$$

The quantities on the right side were evaluated at values of r = 1/4 cm, 1 cm, 2 cm, ... , 25 cm along each of the azimuthal lines 0°, 90° and 270°. Equation (9), with the values of $G(p)$ for p = 50, 70 and 85 cb, gives the desired values of c. The variation of latitude along azimuths 90° and 270° was provided for. Corrections to r for map distortion were omitted [26, p. 180] in this computation. The product of the described evaluation of (12) is a set of values of dh_c/dr at the centers of successive elements of a subdivision of the interval of integration. The first increment is $\frac{1}{2}$ cm in length, the rest are one cm each. Taking the value of contour height at the center of the vortex to be zero, accumulation of the products of dh_c/dr by the corresponding distance increments provides a sequence of values of h_c at the points of subdivision.

The resulting profiles of contour height for the vortex are graphed in fig. 9. The solid lines in that figure are the profiles along the meridians of longitude through the vortex center.

It cannot be supposed that the addition of the vortex center pattern to one similarly derived for the zonal wind field is a good substitute for the geopotential distribution which satisfies the

Figure 9. Height profiles of constant pressure surfaces. See text for method of derivation. East-west profiles along 34°N are in dashed lines. South-north profiles through center of system are in solid lines. (North is at right).

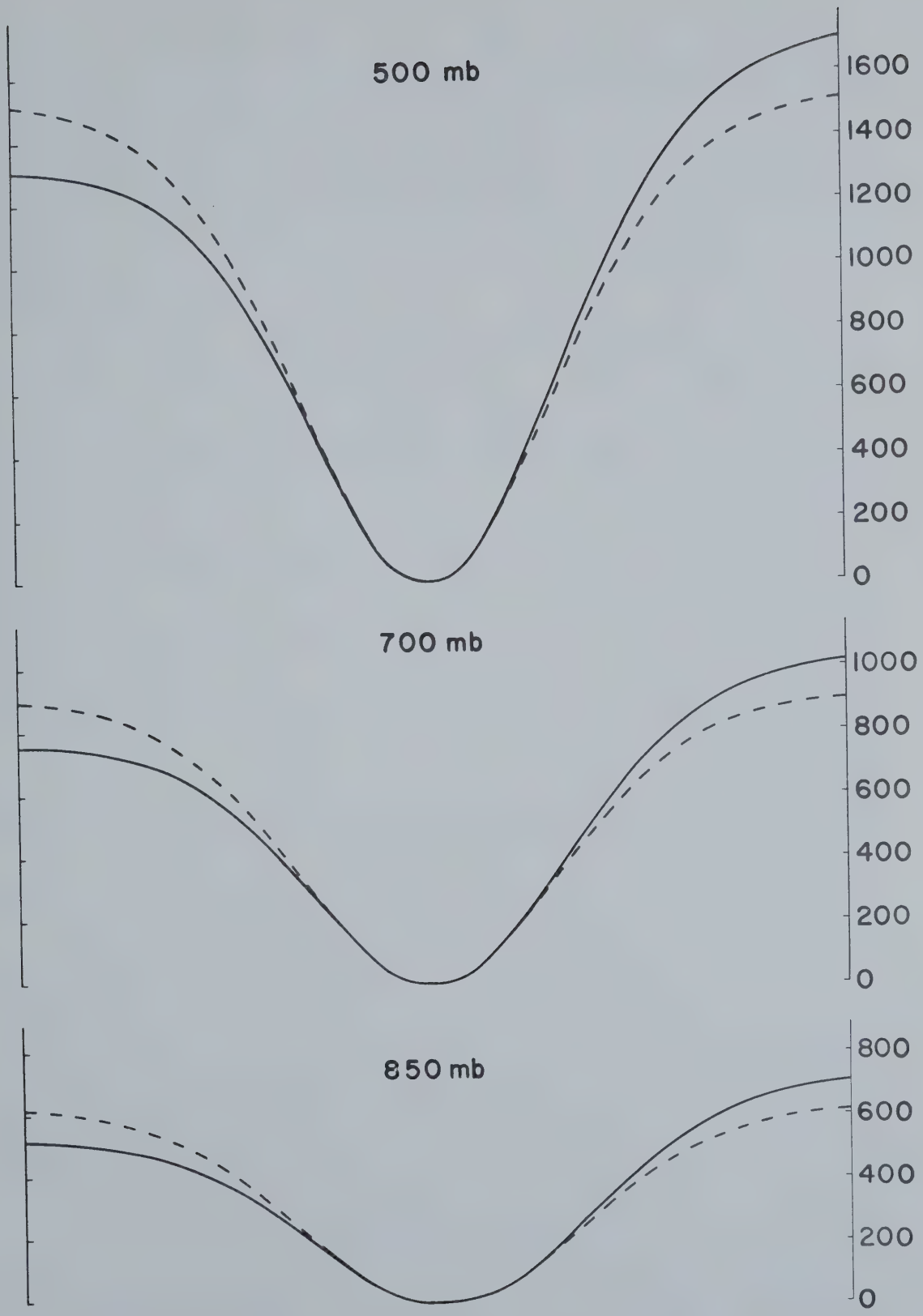
500 mb
1600
1400
1200
1000
800
600
400
200
0
700 mb
1000
800
600
400
200
0
850 mb
800
600
400
200
0

Fig. 9

equation of motion for the combined model wind fields. Even if the tangential component equation is omitted from consideration, addition of the contour fields obtained by integration of the normal-component equation for the vortex and zonal wind fields individually is not a theoretically valid method for getting the geopotential distribution for the combined wind fields.

Nevertheless, there are reasons for the construction of the vortex contour field in the relatively simple manner described. In an early exploratory stage, comparable profiles were obtained along a radial line perpendicular to the axis of some observed cases of intense depressions of pressure surface topography. The purpose of these early studies was to make a model of a cold low in terms of its geopotential field. This idea was given up when it became evident that idealization of contour patterns is no easier to do subjectively than the idealization of wind distributions. The profiles thus obtained were later useful as background information for judging the suitability of a trial model wind field.

There is a limit to the validity of east-west contour profiles derived from the wind field in the manner described. The isohypses derived from the circular vortex wind field are not parallel to the streamlines because of variation of the Coriolis parameter. Considered in connection with the tangential component equation [26],

$$\partial v/\partial t + v\, \delta v/\delta s + g\, \delta z/\delta s = 0 \qquad (13)$$

the presence of a cross-contour component in this preferably steady-state vortex wind field is an evidence of the shortcomings of the

method of deriving the contour field from the wind field. In view of the restricted and qualitative use to be made of the result, these shortcomings are recognized but not remedied.

In spite of the above qualifications on their significance, the vortex height profiles derived from model wind fields were compared with smoothed profiles derived from observations. These comparisons were useful in arriving at the acceptance of the final model of vortex wind.

Other criteria for interpretation of the vortex contour field.- A further criterion which can be applied to the model vortex contours is based on suggestions by James [27] of parameters for characterization of large-scale circular vortices. These parameters are framed in terms of the pressure field.

James' suggested parameters include the spread radius, intensity, and flexure. The spread radius R is the radial distance from the vortex center to the point of maximum pressure gradient. The intensity h is the difference between the pressure at a great distance and the central pressure. The flexure G is defined by

$$G = (\partial p/\partial r)_R \, (h/R)^{-1} ,$$

where p is pressure and r is the radial coordinate. For a given vortex the spread radius and flexure are regarded as constant with height. In the model at hand the characteristic of unvarying spread radius with height is regarded as one of the tentative expedients which should be evaluated by the results of this and similar investigations, and case studies.

Knighting [28] questioned the validity of James' characterization of vortices as having a height-independent spread radius. The reply made by James [29] to clarify his stand on this well-taken point is appropriate for quotation as reason for the use of constant spread radius in this cold-low model. James writes:

> With regard to the measurement of R, this parameter gives the horizontal extent of the cross-section of a vortex at a specified level. . . . R may certainly vary with height, but if the variation is marked, synopticians would surely have noticed by now that the horizontal scale of vortices changes with level. The simple assumption that R is constant with height seems to accord better with synoptic experience and we adopt this assumption tentatively, although there is nothing in vortex theory to prevent our treating $R(z)$ as a variable.

Knighting also questioned the practical possibility of defining the pressure at "a great distance". There is obviously no problem in the latter respect with the present model.

When we modify the definition of flexure for use with constant pressure surface representation, we find that the values of flexure for the model vortex at 850 mb, 700 mb and 500 mb are 0.57, 0.575 and 0.60 respectively. The spread radius is 690 km. These may be compared with values found by James, using estimates provided by Goldie [30] for spread radius, central pressure and maximum tangential speed in 20 extra-tropical sea level depressions. The range of R for the surface systems was 280 to 700 km, with a mean of 400-500 km. The mean flexure was found to be 0.54. While the values for the model are suitable on this basis, the standards of comparison are not sufficiently well established for the favorable comparison to be given any great weight. The absence of negative results is encouraging,

but one recognizes that the discriminating capabilities of these parameters are untested.

The values of flexure obtained for the model contour patterns are not quite as large as the value one obtains for a particular model circular vortex suggested by James. The "general circular vortex" of James has the pressure p given at any radius r by

$$p = P - h\, f(r/R),$$

where P is the pressure at great distance, h is the intensity, and f has the properties:

$$f(o) = 1,$$

$$f(\infty) = 0,$$

$$f'(r/R) \text{ maximum at } r = R.$$

One possible function f is Gauss's function

$$f(x) = \exp[-\tfrac{1}{2} x^2].$$

This gives the normal geostrophic vortex, whose flexure $G = 0.61$ is independent of intensity and spread radius. Normal vortices having the spread radii and the intensities of the 850, 700 and 500 mb model vortex contour patterns were compared with the respective curves of fig. 9. At 500 mb the curves are practically coincident, except that the "wing" of the normal vortex profile is flatter than the model 500 mb curve. This difference is increasingly more pronounced at 700 and 850 mb. Another difference which is absent at 500 mb and becomes more accentuated the lower the level is a more

rapid increase in height outward from the center in the normal vortex. None of the differences are large.

It has been seen that the question of feasible means for getting some idea of geopotential fields corresponding to combined vortex and zonal wind fields presents mathematical difficulties. This is true no matter which direction is taken, either that of splitting up a contour field into a general flow and a vortex in terms of the height fields, or that taken here. More explicitly the second approach considers that vortices not only do exist and have broad structure, but can best be studied by considering the wind fields of synoptic systems as combinations of pure vortex wind fields with unperturbed general flow fields. In the present sample of vortex theory, geopotential has only the minor importance that it is the most familiar context for description of cut-off cyclones as synoptic entities. It is of course recognized that the mass field must be considered in any study of cold lows which is less completely prescribed by modeling assumptions than is the present study.

Approximation of contour distributions implied by the zonal wind field.-Since some idea of the contour patterns in the model was needed for its development, these patterns were obtained by combining the contour fields of the zonal and vortex component wind fields. This entailed derivation of height profiles from the zonal wind fields at 500, 700 and 850 mb. Integration need be carried out along only one meridian of longitude. It is entirely permissible to neglect the curvature of the latitude parallels for the purpose at hand. Then equation (11) becomes simply the geostrophic wind equation

$$dh_U/dY = - 2\Omega F(p)\, U \sin \phi , \qquad (14)$$

where h_U is contour height and U is the zonal wind given by equation (10). Profiles of $h_U(Y)$ were constructed using the procedure of numerical integration described above for the axial profile of $h_c(r)$, and the values of $F(p)$ for 50, 70 and 85 cb. In accordance with arbitrary convention adopted for the vortex profiles, zero height on the zonal profiles occurs at 34°N.

Implied height distributions.-The respective contour fields corresponding to h_c and h_U were plotted on the working map and combined graphically to give the derived height field analyses for the constant pressure surfaces 500 mb, 700 mb and 850 mb. These contour fields are shown in figures 10, 11 and 12.

The three contour charts presented show clearly that there is a high degree of idealization in the model. For example, the configurations at the boundaries clearly do not reproduce what is to be found in synoptic reality. All in all, however, there does not seem to be any reason why a synoptic meteorologist would not accept these contour patterns as generalizations of the subject class of synoptic models, considered apart from the variable substructures within and adjacent to individual cases.

The height fields for the model wind distributions were compared with the corresponding charts for the case of 10 January 1953. Of the analyses which form the basis of comparison only the 500 mb chart is shown here (fig. 13). Using the observed system as a criterion, there are points of good correspondence and points of

Figure 10. 500 mb contour chart corresponding to model wind field.

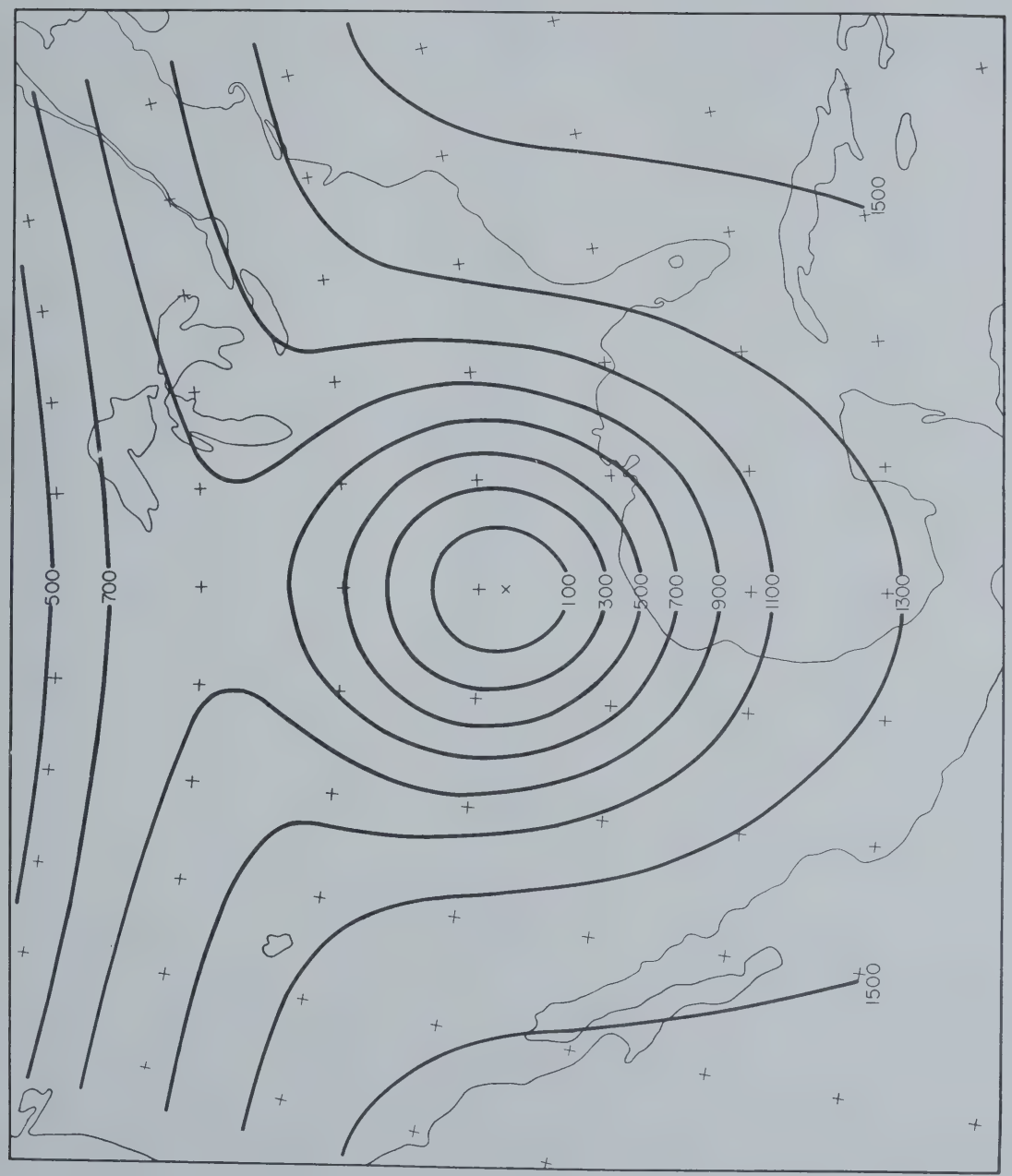

Fig. 10

Figure 11. 700 mb contour chart corresponding to model wind field.

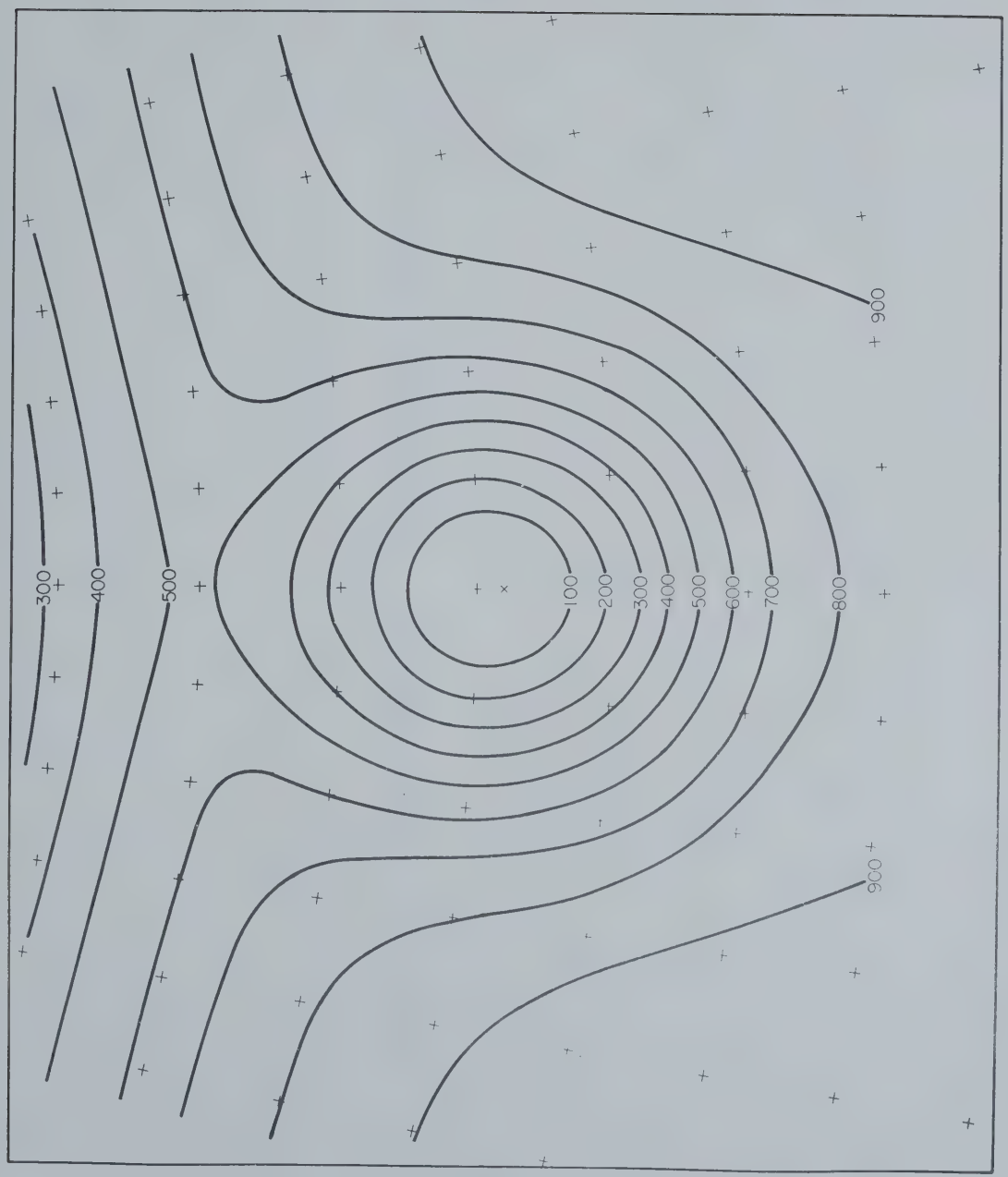

Fig. 11

Figure 12. 850 mb contour chart corresponding to model wind field.

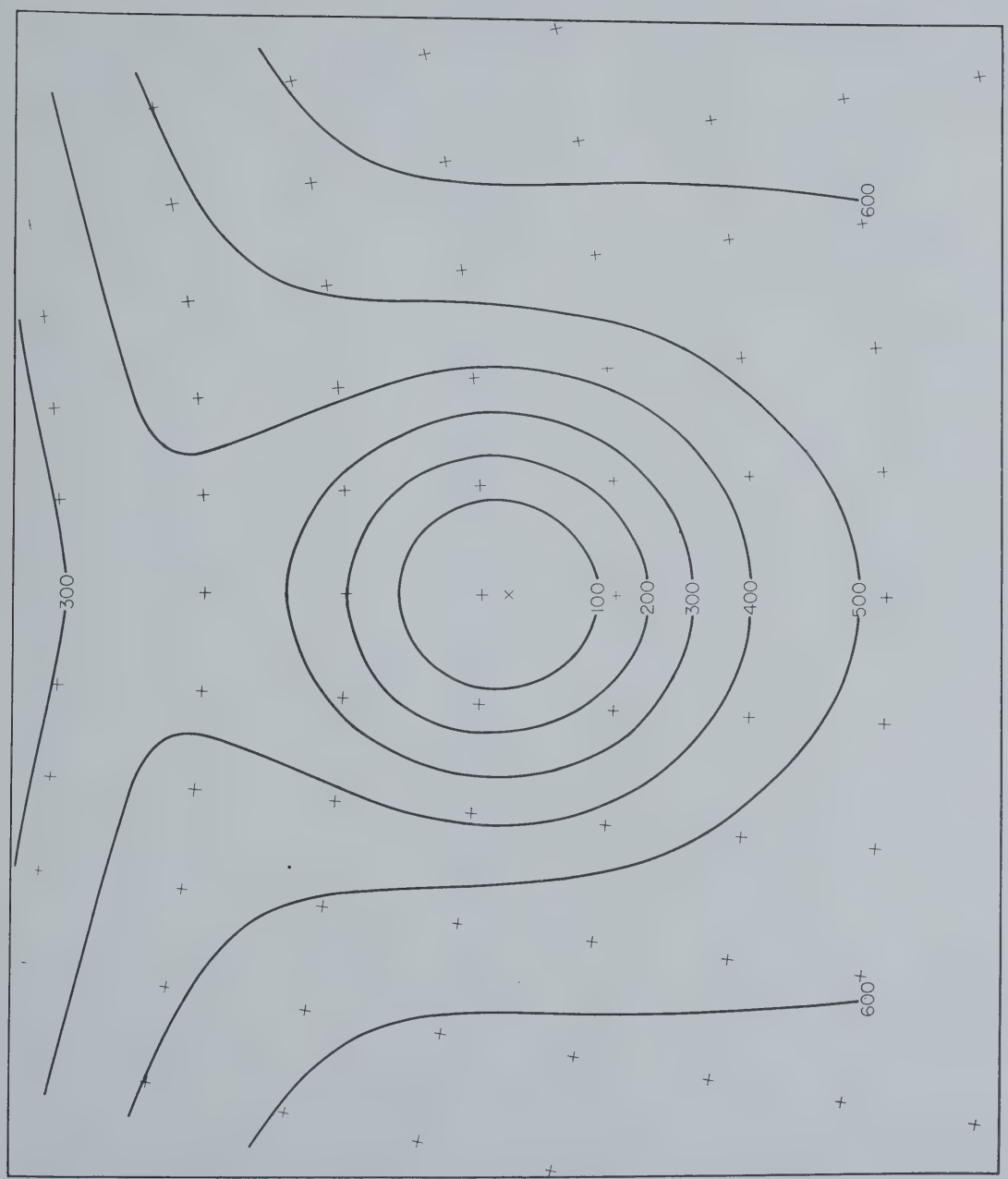

Fig. 12

Figure 13. 500 mb contour chart for cold-low case of 0300 GCT 10 January 1953.

300
500
700
900
1100
1300
1500
1500
700
500
300
100
500
700
900
1100
1300
1500

Fig. 13

possibly significant difference. The aspects which may be pointed out as favoring the realism of the model are the number of closed contours (four at intervals of 200 geopotential feet), the distance and height difference between the low center and the cold point (9 degrees of latitude and 850 feet, respectively) and the overall height difference between low center and adjoining ridges. Asymmetry is among the features which have been eliminated or modified by the generalization. The axis of the observed system at 500 mb tilts eastward, and the ridge to the west is much broader than to the east. In general, the ridge configurations differ in character in ways which follow necessarily from the fact that the observed system merges into adjacent wave structures of the planetary westerlies, while the model merges into a zonal flow which is constant in the east-west direction.

Certain points of difference in regard to configurations of the height pattern are in part consequences of the deliberate disparity between the vortex wind field of the model and that of 10 January 1953. In addition to the symmetry of the vortex imposed by assumption of the framework (8), the model has a more gradual increase of the tangential wind component near the center. This leads to having a larger innermost closed contour in the model than on 10 January 1953. Also the maximum speed in the vortex and the radial distance from the center to this maximum are less in the model. As a result the radial distance at which the maximum gradient of height occurs is less in the model contour field. These differences reflect the effect of the influence of other cases upon the subjective conception

of a general prototype. They are undoubtedly modified to an indeterminable extent by the crudity of the method of derivation of the model contour patterns.

It is believed that the aspects of similarity and difference between the model contour patterns and the case used as a reference are essentially as stated in the preceding two paragraphs. Some differences which show up (e.g. see fig. 4) become more accentuated the lower the level. It is not relevant to make specific comparisons. This is a modeling experiment, not a case study. Other cases with still greater differences of the same kinds can be readily found.

Another study was considered because of lack of information sharply defining the prototype class. Sumner [19] has made a summary of a number of synoptic characteristics of "cold pools". This synoptic model taken as the object of investigation herein is represented among the systems included in Sumner's study.

The primary basis of classification used by Sumner is the thickness pattern of the layer 1000-500 mb. The requirement for inclusion of a system in his compilation was that there be at least two closed 200-foot thickness lines surrounding the cold low center. Of 219 cases studied, 171 had just two closed thickness lines, 41 had three, and the remainder (5 plus 2) had four or five. In the cases occuring in the season December-February, 9 out of 22 cold pools over land were associated with low pressure centers at the surface. These statistics help to place the present model as a roughly median representative of its class.

With the cautioning word that the interpretation cannot be made with too fine a point because of the approximations which have gone into it, it is pertinent to examine the thickness patterns which follow from the derived contour fields of figs. 10-12. The thickness patterns for the layers 500-850 mb and 500-700 mb are shown in fig. 14. On the basis of the examples given by Sumner and of synoptic experience in general, one finds further justification for acceptance of the wind model as suitable material for the proposed experiment.

This was not true, however, at all stages in the development of this model. The present model is the successor of one which had the present 900 mb wind field as the 1000 mb model, and the present reference level field for its 500 mb wind prescription. The model was modified to its present form when it became apparent from examination of the thickness fields that it did not have enough character. At that the model used is by no means as intense as some synoptic examples, e.g. the case of 10 January 1953.

Figure 14. Thickness charts derived from fig. 10-12.
Above: 500-850 mb thickness. Interval of 100 ft. corresponds to mean temperature increment of 3.1C.
Below: 500-700 mb thickness. Interval of 100 ft. corresponds to mean temperature increment of nearly 2C.

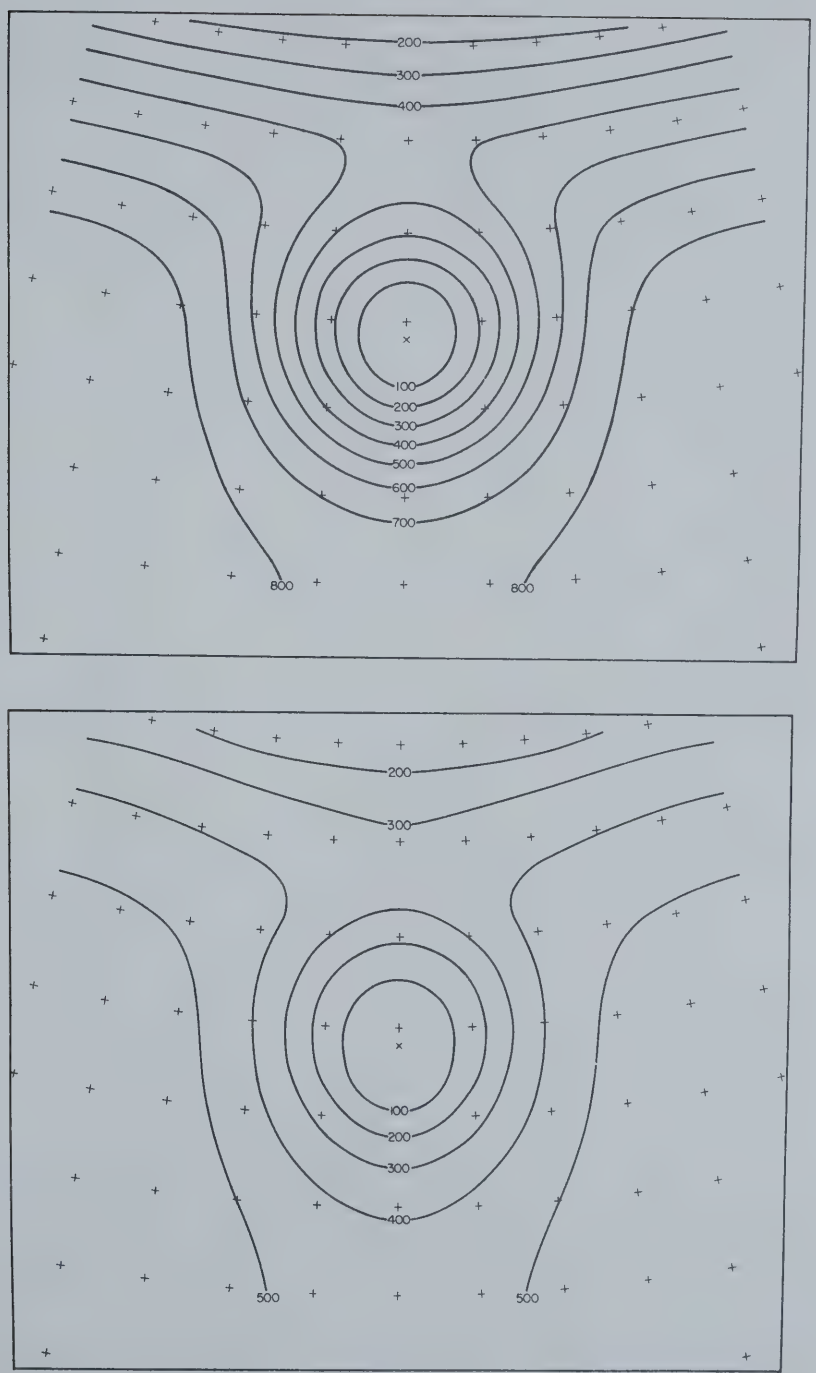
200
300
400
100
200
300
400
500
600
700
800
800
200
300
100
200
300
400
500
500

Fig. 14

5. BOUNDARY CONDITIONS

Vertical motion at the lower boundary.-There is no direct way of estimating an appropriate distribution of vertical motion at the lower boundary of the model system. Several indirect methods of obtaining the large-scale distribution of vertical motion have been used in case studies of atmospheric motions. One possible approach to the modeling problem under consideration here is to use one or more of these techniques on several cases of the desired type, to form a sort of "observational" basis for selection of the boundary values of vertical motion. All of the methods of deducing vertical motions from synoptic data are a great deal of work, however. In consideration of the initial absence of knowledge of the role of lower-boundary vertical motion in the maintenance of a steady state of vorticity by the assigned model wind field, such rigorous modeling would be unwarranted. Furthermore, the main purpose of numerical experimentation is better served by assumption of a simple distribution of vertical motion at the lower boundary. One way of going about it is suggested by Charney's use [3] of the Ekman theory of the wind structure in the layer of surface frictional influence.

It is assumed for the purposes of this model that the integrated effect of the motion in the layer of air below the 90 cb surface is adequately represented by the integrated divergence of the Ekman spiral wind. This is computed with the following

further simplifications of the situation:

(a) latitudinal variation of the Coriolis parameter is neglected;

(b) the cross-isobar angle of the wind is constant on a given pressure surface;

(c) the 90 cb surface is the top of the layer of significant frictional influence ("gradient wind level");

(d) the component of wind along the contours is nondivergent. (This means that the gradient of contour height does not vary along the direction of the contours.);

(e) the relative vorticity of the geostrophic wind may be replaced by the relative vorticity of the model wind on the 90 cb surface;

(f) certain parameters which enter into evaluation of the substantial derivative of pressure at 90 cb by the procedure under discussion may be combined into a single constant;

(g) the continuous distribution of substantial derivative of pressure on the 90 cb surface is replaced by a discrete distribution obtained by evaluation of frictional convergence at points of a finite-difference grid.

We consider the divergence of the wind in a layer from anemometer level to the gradient wind level, under the above assumptions and those of the Ekman spiral derivation [31]. The result of integration from surface pressure to 90 cb is the following formula for the 90 cb distribution of the substantial derivative of pressure:

$$\omega_{90} = - [\rho g (K/2f)^{\frac{1}{2}} \sin 2\theta] \zeta_g , \qquad (15)$$

where ρ is a suitable mean value of density for the layer, g is acceleration of gravity, f is Coriolis parameter, K is eddy viscosity, θ is the angle between anemometer level wind and the contour lines, and ζ_g is the relative vorticity of the geostrophic wind in the friction layer. By assumptions (e) and (f) above, the last quantity is the only variable in the equation and is to be evaluated as the relative vorticity of the model wind field at the 90 cb surface, ζ_{90} .

The numerical value of the coefficient of ζ in equation (15) is obtained by assuming that the horizontal variations of the parameters ρ , K and f balance one another to give the constant value of 1.66. This corresponds to values in the neighborhood of 1.22×10^{-3} t m^{-3}, 5.5 m^2 s^{-1}, and 9×10^{-5} s^{-1} for ρ , K and f respectively, when θ is about 0.5 radian.

Thus

$$\omega = - 1.66 \zeta \qquad (16)$$

is the boundary value prescription of vertical motion at the lower boundary. The pattern given by this formula and assumption (g) above is shown in fig. 19 of section 7.

Lateral boundaries.-The formulation of the problem to which this investigation is directed is completed by consideration of the auxiliary conditions needed for unique determination of the nondivergent wind field $\underline{W}$. In brief recapitulation of the proceedings to this

point, the number of unknown scalars in equation (6) and (7) has been reduced to three, ω and the two components of $\underline{W}$. This was done by setting $\partial\zeta/\partial t = 0$, and by making a model of the nondivergent wind $\underline{V}$ which is similar to velocity fields in real situations when $\partial\zeta/\partial t$ is approximately equal to zero. Equations (6) and (7), together with the fact that the horizontal vector $\underline{W}$ is irrotational, make a complete set for determination of ω and $\underline{W}$. We essay to obtain the solution over the three-dimensional domain (x, y, p) by steps from an initial value of p. The continuity equation (7) links successive values of p, in finite steps performed by a simple method of numerical integration. This integration requires initial knowledge of the dependent variable ω, which is supplied in the preceding section. It also requires knowledge of the divergence as a function of p. In order to obtain the divergence, the vorticity equation with $\partial\zeta/\partial t = 0$ is satisfied by a succession of approximations to the terms involving the unknowns. These successive approximations permit interplay between vertical motion, obtained by successive approximate integrations of divergence with respect to pressure, and divergence. The effects of vertical motion are involved in evaluation of the divergence from the vorticity equation. Beside this interlocking of the continuity equation and the vorticity equation, complete evaluation of the advection terms in the vorticity equation requires that we find an irrotational wind field which itself has the appropriate divergence.

The latter requirement is, as pointed out earlier, nothing more than the commonly encountered problem of solution of the Poisson

type of second-order partial differential equation. For this investigation these equations arise in pairs. One of the components of the divergent wind appears as the dependent variable in each member of a pair. The solution is uniquely determined, provided only that it has suitable continuity (which we shall assume) and is known on the boundary of a suitable region.

The simplest possible prescription of divergent wind at the lateral boundary of each pressure surface of the model is obviously $\underline{W} = 0$. It is worthy of note in this connection that one can tolerate some error in the selection of boundary values of a solution to a Poisson equation. If there is a discrepancy between the assumed boundary value prescription and a hypothetical exactly correct condition, its absolute value is an upper bound to the consequent deviation of the computed solution from the correct solution [32]. This comforting situation is due to the fact that the error in the solution satisfies Laplace's equation at the interior points, and hence is a harmonic function. Since a harmonic function cannot have a maximum absolute value in the interior of a closed region, the error at the interior points is less than or equal in absolute value to the maximum error on the boundary.

In this problem the true boundary values of the components of the divergent wind can reasonably be supposed to be small. There is no reason for considering any more complicated auxiliary condition for the governing Poisson equations than that

$$\underline{W} = 0 \qquad (17)$$

at the boundary on each pressure surface.

6. PROGRAM OF NUMERICAL SOLUTION FOR STRUCTURE

Cartographic considerations.-The functions (9) and (10) which give the model wind field are stated in different coordinate systems. Neither of these is the coordinate system in which equation (6) is to be evaluated. The latter is, as noted earlier, a rectangular coordinate system (x, y) established on Lambert's Conic Projection [33] to the scale 1: 7.5×10^6 at the standard parallels 25°N and 48°30'N. At this point it is desirable to state the relationships used to evaluate the terms of equation (6) for the assumed distributions of $\underline{V}$ given by (9) and (10).

The working rectangular coordinate system has its origin at 34°N, 95°W. That is, its origin coincides with the origin of the polar coordinate system in which $c(r)$ is given. The determination of the value of $c(r)$ and necessary derivatives at a point with coordinates (x, y) is simply a matter of converting from rectangular (x, y) to r by using

$$r = [x^2 + y^2]^{\frac{1}{2}} . \qquad (18)$$

The appearance of the scale factor when conformal charts are used to evaluate expressions involving differentiation along the coordinate curves of the meteorological coordinate system (virtually a spherical coordinate system) is discussed by Eliassen [34]. The considerations explained by him apply here as well, with a

certain difference in application to the coordinate Y in equation (10).

The components of the vortex wind $\underline{c}(r)$ in the x, y coordinate system are shown by

$$\underline{c}(r) = c(r)\ [-y/r\ \underline{i} + x/r\ \underline{j}]\ . \qquad (19)$$

It will be remembered that this is the vortex wind at the reference pressure surface, at which the function $G(p)$ of equation (8) is unity.

Other quantities needed in the evaluation of terms in (6) are the vortex vorticity ζ_c and the gradient $\nabla\zeta_c$. We obtain these quantities for the reference level by working in the polar coordinate system, with provision for the fact that the distance represented by an increment of dr centimeters on the map is equal to $7.5 \times 10^4\ \sigma^{-1}$ dr meters on the mapped surface. The quantity σ is the map distortion factor. It is unity at the standard parallels. The scale factor $\sigma/7.5 \times 10^4$ is conventionally assigned the symbol m, so that we have

$$dr/dr' = m = \sigma/7.5 \times 10^4\ , \qquad (20)$$

where dr' is in meters on the mapped surface and dr is in centimeters on the map. The distortion σ is a function of latitude only.

We interpret the picture of streamlines and isotachs given by c(r) in the polar coordinate system on the map to be the map representation of observations taken in the conventional manner. The associated vorticity at the reference pressure surface is:

$$\zeta_c = m\, dc/dr + \bar{m}\, c/r. \qquad (21)$$

The quantity $\bar{m}$ is a mean value of the scale factor. The appropriate mean value is approximated by the arithmetical mean of the values of σ at the latitudes of the respective end points of the radial line from the origin to the point in question. The use of $\bar{m}/r$ for computing the curvature term in the scalar vorticity is found to be a satisfactory approximation.

Differentiation of (21) with respect to radial distance along the mapped surface gives the magnitude of the gradient of vortex vorticity

$$m\, d\zeta_c/dr = m^2\, d^2c/dr^2 + m\bar{m}/r\,(dc/dr - c/r)\ . \qquad (22)$$

We now turn to the relationship between the rectangular coordinates and the independent variable Y in the expression (10) for the zonal wind. Y is distance along the meridians in map centimeters. It is counted positive in the northward direction from 34°N. For a grid point with coordinates (x, y), we need to know Y, the angle between $\underline{U}$ and the y coordinate direction, and the latitude. Latitude is used in evaluation of the Coriolis parameter, the distortion factor, and a curvature term in the vorticity ζ_U of the zonal wind. These are obtained in the following manner.

On the map, parallels of latitude are arcs of concentric circles. Let the radius of the parallel of latitude ϕ on the map be denoted by R_ϕ. The radius R_{34} corresponds to $Y = 0$. Simple geometry shows that the radius of the latitude arc which

passes through a point (x, y) is

$$R_{\phi} = [(R_{34} - y)^2 + x^2]^{\frac{1}{2}} . \qquad (23)$$

Denoting by α the angle made on the map by the arc of latitude ϕ and the grid line y = constant , trigonometry yields

$$\sin \alpha = x/R_{\phi} , \qquad (24)$$

$$\cos \alpha = (R_{34} - y) R_{\phi} . \qquad (25)$$

These are required when vectors defined with reference to the direction of latitude circles are to be resolved in the rectangular coordinate directions.

The argument Y is the same for all points at a given latitude, but varies along a line of constant value of the rectangular coordinate y . It is simply $R_{34} - R_{\phi}$, and hence is determined from (x, y) by use of (23) and the value of R_{34} which follows from the formulae of cartography applied to the particular map projection used.

The cartographic formulae used to obtain R_{34} and the latitude of a point are those applicable for projection from a spherical surface by conformal conic projection [35].[1]

---

[1]The differences between the sphere of equivalent area and the Clarke spheroid [36] upon which the map is presumably based are insignificant; if it were worthwhile, one could eliminate the differences by a minor change in the interpretation of the model $\underline{V}$. (This would not apply to the use of scale factor for projections from spheres when working with real observations plotted on maps projected from more nearly geoidal shapes - but for these purposes the point is absurd.)

For the Lambert Conformal Conic true at 25° and 48°30', the radius of a parallel of latitude is, in centimeters:

$$R_{\phi} = (a \cos 25°)(7.5 \times 10^{4} n)^{-1} [\tan \tfrac{1}{2}(90-\phi)/\tan 32°30']^{n}, \quad (26)$$

where a = radius of the equivalent sphere and n = cone constant for the projection.

Equation (26) can be solved for latitude ϕ as a function of R_{ϕ}, which is obtained for any point (x,y) by use of (23). In turn, ϕ is used for computation of the Coriolis parameter, ζ_U and $\nabla \zeta_U$ (see below), and the parameter σ. The last depends also upon n, as shown in any standard discussion of cartography.

Application of these quantities in computation of the vorticity field of the zonal wind arises as follows. For a zonal wind of speed U, the vertical component of vorticity is

$$\zeta_U = - 1/a \, (\partial U/\partial \phi - U \tan \phi), \quad (27)$$

where a is distance from the center of the earth. The relationship between the argument Y in the functional expression (10) for the zonal wind and the latitude ϕ is $a^{-1} \, dY/d\phi = m$, as in (20). A constant value of a is used for distance from the center of the earth.

The substitution of $U(Y)$ into (24) leads to

$$\zeta_U = - m \, dU/dY + U \tan \phi / a \quad (28)$$

for the relative vorticity of the zonal wind at the reference pressure surface. The gradient of this field is directed northward,

and has the magnitude

$$d\zeta_U/dY = - m^2 \, d^2U/dY^2 + m \, (dU/dY) \tan \phi / a \, . \qquad (29)$$

A term with the square of a in the denominator has been omitted as negligible. Retention of the second term on the right is a borderline situation in this respect. It is pointed out by Palmen [37], and others, that this curvature term is not quite negligible even for synoptic discussions if the zonal wind is strong. In the use of (29) in this study we would save a relatively unimportant amount of computation by omitting the vorticity effect of horizontal curvature of the latitude circles.

Component parts of the iterative procedure.-The final working formulation of the problem can now be made. We are given the nondivergent wind $\underline{V}$ (x, y, p) as a continuous function of x and y over a chosen region of each of a succession of pressure surfaces spaced at 10 cb intervals, starting with a lower boundary at 90 cb. The irrotational part $\underline{W}$ of the total wind is zero at the lateral boundaries of the region of consideration on each pressure surface, and the substantial derivative of pressure ω is prescribed for the 90 cb surface. The equations to be used are (5), (6) and (7). The next step is neglect of the small non-linear term

$$\underline{k} \cdot \nabla\omega \times (\partial \underline{W}/\partial p)$$

in (6). Making this change and using the conventional symbol ζ_a for the absolute vorticity $\zeta + f$, the system of equation (6) and (7) may be written:

$$D = -\zeta_a^{-1}\left[\underline{V}\cdot\nabla\zeta_a + \underline{W}\cdot\nabla\zeta_a + \omega(\partial\zeta/\partial p) + \underline{k}\cdot\nabla\omega \times (\partial\underline{V}/\partial p)\right], \tag{30}$$

$$D = -(\partial\omega/\partial p) . \tag{31}$$

The problem is to determine the fields of divergence D, divergent wind $\underline{W}$, and substantial derivative of pressure ω, in such a way that equations (30) and (31) are satisfied for the prescribed field of nondivergent wind $\underline{V}$.

Using the relationships between the several horizontal coordinate systems involved, the expanded form for the first term on the right side of (30) is

$$-\zeta_a^{-1}\,\underline{V}\cdot\nabla\zeta_a = -\zeta_a^{-1}(x/r)(R_{34}/R_{\phi})\,G(p)\left\{F(p)\,[c\,d\zeta_U/dY + U\,d\zeta_c/dr] + 2\Omega a^{-1} c\cos\phi\right\}. \tag{32}$$

Here c is given by (9), U by (10), $d\zeta_U/dY$ by (29), $d\zeta_c/dr$ by (22) and

$$\zeta_a = \zeta_c + \zeta_U + f \tag{33}$$

is given by (21), (28) and the Coriolis parameter $f = 2\Omega\sin\phi$.

All quantities involved in the evaluation of (32) are determined by the model wind prescription and cartography. The quantity $-\zeta_a^{-1}\,\underline{V}\cdot\nabla\zeta_a$ is also the major part of the divergence given by equation (30). It is the obvious first approximation to the required divergence. We define the first of a series of approximations

to the divergence of the cold-low system to be

$$D^{(0)} = - \zeta_a^{-1} \underline{V} \cdot \nabla \zeta_a \, . \qquad (34)$$

Most of the computation involved in getting $D^{(0)}$ is common to its evaluation on all pressure surfaces. The program of computations for $D^{(0)}$ was carried out first for the reference surface, where $F(p) = G(p) = 1$. Computations for the other pressure surfaces reported, viz. 90, 80, 70, 60 and 50 cb, are relatively easy rearrangements of terms to introduce the respective values of the vertical variation functions given in table 1.

There are two kinds of improvements to be made to $D^{(0)}$, or for that matter, to the divergence obtained at any stage of the procedure. One is the evaluation of the divergent-wind advection term,

$$\Delta^{(H)}D = -\zeta_a^{-1} \underline{W} \cdot \nabla \zeta_a \, . \qquad (35)$$

This evaluation entails use of the value of $\underline{W}$ determined by the divergence at any current stage of refinement. The other improvement follows from evaluation of ω by (31), and computation of its effects on vorticity, given by

$$\Delta^{(V)}D = - \zeta_a^{-1} (\omega \partial\zeta/\partial p + \underline{k} \cdot \nabla\omega \times \partial\underline{V}/\partial p) \, . \qquad (36)$$

The procedures involved in each of these parts of the program will be discussed individually, followed by description of their alternating use to produce successive approximations to the structure of the system.

The divergent part of the wind field.-The field of irrotational wind $\underline{W}$ which corresponds to a known divergence D is the solution of the following equations (5)

$$k \cdot \nabla \times \underline{W} = 0 ,$$

$$\nabla \cdot \underline{W} = D ,$$

subject to the condition $\underline{W} = 0$ on the lateral boundary.

We choose to represent $\underline{W}$ by its components u and v in the rectangular coordinate system established on the map. The equations (5) are easily transformed into the pair of Poisson problems

$$\nabla^2 u = \partial D/\partial x , \quad u(B) = 0 , \tag{37a}$$

$$\nabla^2 v = \partial D/\partial y , \quad v(B) = 0 , \tag{37b}$$

where ∇^2 is the horizontal Laplacian operator in Cartesian coordinates, and the argument B represents the coordinates of any boundary point.

There are various methods for solution of equations (37). The one used here is chosen from among the numerical approximation methods used in numerical prediction problems [38]. For the purpose of this study, the preferred method is Southwell's relaxation technique [39], modified as recommended by the experience of those who have used it [38, 40].

The finite-difference grid is defined by the intersections of lines of constant x with lines of constant y, forming squares 4 cm on a side. It is shown superimposed on the working map-base in fig. 15. Fourteen rows and fourteen columns of interior grid

Figure 15. Finite difference grid.

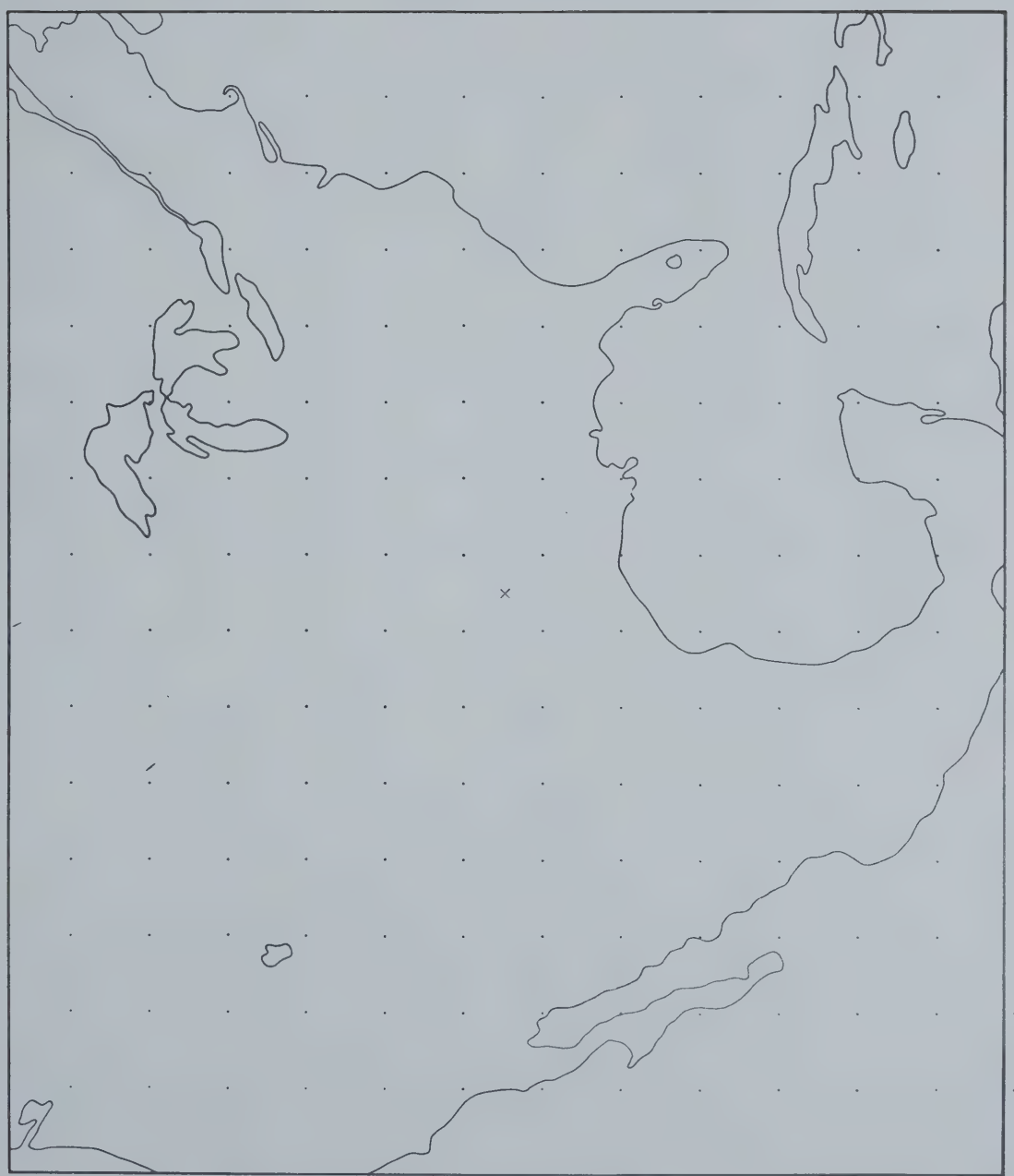

Fig. 15

points are used. Grid point numbering reads from top to bottom for rows and left to right for columns. The format of grid point identification is iijj , with ii and jj respectively running from 01 to 14.

In this grid, the origin of the rectangular coordinate system is at the center of the square formed by the points 0707, 0708, 0807 and 0808. The grid spacing corresponds to 300 km at the standard parallels. This finite-difference interval was chosen for the sake of reduction of the amount of computation necessary. This was an especially important consideration when the project was undertaken, since only desk calculators were available. The use of a 300 km interval is not inconsistent with common practice in numerical studies in atmospheric dynamics [40, 41]. Grid sizes of $2\frac{1}{2}$ degrees latitude or 278 km are usual. The scale of the horizontal variations in the present problem is such that the chosen horizontal mesh size should be adequately small.

In regard to the choice of vertical mesh size, Arnason [41] points out in a similar context that it should be guided by the vertical structure of the quantities involved and should be compatible with the horizontal mesh size. The use of a 10 cb vertical mesh size would seem to be consistent with the scale of the vertical variations of the model wind. There is of course no a priori knowledge of the vertical velocity patterns.

The known functions which appear on the right-hand sides of the Poisson equations (37) can in the case of $D^{(0)}$ be computed by formal differentiation of (32). However, the resulting

expressions are extremely cumbersome. Therefore, at this point in the procedure the modus operandi becomes purely numerical. The finite-difference approximations to partial derivatives and the Laplacians of the components u and v in the grid coordinate directions are standard formulae of discrete analysis.

After rearrangement, the finite-difference equations to be solved become

$$\nabla^2 u_{ij} = \xi_{ij} , \tag{38a}$$

$$\nabla^2 v_{ij} = \eta_{ij} . \tag{38b}$$

Here a two-place subscript is used to denote the interior grid point at which the subscripted quantity applies (i = row number, j = column number), and ξ and η are scaled finite-difference approximations to $\partial D/\partial x$ and $\partial D/\partial y$ respectively. The symbol ∇^2 represents the finite-difference Laplace operator in the grid system. Its form is shown by an example:

$$\nabla^2 u_{ij} = u_{i,\,j-1} + u_{i+1,\,j} + u_{i,\,j+1} + u_{i-1,j} - 4u_{ij} . \tag{39}$$

The solution of the equations (38) yields the components of $\underline{W}$. The particular form of relaxation used was the extrapolated Liebmann process [40]. The application of this technique has been widely discussed in meteorological literature. It will be briefly reviewed here for convenience of discussion.

To solve equation (38a), for example, a sequence of approximations to each of the u_{ij} is generated by making an initial

guess $u_{ij}^{(0)}$, and applying the following iterative formulae:

$$\nabla^2 u_{ij}^{(n,\, n+1)} - \xi_{ij} = R_{ij}^{(n,\, n+1)} , \qquad (40)$$

$$u_{ij}^{(n+1)} = u_{ij}^{(n)} + \gamma R_{ij}^{(n,\, n+1)} , \qquad (41)$$

The residue R_{ij} at each point is computed from (40) by applying the operator ∇^2 to the existing stage of the u values at the point iijj and its four adjacent grid points. The double superscript n, n+1 indicates that as soon as the residue for a point has been computed by (40), it is used in (41) to give the next member in the sequence of values of u_{ij}.

If γ is given the value 1/4 (which may be called the Richardson value), successive application of (40) and (41) at a point reduces the residue at that point to zero. Termination of the iteration is, however, determined by achieving a desired accuracy for all of the u_{ij} on the grid. Any criterion for acceptability of the solution may alternatively be formulated in terms of a maximum magnitude of residuals. It is found (Southwell, [39]) that a given criterion will in general be satisfied in fewer repititions of (40) and (41) if γ is sometimes chosen larger (over-relaxation), sometimes smaller (under-relaxation), than 1/4. The choice of γ is made according to the distribution of the current residue at the adjacent points, according to rules found in any text book on numerical analysis (e.g. Hildebrand [42].

The pair of equations (38) is solved several times at each pressure surface in the present program, once for each $\Delta^{(H)}{}_D$. Two evaluations of this type of contribution to divergence were

made at each of the surfaces 90 cb and 80 cb. The relaxation for these was done entirely by hand computation. All available devices for shortening the work were exploited. For example, in computing the divergent wind from a $D^{(0)}$ field, one can take advantage of the symmetry of the ξ field (or antisymmetry of the η field). The technique of block relaxation [42] was of some help. The flexibility of human computers was used in recommended fashion with regard to choice of δ and selection of route in covering the grid.

One further device tried in order to expedite the relaxation solution was a partial use of Fjørtoft's method [43]. He has shown that approximate solutions of a Poisson equation may be obtained by using various kinds of averages (of the kind now called space-means), formed from the field of values of the known function. The particular averaging intervals and combination of averages which are best suited for a given problem depend upon which components in the double Fourier series expansion of the unknown are considered to be the most important. In the present case, Fjørtoft's approximate solution designed to work best on components with wave lengths about four times the grid interval was tried as a way of getting a good first guess in the relaxation process. Although the circumstances were not suited to comparison with other ways of getting initial approximations, it appeared that this method did not work particularly well. The reason may well lie in discrepancy between the actual dominant wave lengths in the solution pattern and the wave lengths for which the Fjørtoft approximation

is best suited. This is an interesting area of numerical experimentation in itself, but one which it was not feasible to explore.

Regardless of the various attempts to speed the convergence of the relaxation process, and in spite of the considerable skill and ingenuity developed by the persons doing it, the time taken to perform hand-relaxation solutions of equations (38) for 196 grid points was excessive. At about the time that the first relaxation for 70 cb was underway it became possible to plan for the use of an IBM 650 computer. The relaxation solution was hastily programmed and checked out. From 70 cb on, machine computation was used not only for the relaxation problem itself, but also for computation of the finite-difference approximations to the derivatives of D and ω and for the evaluation of the term $\Delta^{(H)}D$ which follows immediately after relaxation solution for the components u and v of the divergent wind.

Divergence required by divergent-wind advection.-The component form of the divergent-wind advection term $\Delta^{(H)}D$ is obtained by expansion of the vector expression $-\zeta_a^{-1}\,\underline{W}\cdot\nabla\zeta_a$,

$$\Delta^{(H)}D = -\zeta_a^{-1}\Big\{[-u\sin\alpha + v\cos\alpha]\,[F(p)\,d\zeta_U/dY + 2\Omega\, a^{-1}\cos\phi] + (u\,x/r + v\,y/r)\,G(p)\,d\zeta_c/dr\Big\}\,. \qquad (42)$$

Divergence required by vertical motion-effects.-The second kind of refinement to be considered is the vertical-motion effect upon divergence, given by (36). The first step in its computation is evaluation of the distribution of the ω_{ij}. At 90 cb ω is provided by the initial value prescription described in section 5.

At subsequent pressure surfaces ω is determined by numerical integration of the continuity equation (31). The essential problem in this integration is the determination of a value of D for the pressure surface at the top of the layer over which the integration is being performed. This may be done in a variety of ways. The description of experimentation in this respect cannot be made until procedures for putting together the two kinds of refinements to divergence have been discussed.

Assuming pro tem that ω has been approximated satisfactorily, evaluation of (36) is in order. The definition (8) of the parts of the model wind as products of functions of pressure and functions of the horizontal coordinates results in a considerable simplification. Thus we have at a pressure surface p :

$$\partial \underline{V}/\partial p = G'(p)\ \underline{c} + F'(p)\ \underline{U}\ , \tag{43}$$

$$\partial \zeta/\partial p = G'(p)\ \zeta_c + F'(p)\ \zeta_U\ . \tag{44}$$

The computations of $\underline{c}$, $\underline{U}$, ζ_c and ζ_U made in getting reference surface values of $D^{(0)}$ constitute most of the work required in evaluation of (43) and (44) in the grid coordinate system. Computation of the vertical motion term further involves the use of the graphical approximations to $F'(p)$ and $G'(p)$ given in table 1.

Expanding the vector expression for the tipping-term part of (36) in the grid coordinate system, we find

$$\underline{k} \cdot \nabla\omega \times \partial \underline{V}/\partial p = (\partial\omega/\partial x)(\partial V_y/\partial p) - (\partial\omega/\partial y)(\partial V_x/\partial p)\ . \tag{45}$$

When the expressions (9) and (10) for $\underline{V}$ at the reference surface are substituted into (43) and this is in turn put into (45), we obtain

$$\underline{k} \cdot \nabla\omega \times \partial\underline{V}/\partial p = \partial\omega/\partial x \, [F'(p) \, U \sin\alpha + G'(p) \, c \, x/r] - \partial\omega/\partial y \, [F'(p) \, U \cos\alpha + G'(p) \, c \, y/r]. \tag{46}$$

Similarly the substitution of the relative vorticity expressions (21) and (28) into (44) provides $\partial\zeta/\partial p$ in the form required for computation from the basic prescriptions (9) and (10).

The computation of derivatives of ω along the coordinate directions at each grid point was done by finite-difference approximations similar to those used to get ξ and η .

Development of a scheme of iterative solution.-Beginning with $D^{(0)}$ at 90 cb, the application of the refinements $\Delta^{(V)}D$ and $\Delta^{(H)}D$ was carried out in that order. The sequence of approximate values of divergence at a particular pressure surface will be represented symbolically by

$$D^{(k)} = D^{(0)} + \Delta^{(V)}D + \Delta^{(H)}D \, , \tag{47}$$

where k is the total number of refinements of either kind, $\Delta^{(V)}D$ or $\Delta^{(H)}D$. These quantities are numbered consecutively $\Delta^{(1)}D$, $\Delta^{(2)}D$, $\Delta^{(3)}D$, etc. In the 90 cb program, $\Delta^{(1)}D$ was the only vertical-motion type of correction applied to $D^{(0)}$. The further approximations to D at 90 cb were obtained by computing successively refined divergent-wind advection terms of the type $\Delta^{(H)}D$.

Since the value of $\Delta^{(V)}D$ at 90 cb is not dependent upon the value of D, the procedure for obtaining a final value $\Delta^{(H)}D$ for the effect of advection of absolute vorticity by $\underline{W}$ was a more simple iterative process than at subsequent pressure steps. To facilitate later descriptions of the iterative process the single iterative loop at 90 cb is now exhibited in detail.

We begin with the second approximation to divergence

$$D^{(1)} = D^{(0)} + \Delta^{(1)}D \,, \tag{48}$$

where $\Delta^{(1)}D$ is computed from (36) and the values ω_{90} described in section 5. Using hand relaxation, $\underline{W}^{(1)}$ was obtained by solution of (38), with ξ and η computed from $D^{(1)}$. Next $\Delta^{(3)}D$ was evaluated by using $\underline{W}^{(1)}$ in (35). (The omission of the superscript 2 in the numbering of these Δ's is intentional. The purpose of doing this is to make the numbering of 90 cb increments parallel that intended for higher levels).

It follows next that

$$D^{(3)} = D^{(1)} + \Delta^{(3)}D \,. \tag{49}$$

This divergence $D^{(3)}$ was in turn used in (38), yielding $\underline{W}^{(2)}$. This was substituted into (32) to give a new value of $\Delta^{(H)}D$, called $\Delta^{(4)}D$. Finally

$$D^{(4)} = D^{(1)} + D^{(4)}D \,. \tag{50}$$

It is clear that the next step in the iterative procedure is to get $\underline{W}^{(3)}$ by solution of $\nabla \cdot \underline{W}^{(3)} = D^{(4)}$ and $\nabla \times \underline{W}^{(3)} = 0$,

and so on. Since it was not certain at this stage just how much the next evaluation of $\Delta^{(H)}D$ would differ from $\Delta^{(4)}D$, a partial third relaxation was done. It was found that the new values of $\underline{W}$ differed negligibly from $\underline{W}^{(2)}$ in regard to their effects upon $\Delta^{(H)}D$, so the iteration at 90 cb was terminated with $\Delta^{(4)}D$ and $D^{(4)}$.

The procedure described above for making successive approximations to $\underline{W}$ is one way of solving the equations

$$\zeta_a \nabla \cdot \underline{W} = - \underline{W} \cdot \nabla \zeta_a + H(x, y) , \qquad (51)$$

$$\nabla \times \underline{W} = 0 , \qquad (52)$$

in which ζ_a and $H(x, y)$ are known functions. These equations can be combined into an elliptic partial differential equation since, by virtue of its irrotational property, $\underline{W}$ is the gradient of a scalar function $\Phi(x, y)$. The first equation then yields (with minor rearrangement):

$$\nabla^2 \Phi + \nabla \Phi \cdot \nabla \ln \zeta_a = H(x, y) . \qquad (53)$$

This equation is quite similar to another elliptic equation with variable coefficients discussed by Thompson [44]. The occasion for Thompson's consideration of this type of equation is its occurrence as a key equation in the theory of large-scale nongeostrophic motions. Thompson discusses the disadvantages of a direct application of relaxation methods to his equation. He also describes an iterative method which amounts to the procedure described above for the solution of (53) for $\nabla \Phi$. He provides

a mathematical demonstration that the sequence of approximations coalesces, and that the limit is the solution of his equation. A straightforward adaptation of Thompson's demonstration shows that the sequence of values of $\underline{W}$ obtained by solving (51) and (52) by the method described will assuredly coalesce under certain well-defined conditions. Feasibility of the iteration procedure for numerical computations follows from the assurance that the procedure converges, albeit conditionally.

Of course, the fact that the iterative procedure for determination of $\underline{W}$ converges when $H(x, y)$ is a known function does not tell what will happen in a situation when $H(x, y)$ also depends upon $\underline{W}$. The latter is the case at pressure surfaces in the interior of the region. Moreover, the way that $H(x, y)$ depends upon $\underline{W}$ is quite complicated. For these reasons, it was not attempted to verify whether or not the coalescence criterion for known $H(x, y)$ is met in this model. At 90 cb, where $H(x, y)$ is known, three applications of the process for getting $\underline{W}$ very definitely indicated coalescence. This, together with the theoretical result derived from Thompson's work, was considered enough to warrant going on to the next pressure step. Once away from the lower boundary, we deal with $H(x, y)$ values that involve $\underline{W}$ in complex ways. The characterization of this investigation as an <u>experiment</u> in the application of numerical methods then has connotations as to its numerical analysis aspects as well as to those of modeling of a large-scale atmospheric motion system. That is, coalescence of

the successive approximations to D is not theoretically demonstrated. As will be seen, this coalescence was surely indicated by the numerical behavior of the results.

The program of computations used at 80 cb was to make two computations of $\Delta^{(V)}D$, numbered with superscripts 1 and 2 :

$$D^{(1)} = D^{(0)} + \Delta^{(1)}D , \tag{54}$$

$$D^{(2)} = D^{(0)} + \Delta^{(2)}D . \tag{55}$$

These were followed by two H-type corrections, $\Delta^{(3)}D$ and $\Delta^{(4)}D$, and a partial determination of $\Delta^{(5)}D$. These H-type corrections follow exactly the same pattern as has already been described for the 90 cb program.

It will be observed, however, that at 80 cb there is the new problem of numerical integration of the continuity equation to get ω for use in $\Delta^{(V)}D$. For the 90-80 cb layer (Δp = 10 cb), the centered finite-difference formula

$$\omega_{80}^{(1)} = \omega_{90}^{(1)} + \tfrac{1}{2}[D_{80}^{(0)} + D_{90}^{(4)}]\,\Delta p \tag{56}$$

was used. With the values of $\omega^{(1)}$ thus obtained, $\Delta^{(1)}D$ was computed. The value of $D_{80}^{(1)}$ which follows by use of (54) was then used in (56), in place of $D_{80}^{(0)}$. The problem of integration of the continuity equation,

$$\partial\omega/\partial p = - D ,$$

with respect to pressure is clearly not simple, because D depends upon ω and its derivatives in a complex way. The numerical

method described above is similar to Euler's modified method [45] for numerical integration of $dy/dx = f(x, y)$. One difference in application is that the very first step can be a centered finite-difference step rather than a one-sided pure extrapolation. This is due to the fact that $D^{(0)}$ constitutes a large part of the true value of D at the top of the layer. Indeed, one lesson learned from the 80 cb procedure was that with two successive applications of $\Delta^{(V)}D$, as in (54) and (55), the second application does not give enough change in D to matter in comparison with the error due to not yet having computed $\Delta^{(H)}D$.

Final scheme of iterative solution.-More than one lesson was learned from the observed behavior of the computation procedures tried at the first two pressure surfaces. The procedures used for 70 cb were based on this experience. Also it was at this stage that much of the work was programmed for the IBM 650. Hence the program for the pressure steps 70, 60 and 50 cb were all the same. At the same time, it became feasible to investigate the need for performing more than one complete cycle of approximations at each pressure surface. It had been evident at the two lower levels that there was no need for more than one cycle of approximations to keep the truncation errors below the desired level, but the increase of magnitudes of D and ω by 70 cb indicated that it was becoming necessary to consider adding another cycle.

Beginning with the 70 cb computations the integration of the continuity equation was made by an improved procedure, requiring the use of values of D at the preceding two pressure surfaces

and the top of the layer. Application of Simpson's method of numerical integration [45] to computation of ω at a pressure surface p_k gives the formula

$$\omega(p_i) = \omega(p_{i-2}) + \Delta p/3[D^{(F)}(p_{i-2}) + 4D^{(F)}(p_{i-1}) + D^{(k)}(p_i)] \quad . \quad (57)$$

This formula connects ω at a given grid point on a pressure surface p_i with values of D at the same location (x,y) on the preceding pressure surfaces. For example, when $p_i = 70$ cb, we have $p_{i-1} = 80$ cb and $p_{i-2} = 90$ cb. The superscript F on a value of divergence signifies that it is the final approximation to divergence for its pressure surface. The superscript k indicates that the divergence used for the pressure surface p_i must be approximated by whatever stage of successive approximations to $D(p_i)$ has been attained. As before, Δp is 10 cb.

Thus (57), and therefore $\Delta^{(V)}D$, are evaluated in steps which are interlocked with evaluations of $\Delta^{(H)}D$. The order used for 70, 60 and 50 cb may be summarized as follows:

Cycle-Step	Initial Divergence Approximation	Quantities Evaluated	Type of Increment
I - 1	$D^{(0)}$	$\underline{W}^{(1)}$, $\Delta^{(1)}D$	H
II - 1	$D^{(1)}$	$\omega^{(1)}$, $\Delta^{(2)}D$	V
II - 2	$D^{(2)}$	$\underline{W}^{(2)}$, $\Delta^{(3)}D$	H
II - 3	$D^{(3)}$	$\underline{W}^{(3)}$, $\Delta^{(4)}D$	H
III - 1	$D^{(4)}$	$\omega^{(2)}$, $\Delta^{(5)}D$	V
III - 2	$D^{(5)}$	$\underline{W}^{(4)}$, $\Delta^{(6)}D$	H
III - 3	$D^{(6)}$	$\underline{W}^{(5)}$, $\Delta^{(7)}D$	H

The relation of the $D^{(k)}$ to the $\Delta^{(k)}$ is as given in equation (47), with $\Delta^{(V)}D$ and $\Delta^{(H)}D$ taken to be the highest approximations available at the time that $D^{(k)}$ is computed.

The foregoing schematic gives the procedure decided upon as most suitable for giving comparable increments of the V and H types in a cycle. Cycle III was performed only at 60 cb. The 70 cb program was run part way through step III - 1, to see if the difference between $D^{(4)}$ and $D^{(5)}$ was enough to make $D^{(7)}$ differ significantly from $D^{(4)}$. The meaning of significance in this context is discussed below. The empirical conclusions drawn about the significance of cycle III at 60 cb are discussed in section 7.

Evaluation of H-type refinements of divergence could of course be made very much more quickly on the IBM 650 computer than by the desk computer procedure used in the layer below 70 cb. Beginning at 70 cb, decisions as to accuracy requirements of the relaxation solutions and number of successive applications of $\Delta^{(H)}D$ corrections could be made with less weight on the time factor. Mechanical computation has the further advantage that generous provision for suppression of round-off error carries virtually no penalty in computation time. As has been indicated above, the procedure followed at 70 cb and up was also better in that the integration of divergence with respect to pressure could be readily done by Simpson's method, thus reducing the truncation error incurred in that step. For these reasons, the results for the layer 70 to 50 cb are regarded to be more important products of this numerical experiment than those for the first two pressure steps.

Accuracy of approximative procedures.-The purpose of this section is to indicate the disposition made of some problems of accuracy control which arise in the course of planning and performance of the computation program. The errors which enter into numerical analysis of given initial data may be classified into three types [46]. This particular classification will be discussed in relation to the present numerical problem, followed by more explicit statements in regard to the digital significance of the results.

First, there are errors in the result of a given computation step due to errors in the input data of that stage of computation. These comprise errors in the given initial data, plus the contributions of the other two types from preceding stages. Such errors may be collectively called propagated error. Such error emerges in the total error of a given step with a magnitude which differs from that with which it entered, to an extent characterized by the ratio of the emergent propagated error to its initial value. This ratio is called the amplification factor. In any but very simple programs the practical situation is such that, as noted by Charney [38], "to calculate the resultant effect of these errors ab initio is a difficult, if not impossible task.".

A second category in this scheme of classification comprises round-off errors and outright mistakes. These errors can never be absolutely eliminated. As soon as they occur, they become part of the propagated error. The number of figures carried in the computations determines the chance of exceeding a given upper bound on accumulated round-off errors. Suppression of arithmetical and

clerical errors is similarly a matter of compromise between avoidance of errors and effectiveness of use of time and labor.

The third type of error is the truncation error, which is error due to termination of an infinite series after a finite number of terms. One can make a case for considering round-off error to be of this type. However, in the nomenclature of numerical analysis, the term "truncation" is applied to any such errors except round-off.

The truncation errors in the present program are of two types. The iterative process as a whole consists of interweaving $\Delta^{(H)}D$ and $\Delta^{(V)}D$ refinements of $D^{(0)}$, and progressing through the pressure steps by numerical integration of the continuity equation. Examination of its mathematical convergence is a major objective of this study. It is dealt with in the section on results.

Smaller subdivisions of the computation procedure are given by the "Steps" in the program summary at the end of the preceding subsection. Each of these unit sub-programs involves truncation errors of less novel types than that of the overall scheme for successive approximation to the solutions of the governing equations. Distinction between truncation errors peculiar to this experiment and those which are routinely found in all numerical solutions of differential equations is drawn for the special purpose of separation of discussion of design of the experiment from discussion of its results.

Both of these kinds of truncation error are inextricably entangled with the truncation error entailed in the use of one set of subdivisions. That is, the problem under consideration is governed by equations involving functions defined on a continuum, but is

solved for a single rather coarse network of discrete points. It is customary to regard the solutions obtained in this manner as being just what is wanted, namely a barring of unwanted small-scale effects. There is little difference between the latter point of view and assertion that we are capable of choosing a priori, from a hypothetical series, a mesh size for which the mathematical convergence of the corresponding series of solutions is satisfactory on some vague physical basis. The above justification for using a finite-difference solution based on the single subdivision of the domain leads to elusiveness in interpretation of truncation errors in finite-difference approximation of derivatives. More will be said on this subject later in this section.

Still another error of the truncation type is that associated with the relaxation solution of the difference equations (38). This error can be given a clear-cut upper bound which is a function of the number of grid points and the maximum absolute residue allowed. Use of this criterion will be made at an appropriate place in the presentation of more explicit statements about accuracy control which follows.

The first step in a systematic consideration of computational errors is with regard to the accuracy of $D^{(0)}$, including cartographic quantities. The latter enter in connection with relating the grid coordinates to the dependent variable Y of the model wind prescription, and into the formulae for gradients of vorticity in the grid coordinate system. The only limitations to the accuracy of $D^{(0)}$ are those of interpolation in table look-up and

number of figures recorded. Since the computation of $D^{(0)}$ at the reference level determines the accuracy of $D^{(0)}$ at all pressure surfaces, this computation was carried out with great care. The tables used for evaluation of the error function, cartographic quantities, and extraction of square roots [47] were chosen for reliability and convenience of arrangement. Whenever the tabulated intervals did not give sufficient accuracy, the necessary interpolation procedures were used. A commensurate amount of care was taken in carrying out the arithmetical operations, so that the maximum error in evaluation of $D^{(0)}$ at any pressure surface can be guaranteed less than 2×10^{-8} sec^{-1}, i.e., 2 in the third decimal place of $10^5 D^{(0)}$. Since any such estimate of accumulation of error is based on a succession of strong inequalities, it is very likely that $D^{(0)}$ values are good to within less than 1×10^{-8} sec^{-1}.

Beyond the $D^{(0)}$ stage of computations at any pressure surface, it becomes virtually impossible to keep track of the new errors and the propagation of computation error from preceding stages except by empirical means. The guiding principle was avoidance of contamination of the third decimal place of $10^5 D$ whenever possible, with the objective that the end result at any pressure surface be accurate to two decimal places times 10^{-5}. That is, the aim was that the final value of divergence would be within $\pm 5 \times 10^{-8}$ sec^{-1} of those implied by the prescribed model wind, the boundary conditions, and the finite-difference analogues of the governing equations. In order to maintain this control enough figures were carried in each $\Delta^{(H)}D$ or $\Delta^{(V)}D$ computation and upward step to

lower pressure to insure that accumulation of round-off error within each such program unit could not in the worst possible situation approach the magnitude of the error already tolerated in $D^{(0)}$. It is impracticable to carry enough figures to provide absolute control of accumulation of round-off error in the whole complex interlocking of computational steps. The answer to this problem was to carry enough figures in all arithmetical operations that there was small chance that rounding-off would contribute error comparable to that of truncation.

The truncation errors associated with finite-difference approximation of horizontal space derivatives are extremely difficult to assess. One set of these derivatives, $\partial D/\partial x$ and $\partial D/\partial y$, is involved in each $\Delta^{(H)}D$ program unit. Similar derivatives of ω enter in each $\Delta^{(V)}D$ step. The formulae used for these derivatives were the 5-point central difference approximation for interior grid points, and comparable non-centered formulae for points adjacent to the boundaries [48].

A considerable amount of effort was put into attempts to estimate the truncation error introduced in these steps. These efforts included inspection of the smoothness of the results, both graphically and by difference tables. The indications were confusing and indecisive. It was determined, however, that of the existing possibilities the approximation formulae noted above were the best choice for the chosen grid size.

It may be noted that the problem of truncation error in computation of finite-difference approximations to space derivatives of

functions known only on a domain of discrete points is bound to be indeterminate in some degree. The finite set of data alone is not a unique specification of a function over the domain continuum, and the very formulae used to get the derivatives imply a further specification of that function. In this sense, any approximation to the derivatives is exactly correct. However, there is usually a physical basis for the preference for patterns of derivatives which imply "smoothness" of the function on the scale of the finite-difference mesh. This is the basis for the use of smoothing functions in extended numerical schemes. Along the same lines, the criterion which was finally applied to control of the truncation errors in the space derivatives of D and ω was subjective judgement of the smoothness of the results. Much experience with the output as interpreted by scalar analysis and graphs was acculumated. It amounted to quite convincing circumstantial evidence that the truncation error in question was being adequately suppressed, in the above sense.

Empirical information on propagated error.-The most concrete statements that can be made about error propagation are based on the occurrence of an arithmetical or clerical mistake. A very substantial error, -0.1236×10^{-5} sec^{-1}, was made at an early stage in the 60 cb program. It occurred in the formation of the quantity $D^{(3)}$. At the $D^{(3)}$ stage the divergence due to advection of vorticity by the model wind has been refined by application of a first approximation to $\Delta^{(V)}D$ and a second approximation to $\Delta^{(H)}D$ (see section 6). The structure of computational procedure happens to be such that the error enters directly into $D^{(4)}$ with unchanged magnitude. It

also has an indirect effect, since the $\underline{W}$ used in equation (35) is obtained from $D^{(3)}$. This indirect propagation was found to give errors of less than nine in the third decimal place of $10^5\ D^{(4)}$ at points in the vicinity of 0803. The indirectly propagated error at point 0803 itself is essentially zero. Hence there is a remarkably strong damping-out of the error as it spreads. This is attributable to the dominance by $D^{(0)}$ of the pattern of derivatives of D.

The error was propagated into $D^{(5)}$ at 60 cb before detection by graphical analysis of results. It was allowed to go on into the 50 cb program by way of the use of $D^{(4)}_{60}$ to get a first approximation of ω at 50 cb, and thence into $D^{(4)}_{50}$. Although not intentional, the introduction of this error was thus made to lead to useful information on several aspects of the propagation of errors in the computation program.

The error under discussion is 60 per cent of the correct value of $D^{(3)}$. The value of $D^{(0)}$ at the same point was about twice the size of the error. As indicated above, the indirect effects of the error upon subsequent $\Delta^{(H)}D$ and $\Delta^{(V)}D$ computations are slight and damp out quickly. Further quantitative evidence of this is obtained by tracing the propagation of the error after the $D^{(4)}$ stage at 60 cb. In $D^{(5)}$ the error is 4×10^{-8} at point 0803, and 6×10^{-8} at 0804. All of the other points affected have errors of less than 1×10^{-8}. The error has been spread quite a bit by the relaxation performed in getting $D^{(4)}$. There are seven points with error of more than one-half in the third decimal place of $10^5\ D^{(5)}$, $\underline{\text{i.e.}}\ 5 \times 10^{-9}$ in $D^{(5)}$, at 60 cb.

It may be seen by inspection of equation (57) that the value of D at 60 cb is a secondary factor in the determination of ω at 60 cb. This helps to explain the small amplification factor in the vertical motion correction $\Delta^{(5)}D$. The effect of an error in $D^{(4)}_{60}$ has a more serious effect upon the first approximation of the 50 cb value of $\omega^{(1)}$ for the grid point. This value was computed using $D^{(4)}_{60}$ as the $D^{(F)}_{p_{i-1}}$ of (57). The resulting error was found to be -0.165×10^{-4} cb sec^{-1}, 20 per cent of the correct value of $\omega^{(1)}_{50}$ at 0803. This enters directly into the computation of $\Delta^{(2)}D$, the first V-type term for 50 cb. The values of $\omega^{(1)}$ at a number of points surrounding 0803 at 50 cb also were affected. These other errors in $\omega^{(1)}_{50}$ are of course much less than that of 0803, the next largest being 0.01×10^{-4} cb sec^{-1} at 0804. The net result of using these values for one V-type and two H-type refinements in the 50 cb routine gave twenty-nine points with values in error by more than one-half in the third decimal place of $10^5 D^{(4)}$. Seventeen points have an error of at least one in that position. The largest errors are +2, -3 and +1 in the second decimal place of $10^5 D^{(4)}$ at 0803, 0804 and 0903. It is noteworthy that half of the total error in $D^{(4)}$ at 0804 on 50 cb is due to error propagated into the vertical motion effect, and half to computation of the effect of vorticity advection by the divergent wind. The perpetuation of the error in the H-type computation at other points is not as marked, and on the whole the worst effect of starting at 50 cb with an incorrect value of ω is in its use in $\Delta^{(2)}D$. The further indirectly-propagated effects are very small.

Thus it is found that upward propagation of the principal discrepancy of 0.12×10^{-5} sec^{-1} at one 60 cb point leads to a maximum total effect of one-fourth as much in the values of $D^{(4)}$ on the following pressure surface. Since the initial error is at least twelve times as large as would be expected to accrue as a result of errors other than human mistakes, it appears quite reasonable that the two-decimal-place values of $10^5 D$ and one-decimal-place values of $10^4 \omega$ presented in the results section are quite dependable. It is true of course that the particular circumstances that form the basis for this induction may be abnormally favorable, but the margin of safety is so large as to make it highly improbable that really deleterious error propagation is the true situation.

One auxiliary observation may be made on the strength of the parallel computation of the stages $D^{(3)}$ through $D^{(5)}$ at 60 cb and $D^{(2)}$ through $D^{(4)}$ at 50 cb, with and without known error at the outset. This is in regard to the effect of errors in ξ and η upon u and v, through solution of (38a) or (38b). The mistake in question gave very much larger error in those quantities than are expected from truncation and propagation errors in approximation of space derivatives of D. Comparison of the resulting correct and incorrect values of u and v shows that the resulting discrepancies are less than 0.05 m sec^{-1}. The latter figure is significant because it is the chosen upper bound for errors in u and v allowable as a result of truncation of the relaxation process. This choice is made effective by prescription of 0.002 as the allowed maximum absolute value of residues at termination

of the relaxation iteration [49, p. 217]. The basis of this choice of 0.05 m sec^{-1} as the allowable truncation error in the components of $\underline{W}$ is that the resulting error in a $\Delta^{(H)}D$ program unit is within the desired limits on error contributed by one such stage.

Reliability of results.-It is believed that the computed results presented in the next section are reliable to the number of figures in which a meteorologist is interested, as far as sources of error other than truncation in the overall scheme are concerned. As previously noted, truncation error of the whole scheme is a proper subject for the results section itself.

It is pertinent to note that percentage errors in the 90 and 80 cb correction terms are probably larger than in the later pressure steps of 70, 60 and 50 cb. There are two reasons why this is so. The earlier pressure steps were more experimental in nature, in regard to the order of iteration steps and choices of finite-difference formulae. Also, the calculations were one on desk computers. For both reasons, the maximum residue used in the hand-relaxation steps were ten times as great as that used when doing relaxations on the stored-program electronic machine. Another point that should be mentioned is that space derivatives of ω at 90 cb were computed by three-point formulae.

In spite of the above-mentioned experimentation in the first steps, it was found that the information transmitted upward to 70 cb was accurate enough. This finding is partly based upon consideration of the results, and partly upon a viewpoint. It was especially true at 90 and 80 cb that

advection of vorticity by the model wind controlled the value of divergence required for maintance of the vorticity field in its steady state. Scalar analyses of the results at frequent points in the computation program were made for any distribution which was suspected of error for any of the reasons noted. These gave no sign of errors at a level detectable by analysis at intervals on the order of 1/10 of the range. Further, we have seen the damping of error which takes place in an upward integration. Because of the small values of $\Delta^{(H)}D$ at 90 and 80 cb, the 70 cb ω's and their implications are certainly accurate at the level of two decimal places in $10^5 D$ for 90 and 80 cb. This is the finding based on consideration of the numbers.

It is likely that such accuracy is enough, judging from the parallel sets of 60 and 50 cb results. However, without a knowledge of the exact size and distribution of the combined errors at 90 and 80 cb, nor a theoretical and/or empirical error-tracing, one might have some qualms about the possible amplification of an unknown error distribution introduced at such an early stage. The information used at 70 cb and above might not be a sufficiently exact consequence of the model and boundary conditions in the layer below from the point of view of rigorous numerical analysis. Although this was recognized, the reason for going ahead anyway was the point of view that the ω distribution at 70 cb need be acceptable only as a lower boundary prescription. As such, it serves just as well for investigation of this application of numerical methods to deduction of structure of the model system at higher

levels. In this point of view, any discrepancies which are ascribable to failings of the information transmitted from below 70 cb are to be regarded as modeling failures, rather than as propagated error.

7. RESULTS

Observed convergence of successive approximations.-The data in tables 2 and 3 are examples of indications furnished by this experiment in regard to mathematical convergence of the procedure of iteration used at 70, 60 and 50 cb. The emphasis in data presentation for this purpose is on 60 cb because repetition of the iterative process was most complete at that pressure. The completion of the 60 cb computations through $D^{(7)}$ was made for two purposes. The first was verification of indications that iteration at 70 cb had progressed far enough when terminated with $D^{(5)}$. The second use of the 60 cb data was as the basis for terminating the 50 cb iteration process with $D^{(5)}$. Comparison of the parallel 60 cb process to that stage indicated that satisfactory approach to a limiting value had occurred at 50 cb. Examples of the latter comparison are provided by showing in table 3 a selection of the 50 cb divergence increments for significant points, most of which are among those used in the 60 cb selection of table 2.

The data in tables 2 and 3 represent a small part of compilations made for each of the five pressure steps computed. The working form of these parent compilations is more extensive than the data shown here, both in greater coverage of the grid and more detailed analysis of the component increments of the iterative process. The implications of all this data from the point of view of a mathematically rigorous knowledge of the behavior of the procedure have not

TABLE 2.-Successive approximate increments of divergence on 60 centibar pressure surface, in units of 10^{-5} per second

Grid Point	$D^{(0)}$	$\Delta^{(1)}D$	$\Delta^{(2)}D$	$\Delta^{(3)}D$	$\Delta^{(4)}D$	$D^{(4)}-D^{(0)}$	$\Delta^{(5)}D$	$\Delta^{(6)}D$	$\Delta^{(7)}D$	$D^{(7)}-D^{(4)}$
0604	-0.26	-0.18	+0.18	-0.18	-0.18	0.00	+0.17	-0.18	-0.18	-0.01
0605	-0.85	-0.26	+0.16	-0.25	-0.25	-0.09	+0.17	-0.25	-0.25	+0.01
0606	-0.80	-0.03	-0.07	-0.01	-0.01	-0.08	-0.07	-0.01	-0.01	0.00
0609	+0.80	+0.03	+0.16	-0.01	-0.02	+0.13	+0.16	-0.02	-0.02	0.00
0610	+0.85	+0.26	-0.08	+0.28	+0.26	+0.19	-0.09	+0.26	+0.26	-0.01
0611	+0.26	+0.18	-0.21	+0.20	+0.20	-0.01	-0.20	+0.19	+0.19	0.00
0704	-0.25	-0.24	+0.21	-0.24	-0.24	-0.03	+0.19	-0.24	-0.24	-0.01
0705	-0.62	-0.23	+0.12	-0.21	-0.20	-0.08	+0.13	-0.20	-0.21	+0.01
0707	-0.21	+0.04	-0.17	+0.06	+0.05	-0.12	-0.18	+0.05	+0.05	-0.01
0708	+0.21	-0.04	-0.08	-0.07	-0.07	-0.14	-0.08	-0.07	-0.07	0.00
0710	+0.62	+0.23	+0.03	+0.22	+0.20	+0.23	+0.02	+0.20	+0.20	-0.01
0711	+0.25	+0.24	-0.22	+0.27	+0.26	+0.05	-0.21	+0.26	+0.26	0.00
0804	+0.02	-0.22	+0.14	-0.21	-0.21	-0.06	+0.12	-0.21	-0.21	-0.02
0805	-0.24	-0.28	+0.18	-0.24	-0.24	-0.06	+0.19	-0.24	-0.24	+0.01
0807	-0.10	-0.02	-0.14	0.00	-0.01	-0.15	-0.14	-0.01	-0.01	0.00
0808	+0.10	+0.02	-0.10	-0.03	-0.02	-0.12	-0.10	-0.02	-0.02	0.00
0810	+0.24	+0.28	-0.01	+0.26	+0.24	+0.22	-0.02	+0.23	+0.24	-0.01
0811	-0.02	+0.22	-0.14	+0.25	+0.24	+0.10	-0.13	+0.24	+0.24	0.00
0904	+0.27	-0.14	+0.02	-0.13	-0.12	-0.10	0.00	-0.12	-0.12	-0.02
0905	+0.10	-0.29	+0.20	-0.25	-0.24	-0.04	+0.19	-0.24	-0.24	-0.01
0906	0.00	-0.22	+0.14	-0.18	-0.19	-0.04	+0.16	-0.19	-0.19	+0.01
0909	0.00	+0.22	+0.03	+0.16	+0.14	+0.17	+0.03	+0.14	+0.14	0.00
0910	-0.10	+0.29	-0.07	+0.29	+0.27	+0.20	-0.07	+0.27	+0.27	0.00
1005	+0.31	-0.16	+0.05	-0.13	-0.12	-0.07	+0.02	-0.12	-0.12	-0.03

been considered. The approach to questions of convergence of this involved approximation scheme has been largely empirical. The indications of convergence in the computed results are taken at face value. The presence or absence of ultimate convergence is not a vital question at this stage of experimentation.

TABLE 3.-Successive approximate increments of divergence on 50 centibar pressure surface, in units of 10^{-5} per second

Grid Point	$D^{(0)}$	$\Delta^{(1)}D$	$\Delta^{(2)}D$	$\Delta^{(3)}D$	$\Delta^{(4)}D$	$D^{(4)}-D^{(0)}$	$\Delta^{(5)}D$
0505	-1.11	-0.45	+0.37	-0.46	-0.46	-0.06	+0.37
0510	+1.11	+0.45	-0.38	+0.48	+0.48	+0.13	-0.38
0604	-0.65	-0.40	+0.51	-0.41	-0.41	+0.13	+0.48
0605	-1.53	-0.44	+0.27	-0.45	-0.44	-0.12	+0.30
0608	+0.48	-0.10	+0.13	-0.16	-0.16	+0.02	+0.13
0609	+1.30	-0.03	+0.32	-0.10	-0.12	+0.26	+0.32
0610	+1.53	+0.44	-0.18	+0.49	+0.47	+0.34	-0.22
0611	+0.65	+0.40	-0.56	+0.43	+0.43	-0.10	-0.53
0704	-0.65	-0.49	+0.49	-0.49	-0.48	+0.05	+0.47
0707	-0.32	+0.10	-0.23	+0.14	+0.13	-0.09	-0.24
0708	+0.32	-0.10	-0.05	-0.15	-0.14	-0.16	-0.05
0710	+1.14	+0.31	+0.04	+0.31	+0.28	+0.38	+0.01
0711	+0.65	+0.49	-0.52	+0.54	+0.53	+0.05	-0.51
0804	-0.21	-0.43	+0.33	-0.42	-0.40	-0.01	+0.30
0806	-0.46	-0.09	-0.04	0.00	-0.02	+0.30	-0.03
0807	-0.17	+0.01	-0.18	+0.05	+0.03	+0.27	+0.18
0808	+0.17	-0.01	-0.08	-0.08	-0.07	+0.15	-0.10
0811	+0.21	+0.43	-0.37	+0.47	+0.46	+0.13	-0.35
0904	+0.23	-0.28	+0.09	-0.26	-0.24	-0.10	+0.05
0909	+0.11	+0.29	+0.04	+0.19	+0.17	+0.28	+0.03
0910	+0.03	+0.46	-0.19	+0.46	+0.43	+0.30	-0.19
1005	+0.33	-0.30	+0.09	-0.24	-0.21	-0.05	+0.04

The increments ΔD of the stages of approximation at 60 cb are given in table 2 for grid points which have been carefully selected to include the largest increment of each kind to be found anywhere on the grid. Additional points are included to balance the selection of grid points between the left and right hand sides of the center line.

The principal purpose of the table is to show the successive increments in evaluation of divergence. To aid in interpretation of the values the scheme of approximations will be restated. $D^{(0)}$ is the divergence required to balance vorticity advection by the model wind. Increments with superscripts 1, 3, 4, 6 and 7 are successive evaluations of the divergence arising from considering divergent wind advection, and $\Delta^{(2)}$ and $\Delta^{(5)}$ are successive evaluations of the divergence which has to be added in for balance when vertical-motion effects are taken into consideration. The difference $D^{(4)} - D^{(0)}$ shows the total effect upon computed divergence of a cycle consisting of:

(a) determination of the divergent wind corresponding to the divergence $D^{(0)}$,

(b) computation of the effect of the divergent wind of step (a), which requires additional divergence $\Delta^{(1)}D$ to cancel its advection of absolute vorticity,

(c) evaluation of the vertical-motion effect $\Delta^{(2)}D$ corresponding to the values of ω at this pressure surface (obtained from the total divergence found in (a) and (b) and divergence values at lower levels), and

(d) replacement of divergent-wind evaluation (b) by $\Delta^{(3)}D$ and $\Delta^{(4)}D$ in turn. The latter are successively improved evaluations of divergent-wind advection. The divergence $D^{(0)} + \Delta^{(2)} + \Delta^{(3)}$ gives $D^{(3)}$, and $D^{(0)} + \Delta^{(2)} + \Delta^{(4)}$ gives $D^{(4)}$.

The difference $D^{(7)} - D^{(4)}$ shows the effect of a second cycle analogous to parts (c) and (d) above. It is to be observed that the tabulated values do not always agree when combined in the various ways in which it is possible to arrive at the same quantity. For example, $D^{(4)} - D^{(0)}$ and $\Delta^{(2)}D + \Delta^{(4)}D$ are the same thing, but at 0609 they differ by one in the second decimal place. This is due to round-off error, which is of course suppressed in the working calculations.

These data are representative of the extreme occurrences of changing evaluations of vertical-motion and divergent-wind effects at 60 cb. They suggest that applications of computations steps (a) to (d) give divergence easily correct to 1×10^{-6}, as far as the successive approximations procedure at a single pressure surface in this model is concerned.

The contribution of the second vertical-motion correction $\Delta^{(5)}D$ at 60 cb differs by less than 3×10^{-7} sec^{-1} from the first evaluation $\Delta^{(2)}D$. From the point of view of short range synoptic considerations, such differences are negligible [34]. The interest here, however, is in the comparison of the several contributions to divergence implied by the model. From the latter point of view the size of $\Delta^{(5)}$ is more significant. At several points on the 60 cb surface the amount

of change from $\Delta^{(2)}$ to $\Delta^{(5)}$ is an appreciable percentage of the total change from $D^{(0)}$ to the final approximation. This is illustrated by the data given below to three decimal places of divergence in units of 10^{-5} sec^{-1}. The two points selected from the set in table 2 for significance in this respect are used for this illustration.

At point 1005, the first approximate divergence $D^{(0)}$ is 0.311. The final approximation $D^{(7)}$ includes a contribution of -0.099 due to divergent-wind advection and vertical-motion effect. Of this increment, 27 per cent is introduced in the second calculation, $\Delta^{(5)}D$, of vertical-motion effects.

At point 0904, $D^{(0)}$ is 0.270. The vertical-motion effect is 0.017 at first evaluation and -0.004 at second evaluation. The net effect of the sequence $\Delta^{(5)}D$, $\Delta^{(6)}D$, $\Delta^{(7)}D$ is to change the approximate divergence by -0.022 out of a net change of -0.126. The extra cycle contributes 17 per cent to the net change, $D^{(7)} - D^{(0)}$. It appears that a second computation of V-type terms at 60 cb is required if truncation error is to be kept out of the second decimal place.

The same two points illustrate another pertinent fact about the behavior of the approximation procedure, namely that the successive values of the divergent-wind advection effect seem to reach stable values rapidly. At 1005 the contribution of the re-evaluation of the divergent wind effect based on $D^{(5)}$ instead of $D^{(2)}$ is 0.002, 2 per cent of the net change from $D^{(0)}$ to $D^{(7)}$. At

0904 the change of value is -0.002 out of the total change of -0.126. The two-place values of the table further show this insensitivity of H-type increments to the third cycle of iteration.

As far as they go, the data obtained by going to the seventh approximation of divergence at 60 cb give favorable indications for the mathematical convergence of the process. The successive evaluations of increments of the same kind, viz. those superscripted 1, 3, 4, 6 and 7 (divergent-wind advection effects) and those superscripted 2 and 5 (vertical-motion effects), show a rapid approach to a value stable in the second decimal place of 10^5 D . Naturally this does not constitute assurance that repeated iteration would not eventually lead to divergence of the series or to some unsatisfactory type of convergence. A rigorous consideration of the conditions under which the process must converge has not been attempted.

The numerical characteristics of the 60 cb results contain information with regard to errors incurred by truncation of iteration at other pressure surfaces. The decision to terminate iteration at 70 cb was made on the basis of a partial computation of $\Delta^{(5)}D$ for certain 70 cb points, selected by inspection of the data for $D^{(4)}$ and experience at lower levels. The difference between $\Delta^{(5)}D$ and and $\Delta^{(2)}D$ did not exceed 0.007×10^{-5} sec^{-1}. It was judged that the difference $D^{(7)} - D^{(4)}$ would amount to less than one in the second decimal place at 70 cb. That the first neglected set of contributions is most of the truncation error is indicated by the trend of the increments of cycles II and III at 60 cb. This

conclusion is made safer at 70 cb by consideration of the smaller magnitude of all refinement terms there.

The selection of points given in table 3 is smaller than in table 2, but it is large enough to show the nature of the progression of approximate increments at 50 cb. It is noted that step for step the divergence increments are generally larger by a factor of about two at the 50 cb surface than at 60 cb. The first vertical-motion increment of divergence affects the evaluation of divergent-wind advection quite noticeably in the second decimal place. The iteration process was stopped after the use of the second vertical-motion approximation, $\Delta^{(5)}D$, at 50 cb. The difference between $\Delta^{(2)}D$ and $\Delta^{(5)}D$ has a maximum nagnitude of 0.056×10^{-5}, found at point 1005. (The two decimal place values of table 5 give 0.05×10^{-5}). A rough estimation of the truncation error, based on indications that the behavior of the approximations is similar at analogous stages on two pressure surfaces, is that the 50 cb values of divergence $D^{(5)}$ are the same as $D^{(7)}$ to within two in the second decimal place.

The foregoing data on convergence behavior for successive pressure steps indicate that slowing of the rate of convergence will require that more iterations be made whenever an initial $D^{(0)}$ pattern has the intensity of the present 50 cb model. For the present model, iteration through $D^{(5)}$ is barely enough at 50 cb to hold the truncation error below the level of 1×10^{-7} sec^{-1}. Whether or not such a standard of accuracy is necessary depends upon the place of this type of truncation error in the error propagation picture

for the total integration procedure. As indicated in the earlier subsection on accuracy of the approximative procedures, there is reason to think that upward propagation of errors upsets the computation of divergence at the next pressure step by an amount smaller than the initial error by nearly an order of magnitude. However, computation of the worst possible situation indicates that such an error could be propagated without diminution.

Scheme of presentation of computed structural elements.-Further presentation of quantities computed by the successive approximation procedure is made in figures 17-41 and tables 4-7.

The figures 17 through 34 show plan views of the computed values of divergence and vertical motion at the five pressure surfaces 90, 80, 70, 60 and 50 cb. These figures are arranged in sets by pressure value. The first figure in each set is an analysis of $D^{(0)}$. This is the divergence required to balance the local rate of change of vorticity implied by advection of the prescribed absolute vorticity by the model wind field. As will be seen, the character of its distribution is important in determining the nature of the computed solution. This of course is a trivial observation in the sense that $D^{(0)}$ is the approximation from which the subsequent approximations are developed, but there is a less predictable aspect to be observed. For this reason, and because most applications of the vorticity method consider the $D^{(0)}$ term alone, it is of interest to examine the individual contributions to it in terms of the zonal-wind and vortex-wind relative vorticities and the planetary vorticity. This is done

by presentation of the component parts of $D^{(0)}$ in table 4, which is discussed in connection with the maps of $D^{(0)}$.

The other maps in the five sets constituting fig. 17-34 show the following for each of the five pressure steps: the net changes in divergence computed from $D^{(0)}$, the resulting approximate divergence $D^{(4)}$, and the associated distributions of the substantial derivative of pressure.

The distribution of final divergence approximation and vertical motion are shown in vertical cross-section by figures 35-38. In regard to stage of termination of the approximation procedure, it should be noted that the data used in the vertical cross-sections are not always the same as in the plan-view figures. In the vertical cross-sections the divergence approximation plotted is $D^{(5)}$ for 50 cb and for 70 cb when available, and $D^{(7)}$ for 60 cb. The values of ω used are $\omega^{(2)}$ throughout for 60 and 50 cb, and wherever the computation was advanced to that stage in the course of experimentation on 70 cb. The differences between these values and uniform use of $D^{(4)}$ and $\omega^{(1)}$ are negligible in view of the resolving power of the intervals used in scalar analysis of the distributions.

Following the discussion of plan views and vertical cross-sections of distributions of divergence and vertical motion, there is given a tabular summary of these and other quantities for points chosen as representative of the principal features of the solution. The main summary is table 5. The data for each grid point are given in a separate subdivision of the table, to facilitate

comparison among the successive pressure surfaces. The space distribution of grid points used is shown by the smaller bordered region in fig. 16.

In addition to repetition of the quantities shown by scalar analysis in the figures, table 5 shows the separate contributions to the final value of divergence by the vertical-motion term and divergent-wind advection term.

Table 6 is an auxiliary analysis of the vertical-motion contribution to the divergence required by the model and the assumptions. It is designed to show the relative importance of the two ways in which the vertical motion enters into this use of the vorticity equation, viz. the vertical-advection effect and the tipping effect.

The divergent part of the total wind system which will maintain the assumed vorticity distribution in the steady state is a product of the computational procedure. The results obtained for it are shown by means of table 7 and figures 39-41. The table shows the grid components of the initial nondivergent wind, the derived divergent wind, and the total wind field. The values presented are chosen for representativeness of the regions of maximum magnitude of divergent wind. The selection of points is indicated by circling in fig. 16. Table 7 is organized in three parts, one for each of the pressure surfaces; 90, 70 and 50 cb.

Figures 39-41 give scalar analyses of the components of divergent wind on the same three pressure surfaces.

Figure 16. Key to selection of grid points in tables 5 and 7. Selection explained in text.

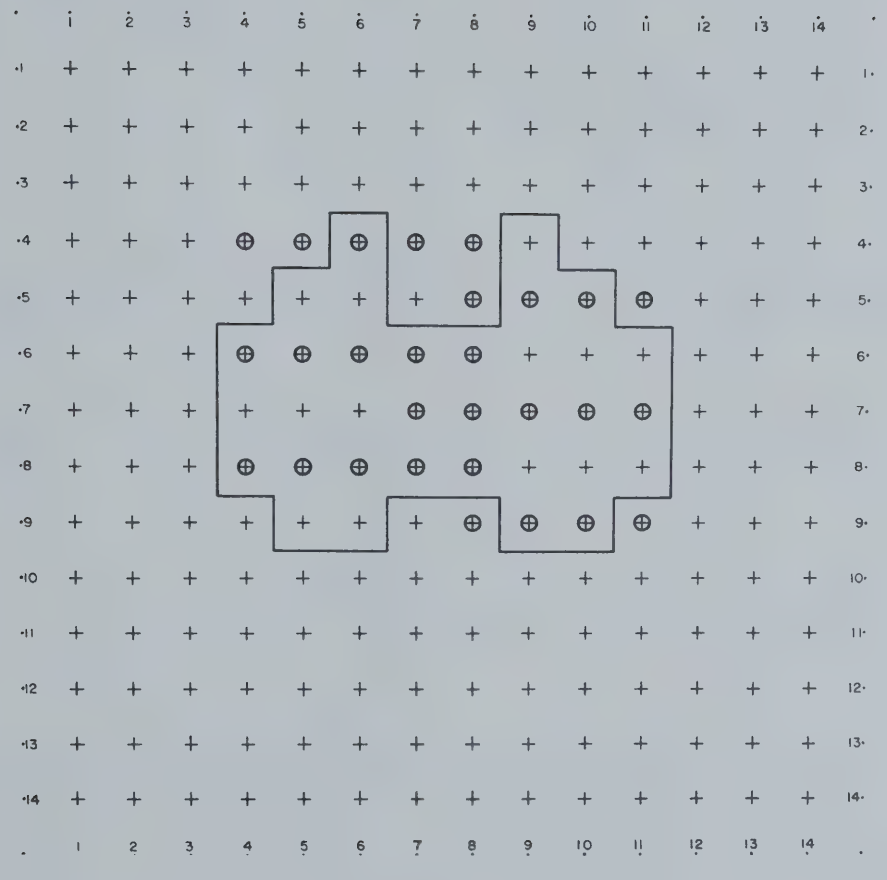

Fig. 16

Divergence and vertical motion on isobaric surfaces.-The starting point in the computation of divergence required to maintain $\partial\zeta/\partial t = 0$ is the quantity $D^{(0)} = -\zeta_a^{-1}\,\underline{V}\cdot\nabla\zeta_a$, i.e., the effect of the advection of absolute vorticity by the nondivergent model wind field. The distributions of this quantity for $p = 90$, 80, 70, 60 and 50 cb are shown in fig. 17, 20, 23, 27 and 31. Each distribution of $D^{(0)}$ is anti-symmetrical about the north-south grid line through the vortex center. The main features are a center of divergence in the northeast quadrant and a crescent-shaped convergence region outside of it, with corresponding convergence and divergence across the y axis in the northwest quadrant. As a result of the change with height of the relative contributions of the zonal and vortex wind and vorticity fields, it is observed that the shapes and relative intensities of these features of the $D^{(0)}$ field change with height. In order to show how the fields of vorticity advection are put together, a tabulation of the individual contributions to the net advection of absolute vorticity will be discussed.

The parallelism of the streamlines of the vortex and zonal wind fields to their respective vorticity isopleths is a conspicuous characteristic of the wind model. Because of it, the only terms in advection of the relative vorticity are $\underline{c}\cdot\nabla\zeta_U$, advection of the zonal wind vorticity by the vortex wind, and $\underline{U}\cdot\nabla\zeta_c$, which is advection of vorticity of the vortex by the zonal wind field. Since lines of constant f are parallels of latitude, $\underline{U}$ has no component perpendicular to them, and the term $\underline{c}\cdot\nabla f$ completes the catalog of terms in $D^{(0)}$. In table 4 these contributions are shown for

the reference pressure surface. The grid points are selected to show the anatomy of $D^{(0)}$, in these terms, at the significant points. Rows 4 through 9 and columns 8 through 11 of the grid take in the points of importance on all of the pressure surfaces. The plus or minus sign tabulated under each of the three advection terms refers to the sign of the contribution to $D^{(0)}$. The percentage indicates the magnitude of each advective contribution, relative to their algebraic sum, $D^{(0)}$.

The occurrence of a divergence center at point 0610 (and therefore a convergence center at 0605) is shown by table 4 to be due to predominance of $\underline{U} \cdot \nabla \zeta_c$. Advection of the cyclonic vorticity of the vortex by the zonal wind is such that for $\partial\zeta/\partial t = 0$ there is a positive divergence contribution at all points east of the axis at which the gradient of vortex vorticity is directed toward the vortex center. As shown by fig. 5 the relative vorticity gradient $\nabla\zeta_c$ is directed radially outward in a small region lying entirely within the grid square containing the vortex center. Its direction is inward along any radial line between the ζ_c maximum at 150 km from the center and the minimum at about 1250 km. Thus, as is evident in table 4, the part of $D^{(0)}$ arising from the advection of vortex vorticity by the zonal wind is the main reason for a divergence center in the northeast quadrant. By symmetry there is corresponding convergence in the northwest quadrant. Over most of these regions where zonal-wind advection of the vortex vorticity is the main effect, the advection of the zonal-wind vorticity by the vortex wind

TABLE 4.—Vorticity advection contributions of zonal and vortex winds

Grid Point	$D^{(0)}$	$\underline{c} \cdot \nabla \zeta_U$		$\underline{U} \cdot \nabla \zeta_c$		$\underline{c} \cdot \nabla f$	
	10^{-5} sec^{-1}	sign	per cent	sign	per cent	sign	per cent
0308	-0.08	-	48	-	8	-	44
0309	-0.30	-	30	-	42	-	28
0310	-0.55	-	17	-	67	-	16
0311	-0.66	-	10	-	80	-	10
0312	-0.53	-	6	-	87	-	7
0408	+0.17	-	22	+	165	-	43
0409	+0.26	-	37	+	212	-	75
0410	-0.14	-	76	+	143	-	167
0411	-0.62	-	11	-	60	-	29
0412	-0.69	-	4	-	82	-	14
0508	+0.39	-	0	+	126	-	26
0509	+0.91	+	0	+	132	-	32
0510	+0.72	+	3	+	155	-	58
0511	-0.12	+	29	+	190	-	319
0512	-0.60	+	5	-	71	-	34
0608	+0.36	+	9	+	118	-	27
0609	+0.95	+	11	+	121	-	32
0610	+1.05	+	17	+	131	-	48
0611	+0.37	+	57	+	192	-	149
0612	-0.37	+	38	-	45	-	93
0708	+0.24	+	19	+	121	-	40
0709	+0.66	+	22	+	125	-	47
0710	+0.78	+	33	+	136	-	69
0711	+0.36	+	88	+	192	-	180
0712	-0.24	+	90	-	6	-	184
0808	+0.12	+	38	+	143	-	81
0809	+0.32	+	46	+	153	-	99
0810	+0.33	+	76	+	189	-	165
0811	+0.05	+	662	+	903	-	1465
0812	-0.27	+	76	-	3	-	173
0908	+0.02	+	163	+	375	-	438
0909	+0.04	+	340	+	685	-	925
0910	-0.06	+	327	+	481	-	908
0911	-0.26	+	86	+	61	-	247
0912	-0.31	+	44	-	12	-	132

has the same sign as the zonal-wind contribution to relative vorticity advection.

The principal effect which counterbalances divergence in the eastern half and convergence in the western half of the system is the effect of a wind component across parallels of latitude, $\underline{c} \cdot \nabla f$. This is the "$\beta v$" term. In this model its relative importance is larger than on most weather maps. However, the relative vorticity advection still dominates the picture. The βv effect, convergence with south winds and divergence with north winds, is overbalanced by the advection of relative vorticity term for a distance of at least 600 km from the center of the vortex on the reference level. The βv term is the source of the peanut-shaped convergence region on the east side of the system and corresponding divergence across the axis, on the $D^{(0)}$ charts.

It is pertinent to note that the vorticity equation governing a model of a purely circular vortex moving as a permanent-type system would have the terms $-\underline{U} \cdot \nabla \zeta_c$ and $\underline{c} \cdot \nabla f$ in the coordinate system in which the system is in the steady state. The vector $\underline{U}$ would be the velocity of propagation in a frame of reference fixed relative to the earth, generally an eastwardly directed vector. Hence there would be convergence wherever the present configuration of the vortex vorticity field calls for divergence, and vice versa, with no change in the effect of the βv term. Such a model has no provision for examination of the effects of latitudinal variation of the basic westerly current and gives little incentive for quantitative work.

We take note of it here for background to a suggestion for improvement of the model, to be made after all results have been explained.

Variations with height of the relative strength of the zonal and vortex parts of the model wind fields result in changing patterns of $D^{(0)}$ to the extent shown in figs. 17, 20, 23, 27 and 31. The divergence center in the northeast quadrant shifts about 300 km toward the east-northeast between 90 cb (fig. 17) and 50 cb (fig. 31), and increases from 5×10^{-7} per second to 1.5×10^{-5} per second. The lobe of convergence farther out from the center has magnitude of just over 2×10^{-6} per second in a center in the northeast quadrant at 90 cb. Going to lower pressure values the maximum effect is observed to shift to the northeast and increase to almost 1×10^{-5} by 50 cb in accordance with a shifting balance among the three parts of the advection of absolute vorticity.

The analyses of the $D^{(0)}$ charts at 90, 80, 70, 60 and 50 cb show the effect of the reversal of the vortex vorticity gradient near the center of the system. Except at 90 cb, this characteristic causes a nearly circular zero isopleth of small radius to be present in the continuously defined $D^{(0)}$ field. This feature lies within the grid point square containing the center. It therefore cannot be accurately reflected in the subsequent computations. The analyses of the subsequently computed fields are made as though there were no such small-scale effect.

Figure 18 shows the final approximate divergence at 90 cb. It gives the net effect of the application of the exact vertical-motion correction for that boundary surface, plus two evaluations of the

Figure 17. Divergence approximation $D_{90}^{(0)}$, units 10^{-5} sec^{-1}.

Figure 18. Divergence approximation $D_{90}^{(4)}$, units 10^{-5} sec^{-1}.

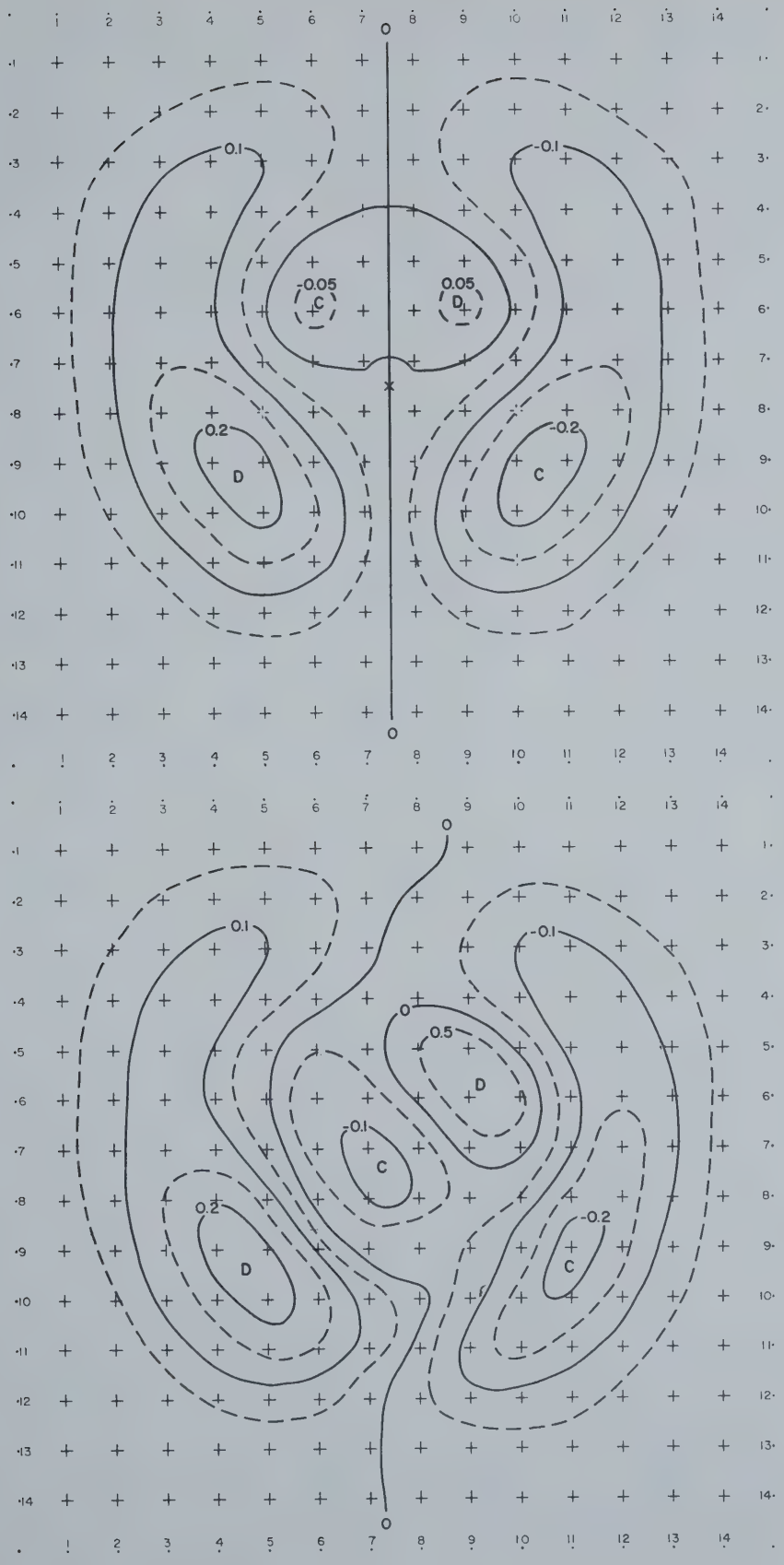

Fig. 17

Fig. 18

Figure 19. Highest approximation to ω at 90 centibars, units 10^{-4} cb sec^{-1}.

Figure 20. Divergence approximation $D_{80}^{(0)}$, units 10^{-5} sec^{-1}.

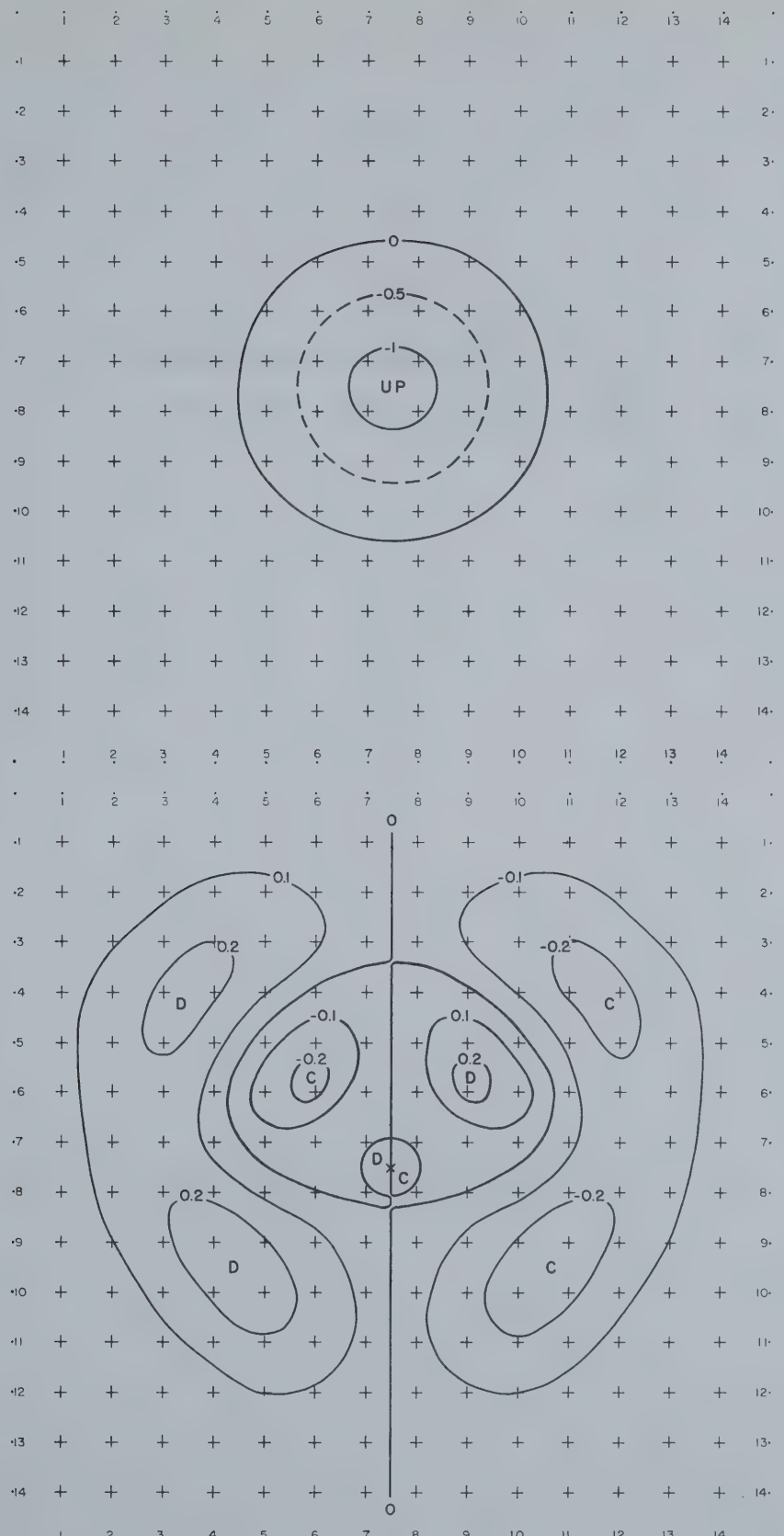

Fig. 19

Fig. 20

Figure 21. Net change of divergence approximations on 80 centibar surface $\left(D_{80}^{(4)} - D_{80}^{(0)}\right)$, units 10^{-5} sec^{-1}.

Figure 22. Divergence approximation $D_{80}^{(4)}$, units 10^{-5} sec^{-1}.

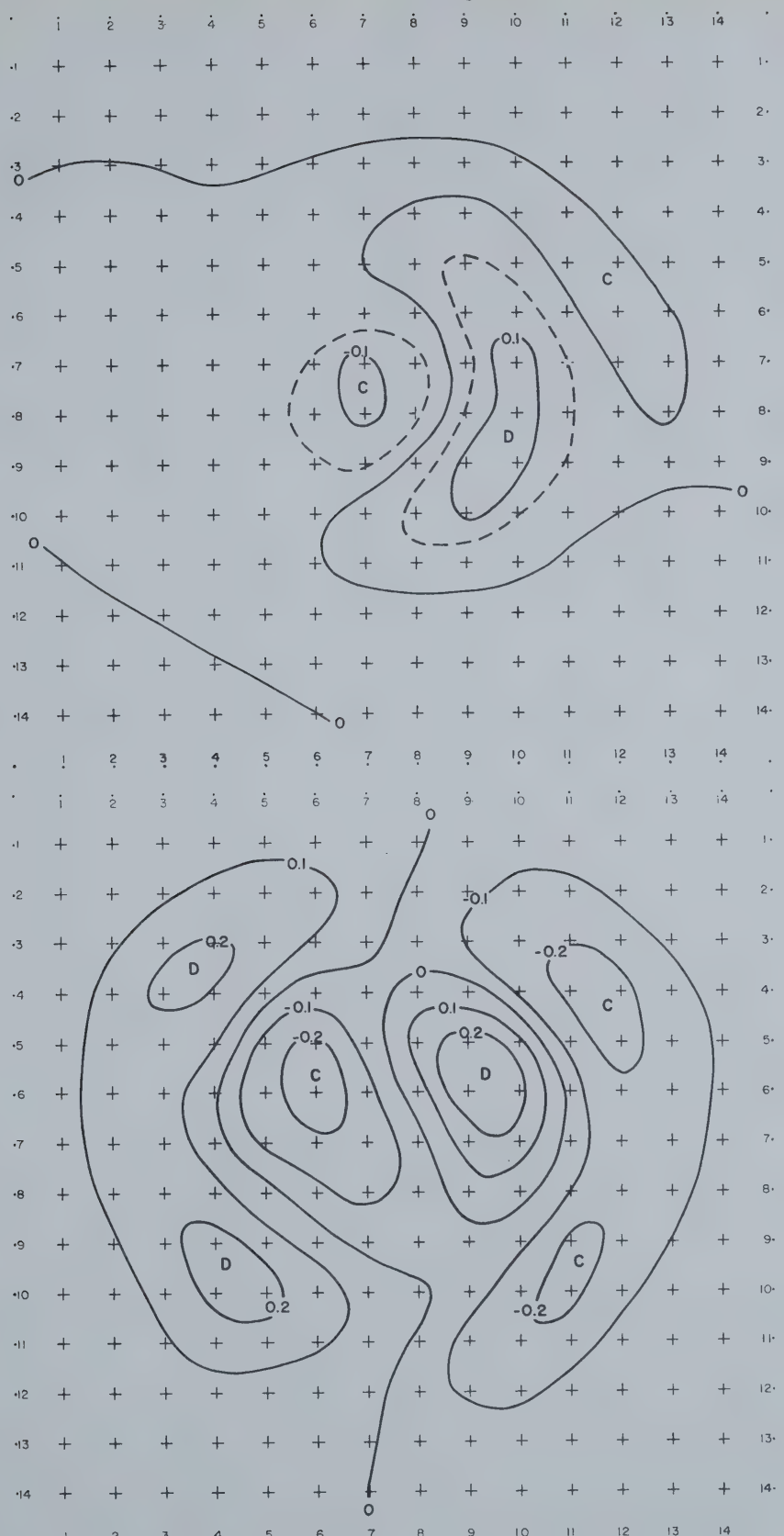

Fig. 21

Fig. 22

90 cb, which was not shown. The ω pattern on the 80 cb surface is also not reproduced. It is much like the 90 cb pattern except where values were so small that even small divergence values such as exist at 90 and 80 cb could shift a zero line great distances. This pattern can be visualized quite well as an intermediate stage between ω_{90} in fig. 19 and ω_{70} in fig. 26.

The sequence of divergence approximations and the vertical motion for 70 cb are pictured in charts of $D^{(0)}$, $D^{(4)} - D^{(0)}$, $D^{(4)}$ and ω in figs. 23-26. This stage in the steps of decreasing pressure is the first at which the relaxation solutions for divergent wind were obtained by high-speed computation. Also, the order of evaluation of the two types of divergence effects is different than at the preceding levels, as explained in section 6. The order of iteration used at 70 cb, having been found preferable to the other possibility, is kept the same for the subsequent pressure steps. For these reasons it is well to keep in mind that in this model, any pressure surface can be looked upon as the lower boundary surface. Of course, in order for the results to have significance as necessary characteristics of the real atmosphere, one must know the action of the layers below the boundary insofar as it affects boundary values of vertical motion. It is useful for some purposes of interpretation of this experiment to look upon the 70 cb surface as the lower boundary. This can be done by re-interpretation of the vertical-motion contributions from the layers below 70 cb.

The distribution of $D^{(0)}$ on the 70 cb surface (fig. 23) continues the trend noted from 90 to 80 cb. The amplitude of the

Figure 23. Divergence approximation $D^{(0)}_{70}$, units 10^{-5} sec^{-1}.

Figure 24. Net change of divergence approximations on 70 centibar surface $\left(D^{(4)}_{70} - D^{(0)}_{70} \right)$, units 10^{-5} sec^{-1}

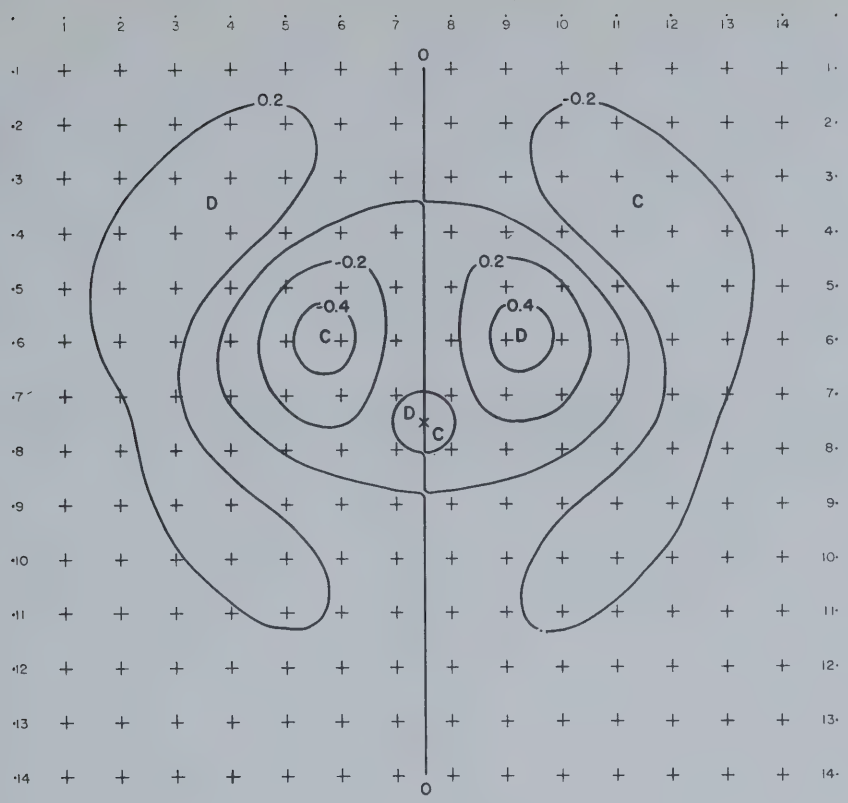

Fig. 23

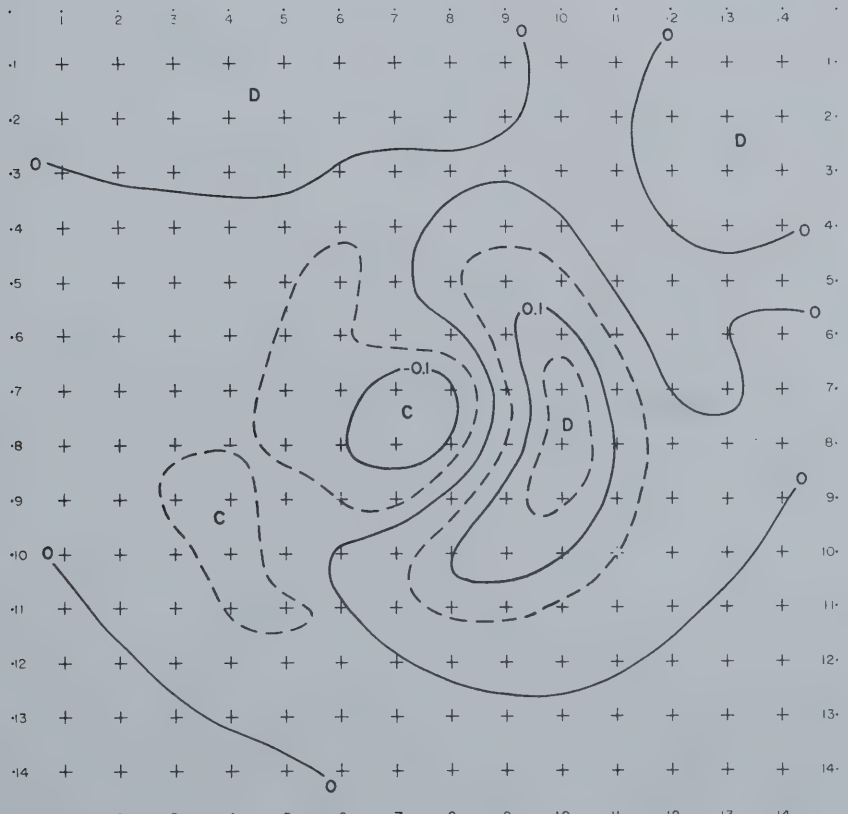

Fig. 24

Figure 25. Divergence approximation $D^{(4)}_{70}$, units 10^{-5} sec^{-1}.

Figure 26. Highest approximation to ω at 70 centibars, units 10^{-4} cb sec^{-1}.

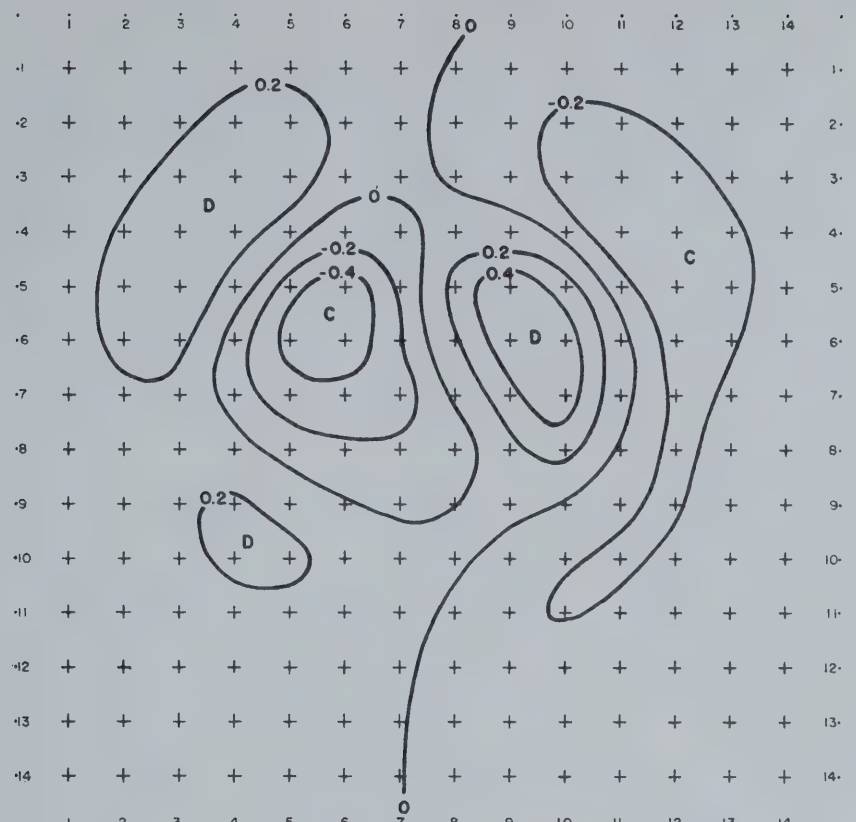

Fig. 25

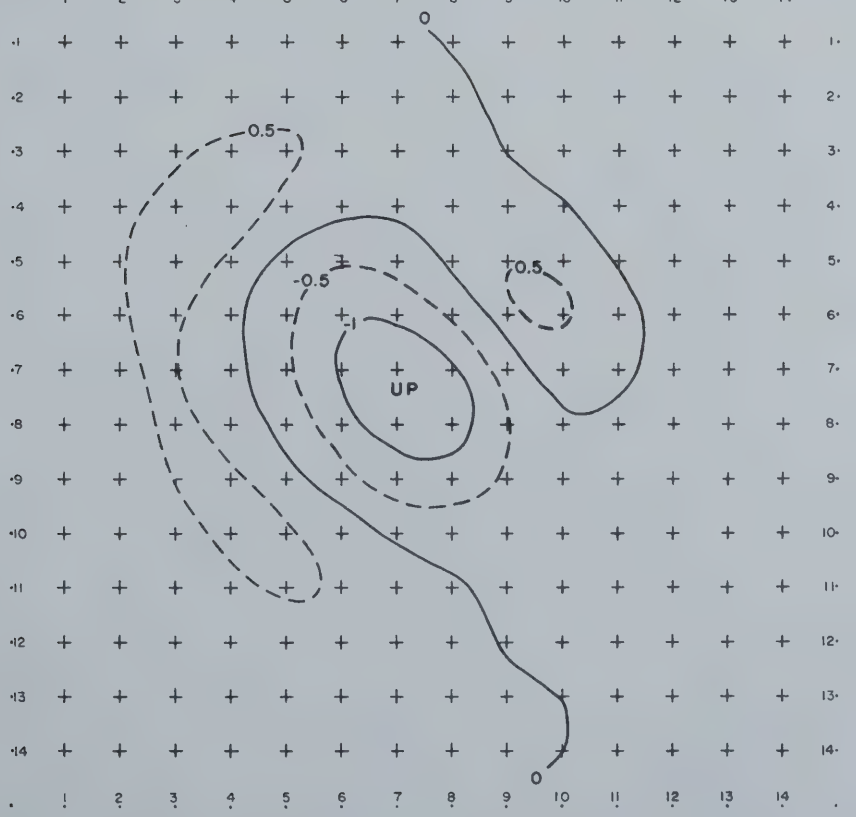

Fig. 26

variations increases a good deal more than the increases of the component wind fields from 80 to 70 cb. The inner centers of divergence are more than doubled in magnitude. The changes in the outer regions where βv dominates are not as great, so that by 70 cb the values associated with the centers on grid row 6, due mainly to zonal-wind advection of vortex vorticity, exceed those in the region of βv domination.

The net changes in computed divergence shown in fig. 24 result in the final approximation to divergence shown in fig. 25. The individual contributions of vertical motion and divergent-wind advection are displayed in the tabular summaries of a later sub-section. It may be noted that the general features of the final divergence pattern are still essentially those of the $D^{(0)}$ pattern, somewhat distorted by the divergent effects.

The pattern of vertical-motion distribution at 70 cb in fig. 26 shows a marked effect of integrated divergence in the 90-70 cb layer in breaking up the simple pattern of ω assumed at the 90 cb boundary surface. There are four distinct regions of alternating downward and upward motion.

The sequence of divergence approximations at 60 cb shown by figs. 27-29 will be discussed as an intermediate stage between the 70 cb and 50 cb stages. The corresponding 70 cb figures are figs. 23-25, discussed above. The corresponding 50 cb patterns are displayed in figs. 31-33.

The patterns of divergence $D^{(0)}$ computed from advection of vorticity by the nondivergent wind at 60 cb and 50 cb, fig. 27 and

Figure 27. Divergence approximation $D^{(0)}_{60}$, units 10^{-5} sec^{-1}.

Figure 28. Net change of divergence approximations on 60 centibar surface $\left(D^{(4)}_{60} - D^{(0)}_{60}\right)$, units 10^{-5} sec^{-1}.

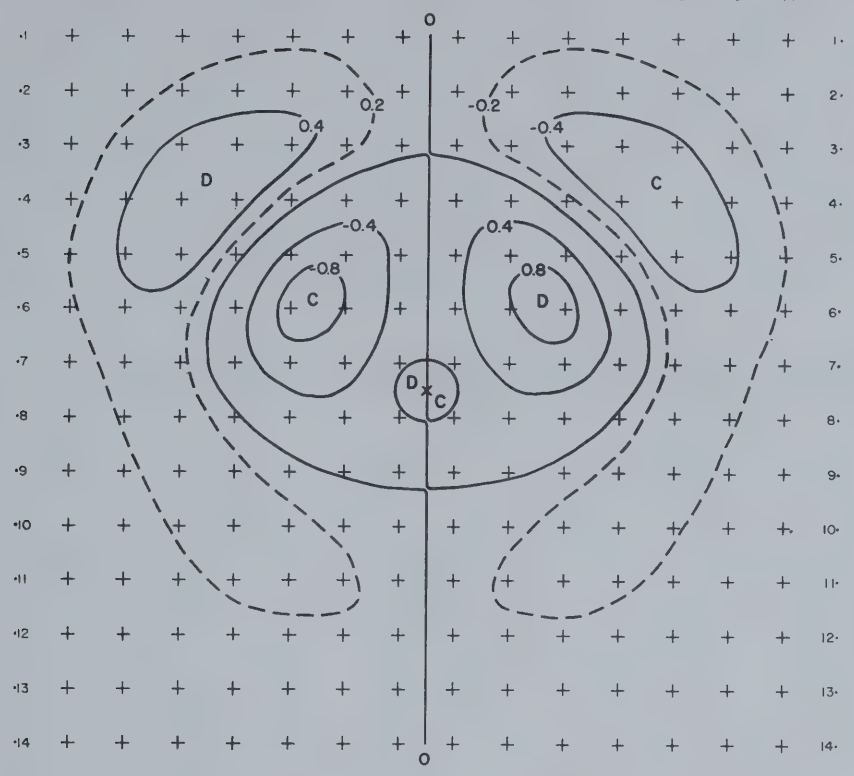

Fig. 27

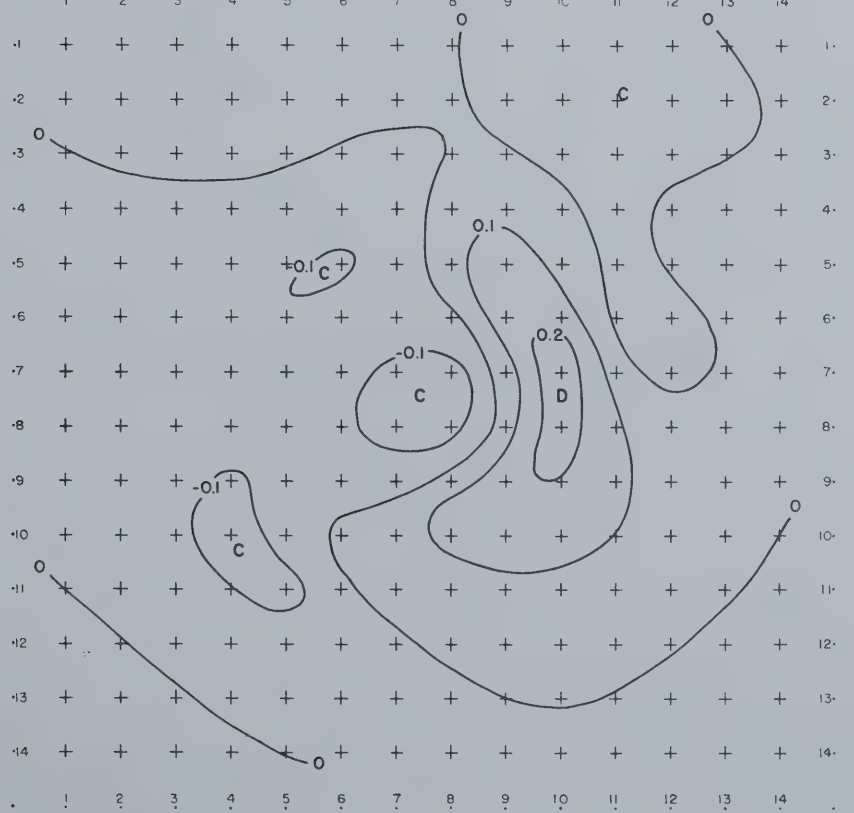

Fig. 28

Figure 29. Divergence approximation $D_{60}^{(4)}$, units 10^{-5} sec^{-1}.

Figure 30. Highest approximation to ω at 60 centibars, units 10^{-4} cb sec^{-1}.

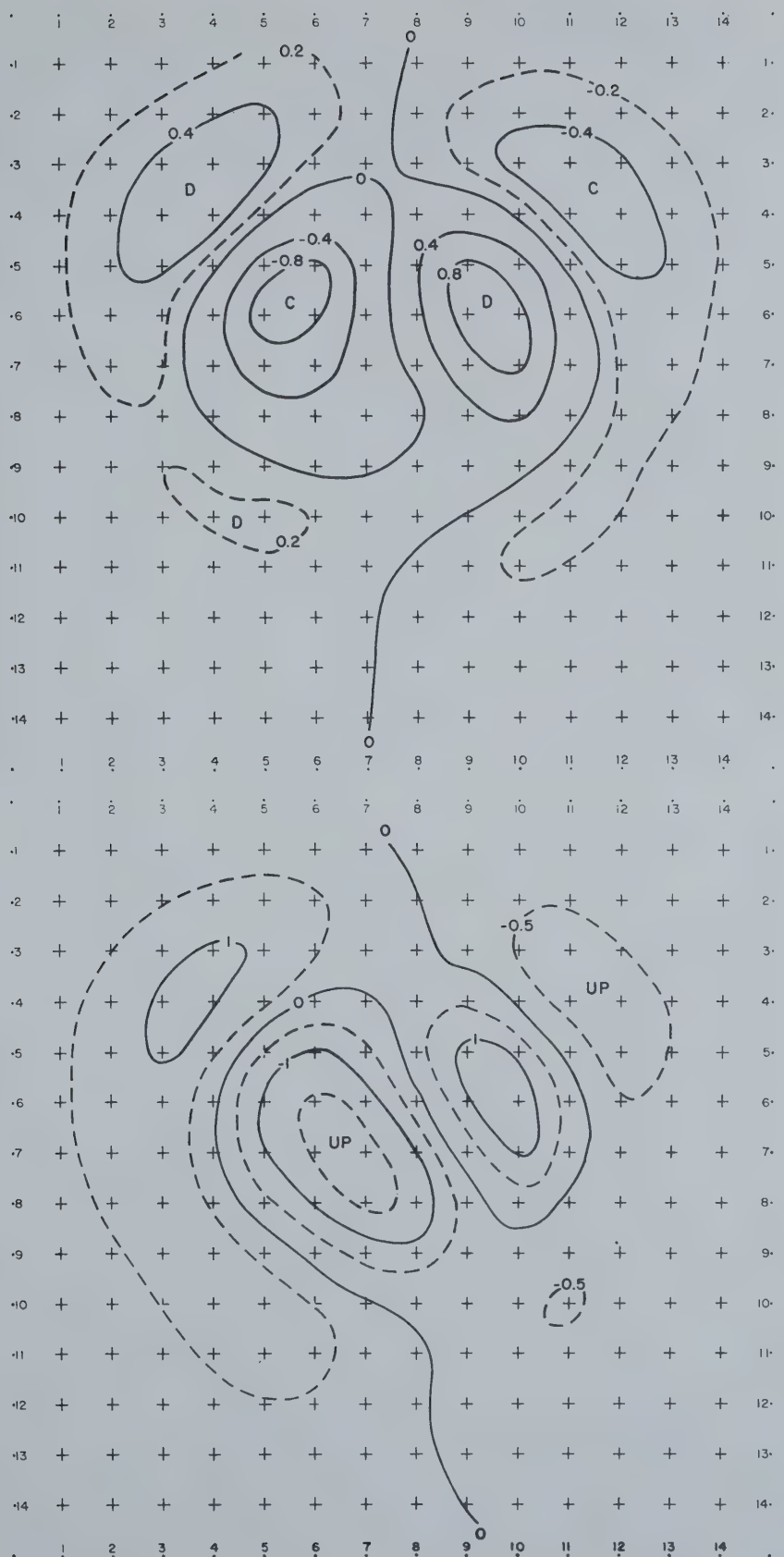

Fig. 29

Fig. 30

31 respectively, have very much the same shape as at 70 cb. The zero isopleth of this divergence field is in roughly the same location on all three charts. The horizontal gradient of the quantity increases in magnitude by a factor of nearly two within the central region enclosed by the zero isopleth. The exact centers of the symmetrically located centers of divergence and convergence shift very slightly away from the axis with height. Outside the zero line, in the region of control by the βv term, the proportionate increases in amplitude of the pattern are less. The ratio of increase is on the order of five-thirds from 70 to 60 cb, and eight-fifths from 60 to 50 cb. This portion of the pattern, spoken of as "peanut-shaped" for lack of a better appellation, has its axis on the plan views shifted slightly outward from the center of the system with increasing height. Close examination of the data on more complete working analyses shows that the zero line has a similar small displacement. A more evident change in the outer features of the pattern is the decreasing importance of the southern kernels of the configuration, relative to the other portions at higher latitudes. Close examination shows that this is due to changing importance of the vortex wind c and the gradient of its vorticity ζ_c. It shows the part that even these relatively remote portions of the vortex wind and vorticity patterns play in shaping the pattern of $D^{(0)}$.

The distribution and magnitude of the net divergence change $D^{(4)} - D^{(0)}$ have systematic but complicated trends from 70 to 60 cb (figs. 24 and 28), and on to 50 cb (fig. 32). The magnitude of the central values increases in the neighborhood of 50 percent with

Figure 31. Divergence approximation $D^{(0)}_{50}$, units 10^{-5} sec^{-1}.

Figure 32. Net change of divergence approximations on 50 centibar surface $\left(D^{(4)}_{50} - D^{(0)}_{50}\right)$, units 10^{-5} sec^{-1}.

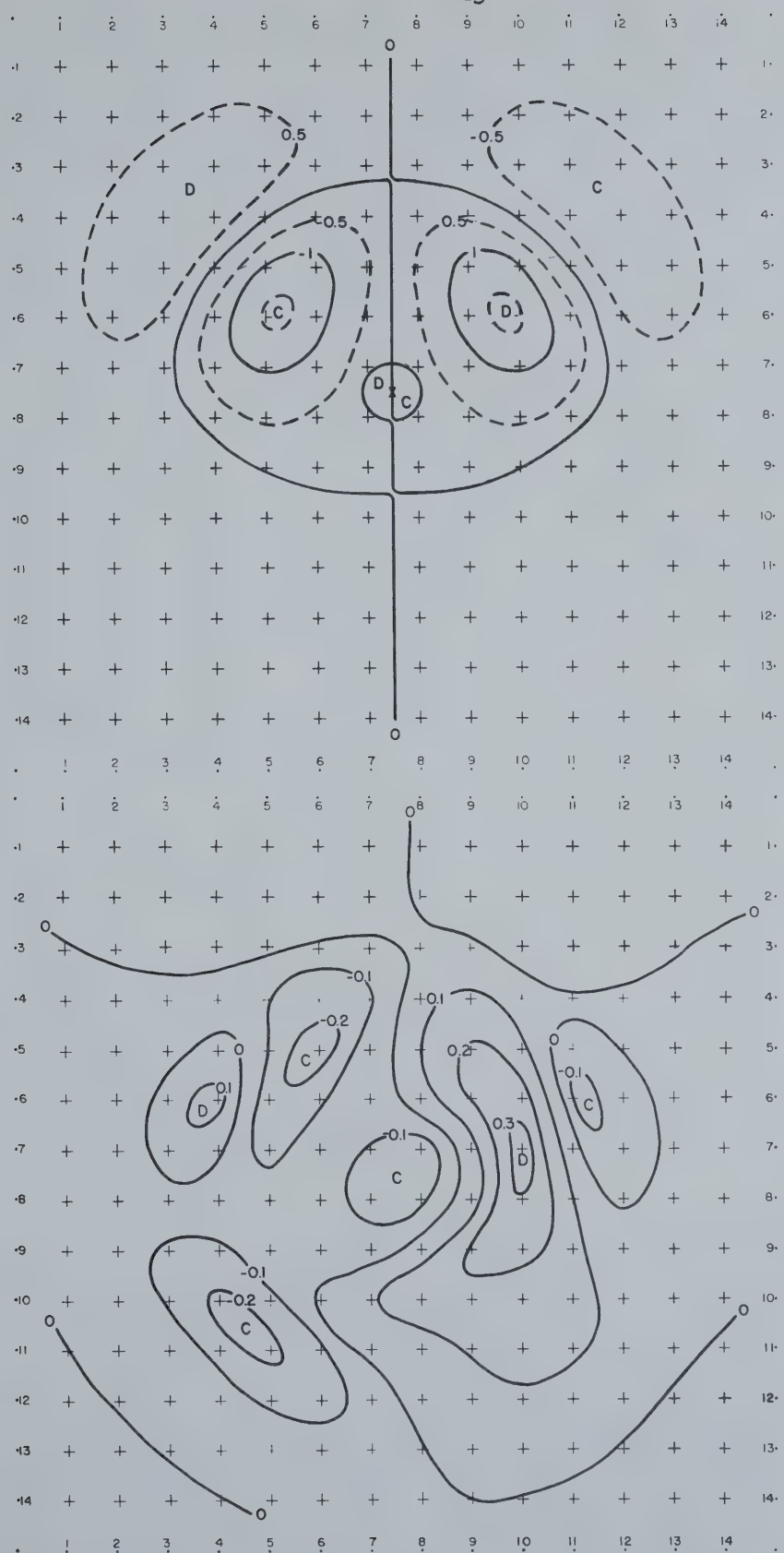

Fig. 31

Fig. 32

each step. These values are not large enough in comparison with $D^{(0)}$ at the respective pressure surfaces to alter the patterns of final approximations $D^{(4)}$ at 60 cb and 50 cb (fig. 29 and fig. 33) by very much. It is interesting, however, to note that the distributions of corrections $D^{(4)} - D^{(0)}$ are far less symmetric in their trends with height than the perfectly symmetric parent fields. There is a shifting balance among the various effects.

It is pertinent to make preliminary note here of a persistent tendency in the consitution of the $D^{(4)} - D^{(0)}$ pattern. The individual parts of this increment, $\Delta^{(2)}D$ and $\Delta^{(4)}D$, are at their respective maxima a good deal bigger than their sum. The patterns of distribution of each are quite unlike in detail, but in the net there is very frequent occurrence of cancellation between contributions of opposite sign. This becomes especially apparent upwards from the 70 cb surface, partly because it is more true there and partly because the magnitudes of these contributions reach more respectable proportions and make it especially clear-cut. This feature of cancellation between the vertical-motion term and the divergent-wind advection term is exhibited in the tabular summaries of a later sub-section.

Figures 30 and 34 show the vertical motions on the 60 cb and 50 cb surfaces respectively. The effect of the divergence in the successive layers is very clearly shown. It is interesting to note a gradual shift with height of a center of upward motion from location over the center of the system to a position well to the northwest. This region is connected by a weakening link through the

Figure 33. Divergence approximation $D^{(4)}_{50}$, units 10^{-5} sec^{-1}.

Figure 34. Highest approximation to ω at 50 centibars, units 10^{-4} sec^{-1}.

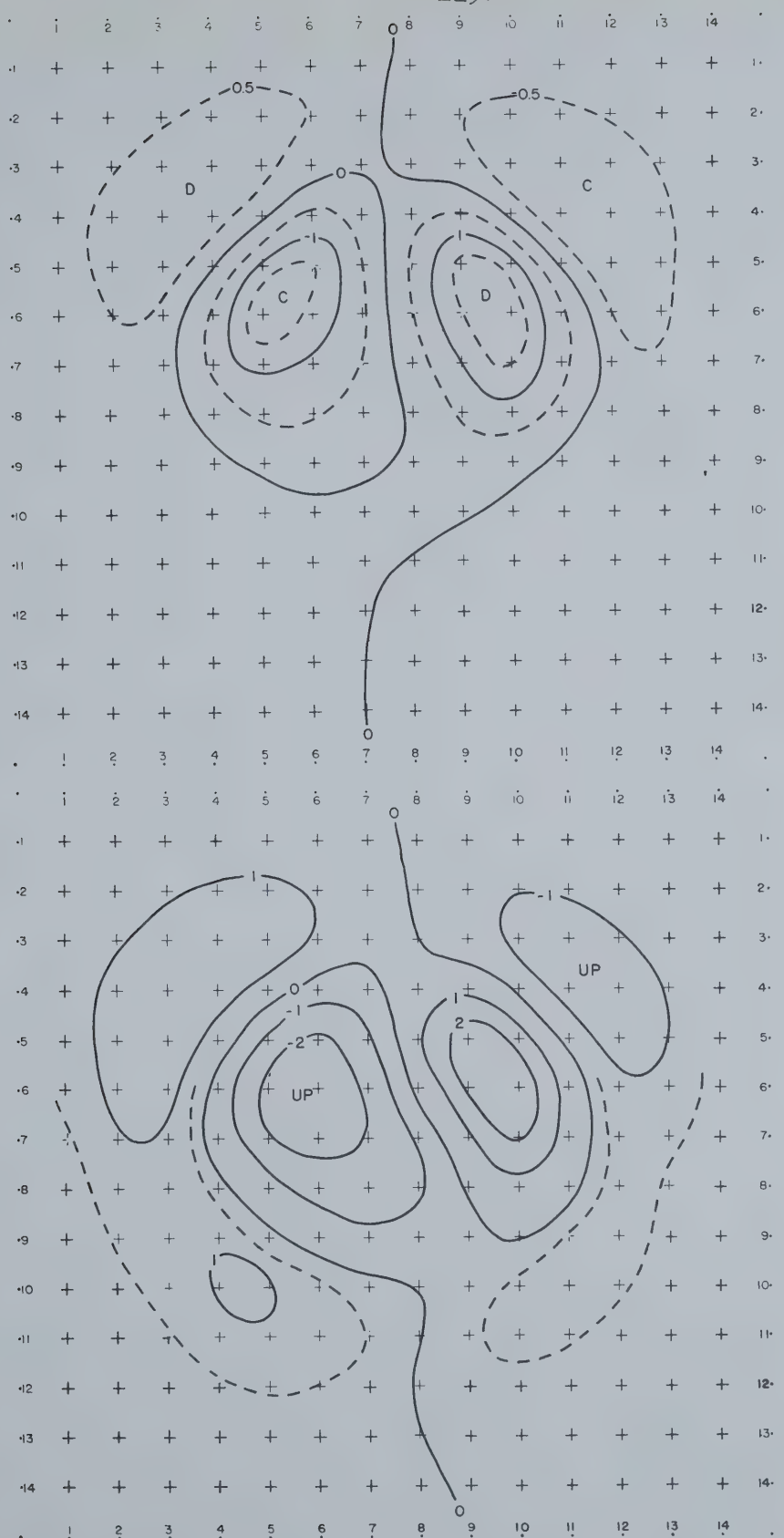

Fig. 33

Fig. 34

southeast quadrant to upward motion in a weaker center in the farther northeast section. In between these upward drifts there is downward motion centered in the northeast quadrant. Examination of the ω maps in ascending sequence indicates imminent cutting-off of another link across the northern part of the axis between this northeast quadrant descent region and a lobe of downward motion west of the axis. A new connection between the latter two across the southern part is indicated. The influence of the lower boundary distribution of ω as such is no longer discernible at the 50 cb level.

Vertical cross-sections of divergence and vertical motion.-The vertical distributions of the computed values of the final approximations to divergence, $D^{(F)}$, and substantial derivative of pressure, $\omega^{(F)}$, are presented in this section. For convenience of discussion, ω will continue to be referred to as vertical motion. Direct conversion of ω to the vertical component of velocity by $\omega = -\rho g w$ can be made with the table of conversion factors below. These factors use mean densities obtained by inspection of the temperature field in the 10 January 1953 case. A value of ω in units of 10^{-4} cb sec^{-1} is converted to w in cm sec^{-1} by multiplying ω by the indicated factor.

pressure (cb)	50	60	70	80	90
conversion factor	-1 1/2	-1 1/4	-1 1/7	-1	-11/12

Analyses of distribution of $D^{(F)}$ and $\omega^{(F)}$ in vertical cross-section are given in pairs by figs. 35-38. Fig. 35 and 36 are perpendicular to and parallel to the axis, respectively, and intersect in a vertical line through point 0707. Figures 37 and 38 are diagonal cross-sections, oriented from northwest to southeast and from southwest to northeast, respectively. On the east-to-west and north-to-south cross-sections the scale of distances is given by the vertical ticks on each constant pressure line. The distance between ticks is 300 km, plus or minus less than three per cent due to variation of scale factor. The numbering along the lower border is row or column number as indicated in the caption. The locations of the grid points on diagonal cross-sections are given by dots along the bottom margin of the figure and on the 50 cb line. The numbering of the dots is also explained in the figure captions. The distance between two adjoining dots represents 425 km on the standard-parallel scale of reduction.

All of the patterns of distribution in vertical cross-section are elongated vertically. The vertical scale of these diagrams is stretched conventionally, and in that sense the axes of divergence centers and vertical-motion centers are steeply inclined. In most cases the magnitudes of the quantities increase with height to the tops of the sections.

The analysis of the distributions in vertical cross-section are, by and large, rather obvious after consideration of the plan views in the earlier figures of this section. They do, however, bring out a few additional characteristics of the structure of

horizontal divergence and vertical motion implied by the requirement that the system maintains its vorticity in the steady-state condition.

The west-to-east cross-sections of fig. 35 show the extent to which the anti-symmetry across the meridional axis is changed by the additional divergence effects. There is very little convergence on the center line. The zero lines of divergence are essentially vertical, especially above 70 cb. The associated slope with height of the centers of the divergence patterns can be seen, especially in the lower 300 mb. The patterns of vertical motion are the result of the boundary prescription modified with height by the divergence contributions in the successive layers. The combination of these effects makes the axes of the ω patterns have greater inclination to the vertical than those of the divergence patterns.

The north-to-south sections in fig. 36 bring out the fact that the small asymmetry across the axis results in the presence of weak convergence on the axis, from roughly 1200 km north of the center to some distance south of the center. The distance of this zero line south of the center varies from 450 km at 90 cb to 600 km at 50 cb. The vertical motion pattern is centered at the intersection of row 7 with the cross-section plane. It should be kept in mind that this plane is 150 km west of the meridional plane containing the vortex centers.

The diagonal cross-sections of figs. 37 and 38 reflect the characteristic of the pattern, apparent on the plan views, that the relative maxima of magnitudes are found in the northern quadrants. The northwest-to-southeast diagonal section of ω, at the bottom

Figure 35. West-east cross-section of final approximate divergence (top, units 10^{-5} sec^{-1}), and vertical motion measure ω (bottom, units 10^{-5} cb sec^{-1}). Line of cross section is along grid row i = 7 , 150 km north of center of model vortex. Crosses indicate columns on grid.

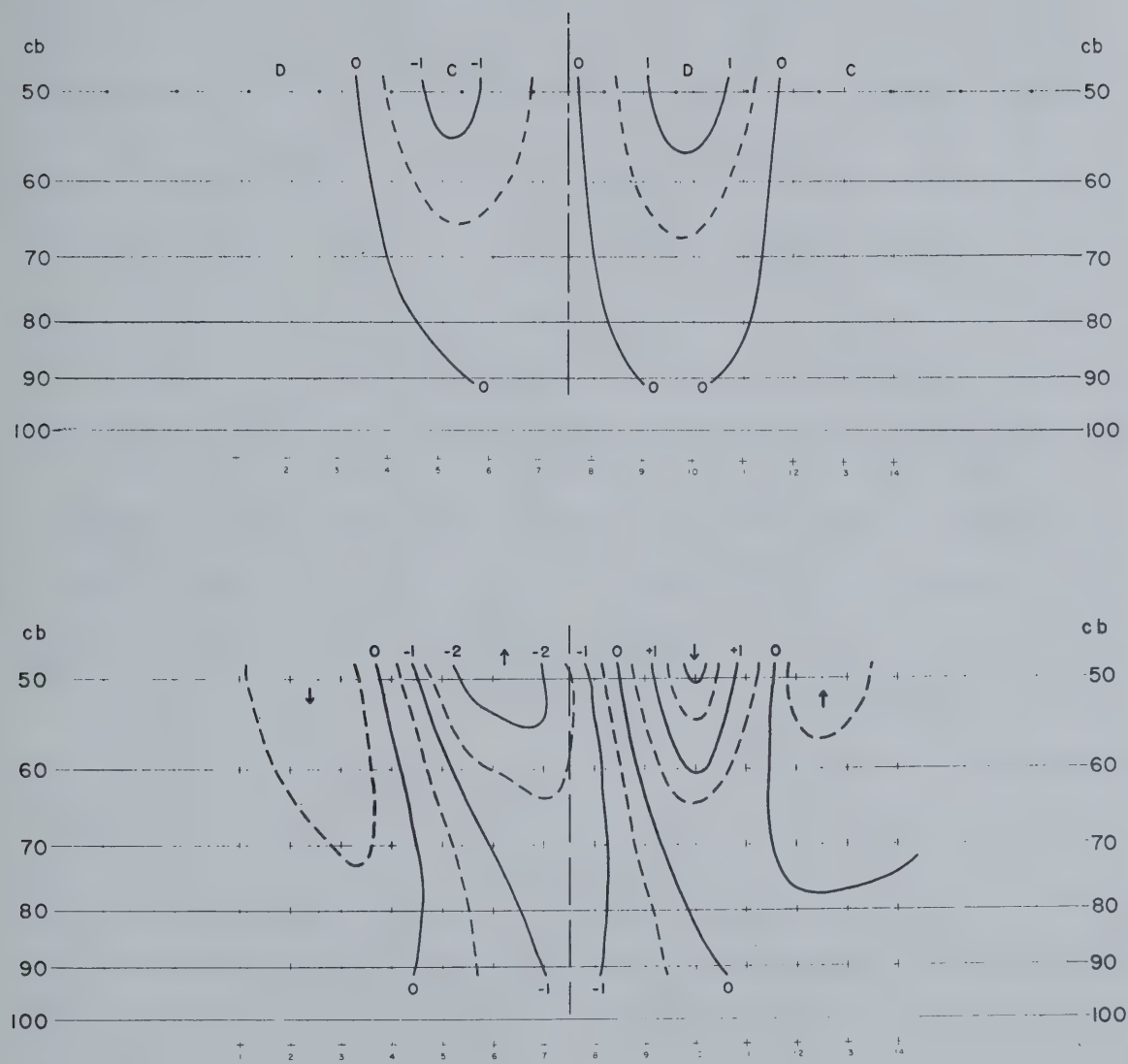

Fig. 35

Figure 36. South-north cross-section of final approximate divergence D (top, units 10^{-5} sec^{-1}), and vertical motion measure ω (bottom, units 10^{-5} cb sec^{-1}). Line of cross-section is along grid column j = 7 , 150 km west of center of model vortex. Crosses indicate rows on grid.

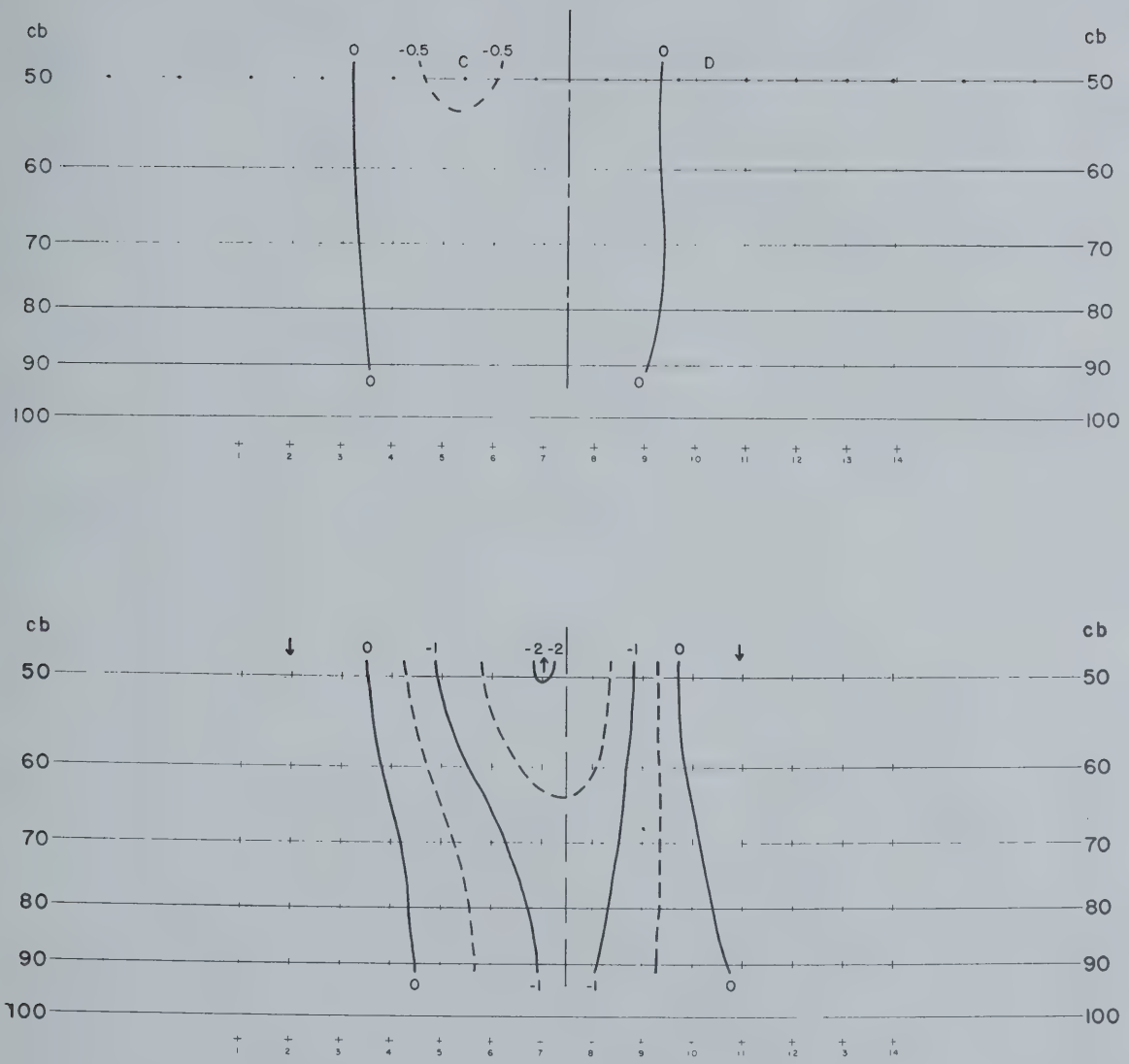
cb
50
60
70
80
90
100
0
-0.5
C
-0.5
0
D
0
0
cb
50
60
70
80
90
100
cb
50
60
70
80
90
100
0
-1
-2 -2
-1
0
0
-1
-1
0
cb
50
60
70
80
90
100

Fig. 36

in fig. 37, has the interesting feature that it cuts through two regions of upward motion without a change of sign in the intervening area of relative minimum upward motion.

The right-hand sides of the vertical motion cross-sections in figs. 35, 37 and 38 all show a region of appreciable horizontal extent in which weak downward motion in the lowest ten to fifteen centibars is replaced by upward motion. The indicated locations are far out on the eastern end of the west-to-east axis and in the southeast and northeast quadrants. One can visualize the surface of $\omega = 0$ in the more remote portions of the eastern side of the system as having considerable stretches of nearly horizontal orientation. This is noted to point out that most of the curves of intersection of the cross-section planes with the zero surface of vertical motion have relatively little inclination to the vertical.

The final divergence and vertical-motion distributions along the southwest-to-northeast vertical plane (fig. 38) complete the presentation of scalar analyses of results with little additional information. It may be observed that all four cross-sections of divergence show a central convergence region. The increase with height of the magnitude of this convergence is less strong in the present cross-section than in the others. This goes along with the fact that there is a central column of vertical motion on all cross-section planes. Further, there is smaller vertical gradient of vertical motion in the southwest-northeast vertical plane of fig. 38 than in any of the others.

Figure 37. Northwest-southeast cross-section of final approximate divergence D (top, units 10^{-5} sec^{-1}), and the vertical motion measure ω (bottom, units 10^{-4} cb sec^{-1}). Line of cross-section passes through center of model vortex. Dots show positions of grid points. Numbering of a dot gives both row and column number of grid point.

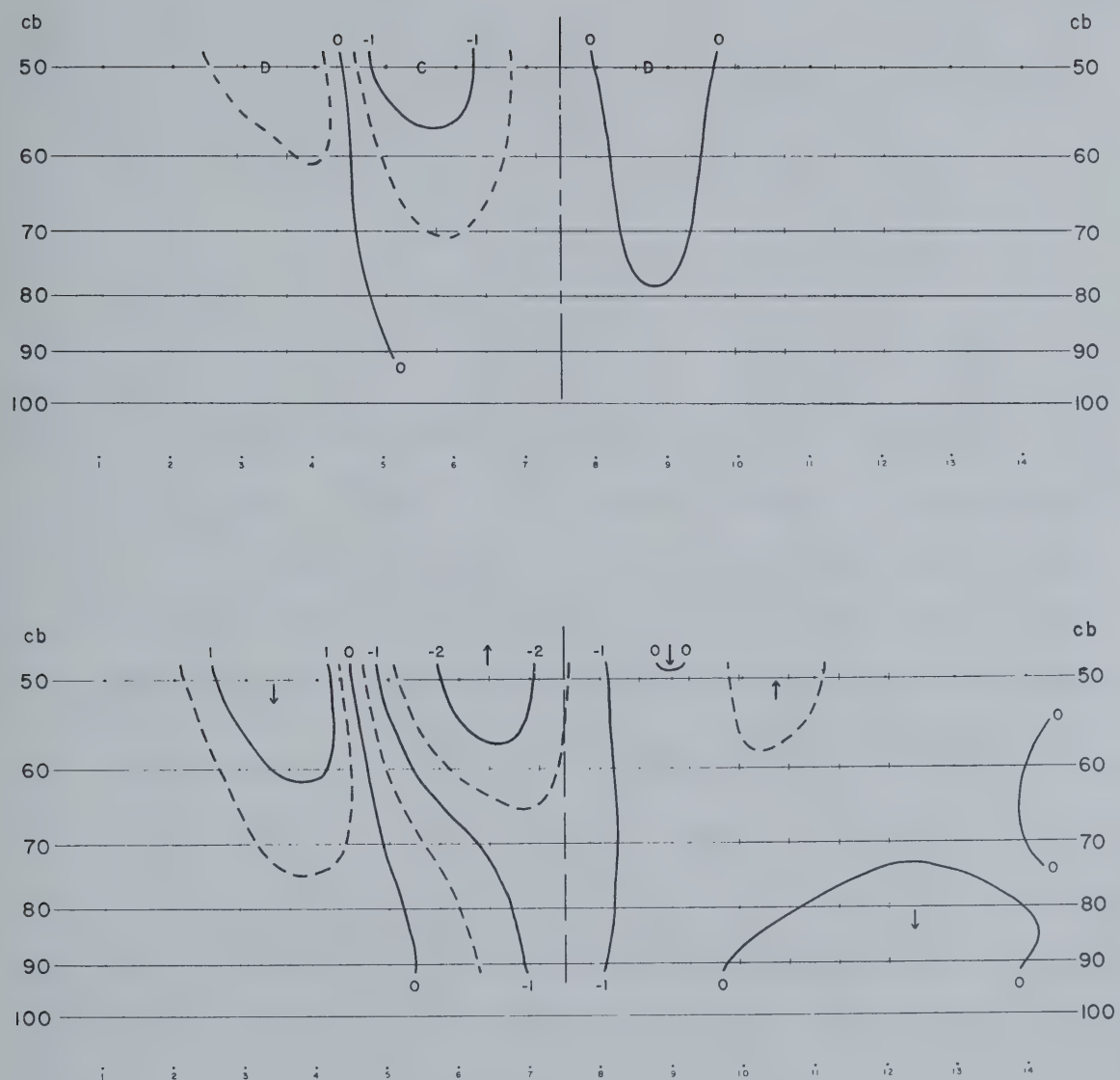

Fig. 37

Figure 38. Southwest-northeast cross-section of final approximate divergence D (top, units 10^{-5} sec^{-1}), and vertical motion measure ω (bottom, units 10^{-4} cb sec^{-1}). Line of cross-section passes through center of model vortex. Dots show positions of grid points. Numbering of a dot gives its column number and 14 minus its row number.

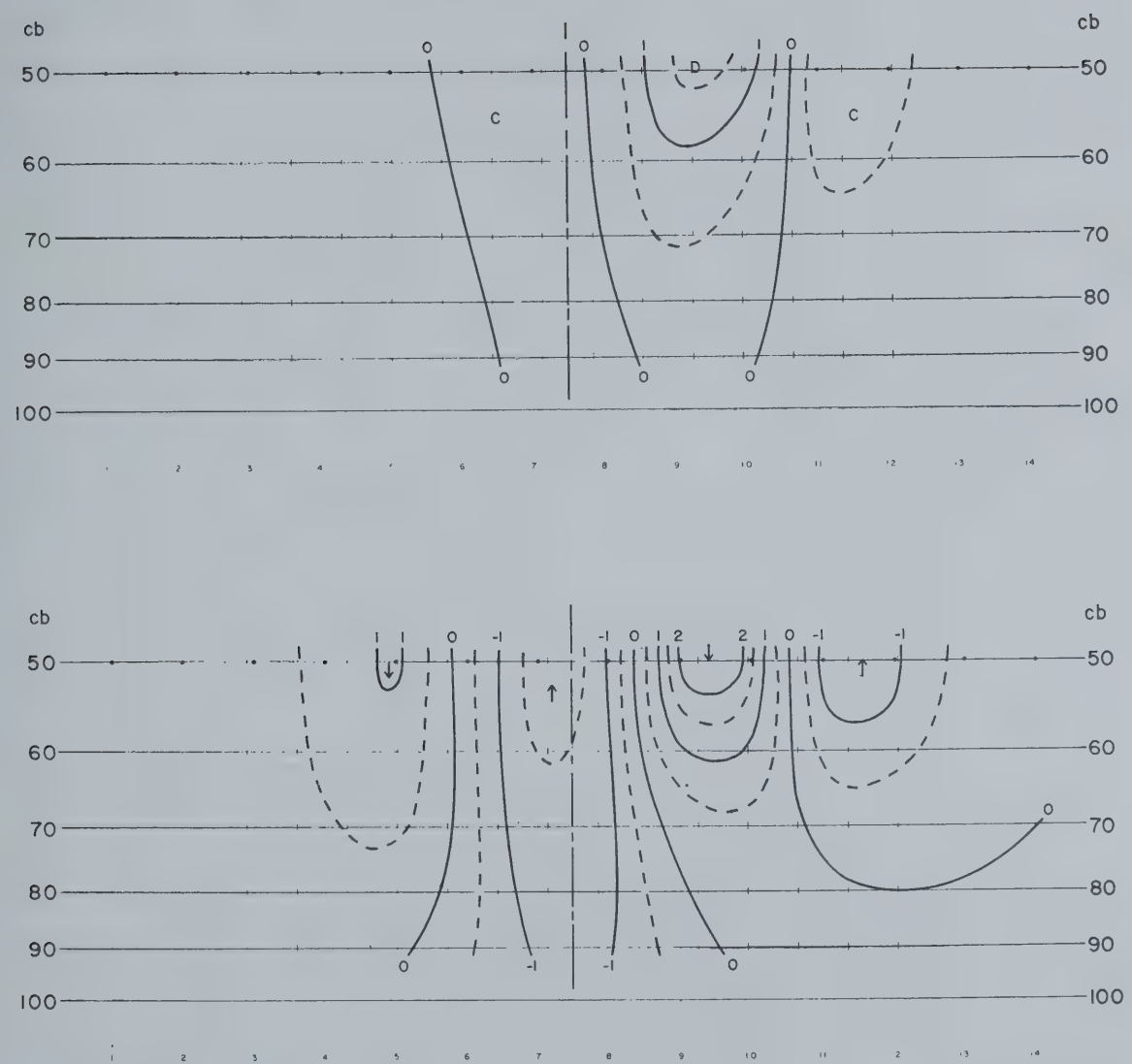

Fig. 38

Tabular summaries of structural elements at selected points.- The foregoing examination of the three-dimensional distribution of computed final approximations to divergence and vertical motion raises many questions of meteorological importance. Before pointing out these questions it is desirable to complete the presentation of computed results. Discussion of the data of table 5 in this section will serve to fill in the picture of distributions of the computed structural elements, and to give further insight into the numerical properties of the model. The quantities presented in table 5 are labeled with superscripts 0 and F , denoting their stages in the approximative procedure. The new superscript F is used to indicate the final (highest) approximation to divergence or vertical motion. The selection of grid points is indicated on fig. 16 by the inner bordered region. This selection takes in all points for which the listing of quantities will help to delineate patterns of results or show the behavior of the iterative output.

The magnitude of the first approximation to divergence increases very strongly with height at most of the points in the table. At several points $D^{(0)}$ approximately doubles from the bottom to the top of a 10 cb layer. The relatively smaller rates of increase of $D^{(0)}$ with height are found at points of the central region, in rows and columns 7 and 8. The selection of values given also shows that rates of increase of $D^{(0)}$ with height are relatively small in row 9. Some of the factors which lead to having increases of advective effects five to ten times as great as those of the advecting wind have been indicated in discussion of $D^{(0)}$ plan-view maps.

TABLE 5.-Summary of divergence contributions and vertical motion at selected grid points

p	$D^{(0)}$	$\Delta^{(V)}D$	$\Delta^{(H)}D$	$D^{(F)}-D^{(0)}$	$D^{(F)}$	$\omega^{(F)}$
cb	10^{-5} sec^{-1}					10^{-4} cb sec^{-1}
			Grid Point 0406			
90	+0.02	-0.01	-0.01	-0.02	0.00	+0.19
80	-0.02	-0.01	-0.01	-0.02	-0.04	+0.17
70	-0.08	-0.02	-0.03	-0.05	-0.13	+0.10
60	-0.20	-0.03	-0.07	-0.10	-0.30	-0.11
50	-0.42	-0.04	-0.15	-0.18	-0.60	-0.55
			Grid Point 0409			
90	-0.02	-0.01	0.00	0.00	-0.02	+0.19
80	+0.02	-0.01	+0.01	0.00	+0.02	+0.18
70	+0.08	-0.01	+0.03	+0.02	+0.10	+0.24
60	+0.20	+0.01	+0.06	+0.07	+0.27	+0.42
50	+0.42	+0.01	+0.15	+0.16	+0.58	+0.83
			Grid Point 0505			
90	+0.02	0.00	-0.02	-0.01	+0.01	+0.15
80	-0.08	+0.01	-0.04	-0.03	-0.10	+0.11
70	-0.25	+0.05	-0.10	-0.05	-0.29	-0.09
60	-0.56	+0.14	-0.21	-0.07	-0.63	-0.53
50	-1.11	+0.37	-0.46	-0.09	-1.20	-1.42
			Grid Point 0506			
90	-0.05	+0.01	-0.02	0.00	-0.05	-0.01
80	-0.18	+0.02	-0.04	-0.02	-0.20	-0.14
70	-0.39	+0.03	-0.09	-0.06	-0.45	-0.45
60	-0.74	+0.04	-0.15	-0.12	-0.86	-1.10
50	-1.30	+0.05	-0.26	-0.21	-1.51	-2.26

TABLE 5.-Continued

p	$D^{(0)}$	$\Delta^{(V)}_D$	$\Delta^{(H)}_D$	$D^{(F)}-D^{(0)}$	$D^{(F)}$	$\omega^{(F)}$
cb	10^{-5} sec^{-1}					10^{-4}cb sec^{-1}
			Grid Point 0509			
90	+0.05	+0.01	+0.02	+0.03	+0.08	-0.01
80	+0.18	+0.01	+0.05	+0.06	+0.24	+0.15
70	+0.39	+0.01	+0.08	+0.09	+0.49	+0.49
60	+0.74	0.00	+0.15	+0.15	+0.89	+1.17
50	+1.30	-0.01	+0.27	+0.26	+1.56	+2.38
			Grid Point 0510			
90	-0.02	0.00	+0.02	+0.02	-0.01	+0.15
80	+0.08	-0.01	+0.05	+0.03	+0.11	+0.20
70	+0.25	-0.05	+0.10	+0.05	+0.30	+0.40
60	+0.56	-0.15	+0.22	+0.07	+0.63	+0.85
50	+1.11	-0.38	+0.48	+0.10	+1.21	+1.74
			Grid Point 0604			
90	+0.10	0.00	-0.01	-0.01	+0.09	+0.18
80	+0.05	+0.01	-0.04	-0.03	+0.03	+0.25
70	-0.05	+0.06	-0.08	-0.02	-0.07	+0.23
60	-0.26	+0.17	-0.18	-0.01	-0.27	+0.07
50	-0.65	+0.48	-0.41	+0.07	-0.58	-0.32
			Grid Point 0605			
90	0.00	+0.03	-0.04	-0.01	0.00	-0.02
80	-0.16	+0.05	-0.07	-0.02	-0.18	-0.10
70	-0.39	+0.09	-0.15	-0.06	-0.45	-0.41
60	-0.85	+0.17	-0.25	-0.08	-0.93	-1.08
50	-1.53	+0.30	-0.44	-0.14	-1.68	-2.38

TABLE 5.-Continued

p	$D^{(0)}$	$\Delta^{(V)}_D$	$\Delta^{(H)}_D$	$D^{(F)}-D^{(0)}$	$D^{(F)}$	$\omega^{(F)}$
cb	10^{-5} sec^{-1}					10^{-4} cb sec^{-1}
			Grid Point 0606			
90	-0.05	+0.02	-0.03	-0.01	-0.07	-0.35
80	-0.22	+0.02	-0.04	-0.02	-0.24	-0.50
70	-0.47	-0.01	-0.04	-0.05	-0.52	-0.86
60	-0.80	-0.07	-0.01	-0.08	-0.87	-1.57
50	-1.30	-0.20	+0.09	-0.11	-1.41	-2.68
			Grid Point 0607			
90	-0.03	-0.02	-0.02	-0.04	-0.07	-0.63
80	-0.09	-0.03	-0.01	-0.04	-0.13	-0.72
70	-0.18	-0.05	0.00	-0.05	-0.23	-0.89
60	-0.31	-0.09	+0.04	-0.05	-0.36	-1.19
50	-0.48	-0.16	+0.12	-0.05	-0.53	-1.62
			Grid Point 0608			
90	+0.03	-0.02	0.00	-0.02	+0.01	-0.63
80	+0.09	-0.01	0.00	-0.01	+0.08	-0.58
70	+0.18	+0.01	-0.03	-0.02	+0.16	-0.46
60	+0.31	+0.06	-0.08	-0.02	+0.29	-0.24
50	+0.48	+0.13	-0.16	-0.02	+0.46	+0.12
			Grid Point 0609			
90	+0.05	+0.02	+0.02	+0.04	+0.09	-0.35
80	+0.22	+0.03	+0.03	+0.06	+0.28	-0.17
70	+0.47	+0.07	+0.02	+0.09	+0.56	+0.23
60	+0.80	+0.16	-0.02	+0.14	+0.93	+0.98
50	+1.30	+0.32	-0.13	+0.20	+1.50	+2.16

TABLE 5.-Continued

p	$D^{(0)}$	$\Delta^{(V)}D$	$\Delta^{(H)}D$	$D^{(F)}-D^{(0)}$	$D^{(F)}$	$\omega^{(F)}$
cb	10^{-5} sec^{-1}					10^{-4} cb sec^{-1}
			Grid Point 0610			
90	0.00	+0.03	+0.03	+0.06	+0.06	-0.02
80	+0.16	+0.02	+0.08	+0.10	+0.25	+0.13
70	+0.39	-0.01	+0.15	+0.14	+0.53	+0.52
60	+0.85	-0.09	+0.26	+0.17	+1.02	+1.27
50	+1.53	-0.22	+0.47	+0.26	+1.79	+2.67
			Grid Point 0611			
90	-0.10	0.00	+0.01	+0.01	-0.09	+0.18
80	-0.05	-0.01	+0.04	+0.03	-0.03	+0.13
70	+0.05	-0.07	+0.09	+0.02	+0.07	+0.14
60	+0.26	-0.20	+0.19	-0.01	+0.25	+0.30
50	+0.65	-0.53	+0.43	-0.10	+0.55	+0.67
			Grid Point 0704			
90	+0.14	+0.02	-0.02	0.00	+0.14	+0.13
80	+0.09	+0.02	-0.05	-0.03	+0.06	+0.23
70	-0.03	+0.08	-0.12	-0.04	-0.07	+0.23
60	-0.25	+0.19	-0.24	-0.04	-0.29	+0.07
50	-0.65	+0.47	-0.48	-0.02	-0.67	-0.38
			Grid Point 0705			
90	+0.06	+0.04	-0.06	-0.02	+0.05	-0.17
80	-0.07	+0.07	-0.09	-0.03	-0.10	-0.19
70	-0.28	+0.09	-0.15	-0.06	-0.34	-0.40
60	-0.62	+0.13	-0.21	-0.08	-0.70	-0.91
50	-1.14	+0.16	-0.27	-0.11	-1.25	-1.88

TABLE 5.-Continued

p	$D^{(0)}$	$\Delta^{(V)}D$	$\Delta^{(H)}D$	$D^{(F)}-D^{(0)}$	$D^{(F)}$	$\omega^{(F)}$
cb	10^{-5} sec^{-1}					10^{-4} cb sec^{-1}
			Grid Point 0706			
90	0.00	-0.01	-0.05	-0.06	-0.06	-0.64
80	-0.12	0.00	-0.05	-0.06	-0.18	-0.76
70	-0.30	-0.03	-0.04	-0.07	-0.37	-1.02
60	-0.55	-0.08	+0.02	-0.06	-0.61	-1.51
50	-0.89	-0.20	+0.16	-0.03	-0.92	-2.27
			Grid Point 0707			
90	-0.01	-0.09	-0.02	-0.11	-0.11	-1.02
80	-0.06	-0.10	-0.01	-0.11	-0.16	-1.16
70	-0.12	-0.13	+0.01	-0.12	-0.24	-1.35
60	-0.21	-0.18	+0.05	-0.13	-0.33	-1.63
50	-0.32	-0.24	+0.13	-0.12	-0.44	-2.01
			Grid Point 0708			
90	+0.01	-0.09	+0.01	-0.08	-0.08	-1.02
80	+0.06	-0.09	0.00	-0.09	-0.03	-1.07
70	+0.12	-0.09	-0.02	-0.11	+0.01	-1.08
60	+0.21	-0.08	-0.07	-0.15	+0.06	-1.05
50	+0.32	-0.05	-0.14	-0.19	+0.13	-0.95
			Grid Point 0709			
90	0.00	-0.01	+0.02	+0.01	+0.02	-0.64
80	+0.12	+0.01	+0.03	+0.03	+0.16	-0.55
70	+0.30	+0.04	0.00	+0.04	+0.34	-0.31
60	+0.55	+0.13	-0.07	+0.06	+0.60	+0.15
50	+0.89	+0.26	-0.22	+0.04	+0.93	+0.90

TABLE 5.-Continued

p	$D^{(0)}$	$\Delta^{(V)}D$	$\Delta^{(H)}D$	$D^{(F)}-D^{(0)}$	$D^{(F)}$	$\omega^{(F)}$
cb	10^{-5} sec^{-1}					10^{-4} cb sec^{-1}
			Grid Point 0710			
90	-0.06	+0.04	+0.04	+0.09	+0.03	-0.17
80	+0.07	+0.03	+0.09	+0.12	+0.19	+0.06
70	+0.28	+0.03	+0.14	+0.17	+0.46	+0.25
60	+0.62	+0.02	+0.20	+0.22	+0.85	+1.03
50	+1.14	+0.01	+0.28	+0.30	+1.44	+2.03
			Grid Point 0711			
90	-0.14	+0.02	+0.02	+0.04	-0.10	+0.13
80	-0.09	0.00	+0.06	+0.06	-0.02	+0.06
70	+0.03	-0.06	+0.14	+0.08	+0.10	+0.10
60	+0.25	-0.21	+0.26	+0.04	+0.29	+0.29
50	+0.65	-0.51	+0.53	+0.02	+0.67	+0.75
			Grid Point 0804			
90	+0.19	+0.02	-0.02	0.00	+0.20	+0.12
80	+0.18	+0.02	-0.05	-0.03	+0.15	+0.30
70	+0.13	+0.06	-0.11	-0.05	+0.08	+0.41
60	+0.02	+0.12	-0.21	-0.09	-0.07	+0.44
50	-0.21	+0.30	-0.40	-0.10	-0.31	+0.28
			Grid Point 0805			
90	+0.15	+0.05	-0.07	-0.02	+0.13	-0.18
80	+0.08	+0.08	-0.11	-0.04	+0.04	-0.09
70	-0.04	+0.12	-0.18	-0.06	-0.10	-0.12
60	-0.24	+0.19	-0.24	-0.05	-0.29	-0.30
50	-0.55	+0.22	-0.32	-0.09	-0.61	-0.76

TABLE 5.-Continued

p	$D^{(0)}$	$\Delta^{(V)}D$	$\Delta^{(H)}D$	$D^{(F)}-D^{(0)}$	$D^{(F)}$	$\omega^{(F)}$
cb	10^{-5} sec^{-1}					10^{-4}cb sec^{-1}
			Grid Point 0806			
90	+0.07	-0.01	-0.08	-0.08	-0.01	-0.66
80	0.00	+0.02	-0.10	-0.08	-0.08	-0.70
70	-0.10	+0.01	-0.10	-0.10	-0.20	-0.83
60	-0.25	+0.01	-0.09	-0.08	-0.33	-1.09
50	-0.46	-0.03	-0.02	-0.04	-0.50	-1.51
			Grid Point 0807			
90	+0.02	-0.09	-0.03	-0.12	-0.10	-1.03
80	-0.01	-0.09	-0.03	-0.12	-0.13	-1.15
70	-0.05	-0.11	-0.03	-0.14	-0.18	-1.30
60	-0.10	-0.14	-0.01	-0.15	-0.25	-1.52
50	-0.17	-0.18	+0.03	-0.15	-0.32	-1.80
			Grid Point 0808			
90	-0.02	-0.09	+0.01	-0.08	-0.10	-1.03
80	+0.01	-0.09	+0.01	-0.08	-0.08	-1.12
70	+0.05	-0.10	0.00	-0.10	-0.05	-1.18
60	+0.10	-0.10	-0.02	-0.12	-0.03	-1.22
50	+0.17	-0.10	-0.07	-0.16	+0.01	-1.23
			Grid Point 0809			
90	-0.07	-0.01	+0.04	+0.03	-0.04	-0.66
80	0.00	-0.01	+0.06	+0.05	+0.05	-0.65
70	+0.10	+0.01	+0.05	+0.07	+0.17	-0.55
60	+0.25	+0.05	+0.03	+0.08	+0.33	-0.30
50	+0.46	+0.12	-0.05	+0.07	+0.53	+0.11

TABLE 5.-Continued

p	$D^{(0)}$	$\Delta^{(V)}D$	$\Delta^{(H)}D$	$D^{(F)}-D^{(0)}$	$D^{(F)}$	$\omega^{(F)}$
cb	10^{-5} sec^{-1}					10^{-4} cb sec^{-1}
			Grid Point 0810			
90	-0.15	+0.05	+0.05	+0.10	+0.05	-0.18
80	-0.08	+0.04	+0.10	+0.14	+0.06	-0.18
70	+0.04	+0.02	+0.17	+0.18	+0.23	-0.05
60	+0.24	-0.02	+0.24	+0.22	+0.46	+0.29
50	+0.55	-0.05	+0.33	+0.28	+0.83	+0.93
			Grid Point 0811			
90	-0.19	+0.02	+0.02	+0.04	-0.15	+0.12
80	-0.18	+0.01	+0.06	+0.07	-0.11	-0.02
70	-0.13	-0.03	+0.13	+0.10	-0.04	-0.10
60	-0.02	-0.13	+0.24	+0.11	+0.09	-0.08
50	+0.21	-0.35	-0.46	+0.12	+0.33	+0.11
			Grid Point 0905			
90	+0.21	+0.05	-0.05	0.00	+0.21	-0.06
80	+0.20	+0.07	-0.10	-0.03	+0.18	+0.15
70	+0.17	+0.12	-0.16	-0.04	+0.13	+0.29
60	+0.10	+0.19	-0.24	-0.05	+0.05	+0.40
50	-0.03	+0.30	-0.36	-0.06	-0.09	+0.39
			Grid Point 0906			
90	+0.13	+0.03	-0.08	-0.04	+0.09	-0.40
80	+0.11	+0.07	-0.12	-0.05	+0.06	-0.31
70	+0.07	+0.10	-0.16	-0.06	+0.01	-0.28
60	0.00	+0.16	-0.19	-0.03	-0.03	-0.29
50	-0.11	+0.21	-0.21	0.00	-0.11	-0.38

TABLE 5.-Continued

p	$D^{(0)}$	$\Delta^{(V)}D$	$\Delta^{(H)}D$	$D^{(F)}-D^{(0)}$	$D^{(F)}$	$\omega^{(F)}$
cb	10^{-5} sec^{-1}					10^{-4} cb sec^{-1}
			Grid Point 0909			
90	-0.13	+0.03	+0.05	+0.08	-0.05	-0.40
80	-0.11	+0.03	+0.08	+0.11	0.00	-0.42
70	-0.07	+0.03	+0.11	+0.14	+0.07	-0.39
60	0.00	+0.03	+0.14	+0.17	+0.17	-0.27
50	+0.11	+0.03	+0.17	+0.20	+0.31	-0.03
			Grid Point 0910			
90	-0.21	+0.05	+0.04	+0.09	-0.12	-0.06
80	-0.20	+0.03	+0.09	+0.12	-0.08	-0.16
70	-0.17	-0.01	+0.17	+0.16	-0.01	-0.20
60	-0.10	-0.07	+0.27	+0.19	+0.09	-0.16
50	+0.03	-0.19	+0.43	+0.24	+0.27	+0.01

Increases of the magnitude of divergence increments are similarly quite large, at least from 70 cb up. Two interesting observations can be generalized from qualitative interpretation of the $\Delta^{(V)}D$ and $\Delta^{(H)}D$ data. First, the individual values of these contributions are of the same magnitude as the advective effect of the nondivergent wind. In the regions of $D^{(0)}$ maxima, one or the other of the increments $\Delta^{(H)}D$ or $\Delta^{(V)}D$ is often 30 to 40 percent as large as $D^{(0)}$. Not infrequently both are appreciable fractions of $D^{(0)}$. In such situations there is a definite tendency for these contributions to cancel one another. This is the second generalization of interest. If it were not for this frequent

cancellation of vertical motion effects by the horizontal divergent-wind advection, the patterns of final divergence approximation would be much more unlike those of the divergence required to balance only the nondivergent-wind advection in a steady-state situation.

Table 6 gives a comparison of the vertical advection of vorticity and the tipping term. The points included were chosen because of having large values of either or both of these parts of $\Delta^{(V)}D$. The divergence contribution of vertical advection of vorticity is denoted in the table and this discussion by A, and that of differential vertical advection by T. From table 6 it is found that at 90 cb |A| averages twice as much as |T|, while at 70 cb these two terms average just about the same in absolute value. The 70 cb |T| is almost three times as large as it was at 90 cb. At 50 cb |T| averages more than twice as much as |A|, and is five times as large as the mean |T| at 70 cb. The largest value of |T| in the selection, found at 50 cb, is also twice as large as the largest value of |A|. In lower layers |T| at its largest is smaller than the maximum |A|. The tendency toward cancellation of A by T is unanimous in the 90 cb selection. Occurrence of opposite signs is also more common than reinforcement at 70 cb. At 50 cb, reinforcing contributions are the rule by eleven to five.

The data in tables 5 and 6 for the four points 0707, 0708, 0807 and 0808 show that at the lower boundary and at 70 cb the vertical advection of vorticity was actually the predominant effect near the center of the system. This term accounts for a negative final approximation

to divergence over the center of the system, as shown, for instance, by fig. 35. The 50 cb final divergence at these same central points is also strongly affected by the vertical advection effect. The points at which the tipping term is the more important vertical-motion effect are farther out from the center. It seems characteristic that at such points the divergent-advection effect is systematically opposed to $\Delta^{(V)}D$, with the net result that the pattern of final divergence is little different from that of $D^{(0)}$.

TABLE 6.-Comparison of vertical advection of vorticity term (A) and tipping term (T) evaluated as divergence contributions.

Grid Point	90 cb		70 cb		50 cb	
	A*	T‡	A	T	A	T
	10^{-5} sec^{-1}					
0505	-0.01	+0.01	+0.01	+0.05	+0.12	+0.25
0510	-0.01	+0.01	-0.02	-0.03	-0.14	-0.23
0604	-0.01	+0.01	-0.01	+0.07	+0.03	+0.44
0607	-0.04	+0.02	-0.06	+0.01	-0.13	-0.03
0608	-0.04	+0.02	-0.03	+0.04	+0.01	+0.12
0609	-0.01	+0.03	+0.01	+0.06	+0.12	+0.20
0611	-0.01	+0.01	-0.01	-0.06	-0.07	-0.46
0704	0.00	+0.02	-0.01	+0.09	+0.03	+0.44
0707	-0.10	+0.01	-0.13	0.00	-0.22	-0.02
0708	-0.10	+0.01	-0.11	+0.02	-0.11	+0.05
0711	0.00	+0.02	-0.01	-0.05	-0.06	-0.45
0804	0.00	+0.02	-0.02	+0.08	-0.02	+0.32
0806	-0.05	+0.04	-0.07	+0.08	-0.14	+0.12
0807	-0.11	+0.01	-0.13	+0.02	-0.21	+0.03
0808	-0.11	+0.01	-0.12	+0.02	-0.14	+0.05
0811	0.00	+0.02	0.00	-0.04	-0.01	-0.34

*$A = -\zeta_a^{-1}\omega\,\partial\zeta/\partial p$ ‡$T = -\zeta_a^{-1}\,\underline{k}\cdot\nabla\omega \times \partial\underline{V}/\partial p$

The data presented in this section show that for this model, at least, one cannot make any safe statements of consistently dominating terms in the vorticity equation. Even the incomplete dominance by nondivergent-wind advection is in large part a matter of cancelling combinations of individually non-negligible terms. That this is more or less consistently the case in this model is the natural result of the process of analysis which bases deduction of the structure essentially upon assumption of $D^{(0)}$. It is to be expected that certain patterns of $D^{(0)}$ imply certain patterns of the computed quantities, and that these should have systematic relationships to one another. Even so, the resulting combinations are a complicated interplay. It is likely that the symmetry of the present model is responsible for under-estimation, if anything, of the importance of the structural characteristics which depend on there being a divergent component in the cold-low wind field.

Divergent wind contribution to total wind system.-The present treatment of the equations of motion makes it easy to examine the divergent part of the wind directly. It does this by restrictive assumptions, which also restrict the applicability of the conclusions. However, in many numerical approaches it is assumed that at least some of the effects of the divergent wind are negligible effects. Most examples of application of numerical methods to atmospheric dynamics are in the field of numerical weather prediction. The amount of constraint on the effects of divergence and divergent wind varies from one prediction model to another. Baroclinic models are in general characterized by the inclusion of the direct effect of

divergence upon the substantial derivative of vorticity. The quasi-divergent nongeostrophic models are among these. Representation of the wind as the sum of a divergent irrotational part and a nondivergent rotational part is a prominent device in such prediction formulations, [50], as it is in the procedure of this investigation. Of course, formulations for the purpose of prediction are more complex. The assumptions of steady-state vorticity and prescription of the nondivergent rotational wind are excluded from them by definition. Nevertheless the information that the present investigation gives about the nature of the divergent wind has potential usefulness in connection with evaluation of simplifications made in dealing with prediction problems. It has been shown by a theoretical study [51] that one such simplification, neglect of a term which is essentially our $\Delta^{(H)}_D$ term, may account for certain troublesome defects of baroclinic forecasts. In the cited study, Thompson points to an effect of discrepant exaggeration of pressure gradients between surface lows and highs, when advection of vorticity with the divergent component of the wind is not properly taken into account. It becomes more serious as the flow becomes more and more baroclinic. The fact that such considerations have arisen is good reason for interest in explicit information about the divergent wind.

The mere existence of the possibility for representing a wind field in two parts will cause some people to wish to see what atmospheric wind systems look like in these terms. Any structural investigation which produces horizontal divergence has of course the same

possibilities as the present analysis for separating out the divergent wind, but to date it has not been done.

For the reasons set forth above, the results for the divergent wind are presented in this section. Figures 39-41 show the final approximations to the components of $\underline{W}$ at the pressure surfaces 90, 70 and 50 cb, respectively. The top part of each figure is the scalar analysis of the grid-system x component (u) in m sec^{-1}, and the lower half gives the y component (v). For simplicity, terminology such as "westerly" and "southerly", or equivalents, will be used in reference to grid directions. The patterns at the lower boundaries are very weak, but at 70 and 50 cb the respective u and v distributions have characteristic clear-cut patterns. When the 90 cb patterns are analyzed for a smaller interval than the 0.5 m sec^{-1} interval of the figures, the rudiments of the higher-level patterns are apparent. The patterns of u in figs. 40 and 41 are characterized by three centers, roughly along a west-east line some 500 km north of the center of the system. A center of easterly component appears on the north-south axis at the 70 cb level and is more than 3 m sec^{-1} in central value at 50 cb. Centers of maximum westerly component up to 5 m sec^{-1} are found along this line at $3\frac{1}{2}$ grid spacings on either side of the axis. The central value in the northeastern quadrant increases more rapidly with height than in the symmetrical location across the axis, and by 50 cb is stronger by at least a meter per second.

The south-to-north components of the divergent wind are of slightly smaller magnitudes than those in the x direction. The patterns have one center per vortex quadrant, with a change of sign for each 90

Figure 39. Computed divergent wind at 90 centibars.

Top: component in grid system x direction.

Bottom: component in grid system y direction.

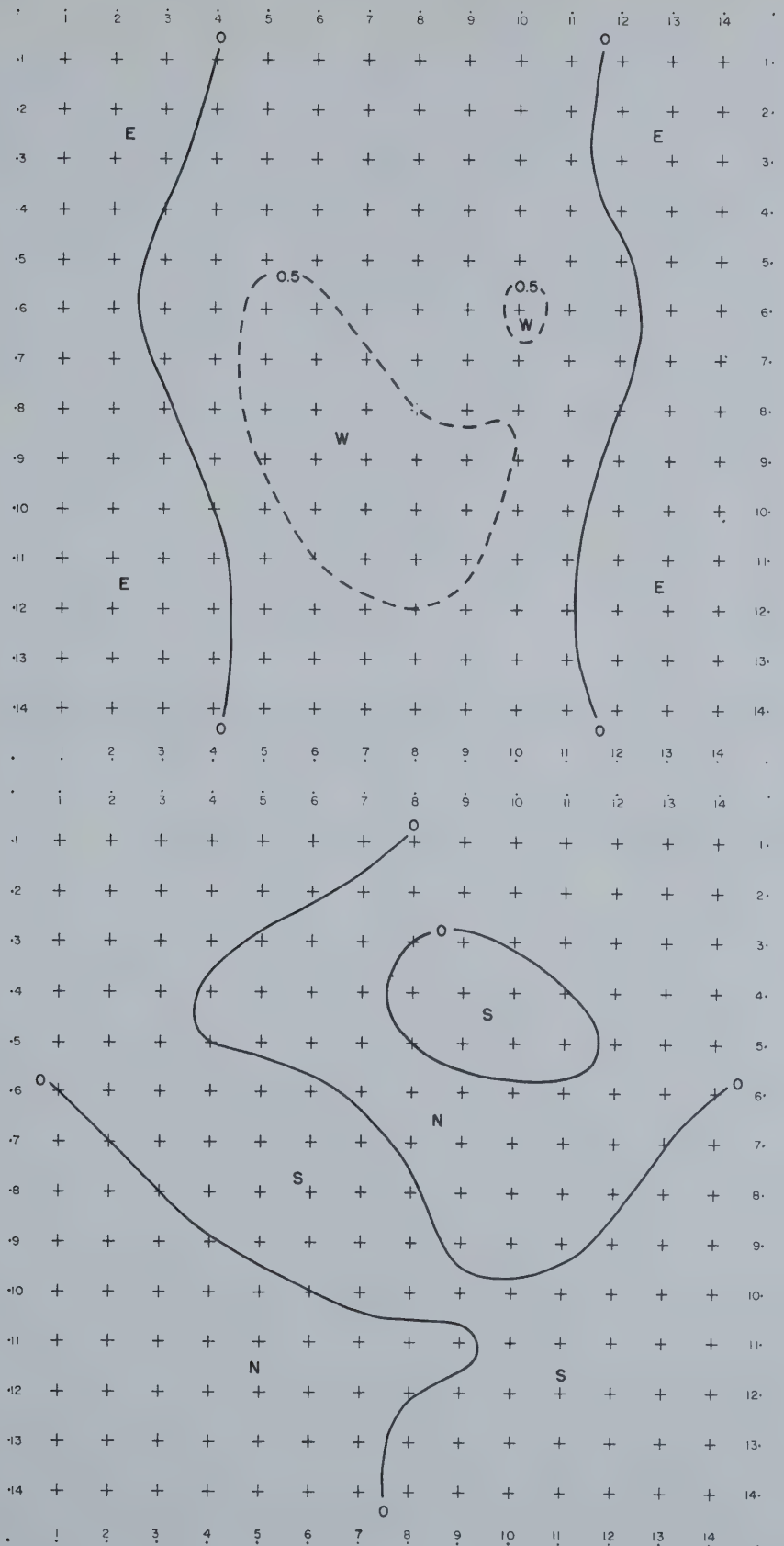

Fig. 39

Figure 40. Computed divergent wind at 70 centibars.

Top: component in grid system x direction.

Bottom: component in grid system y direction.

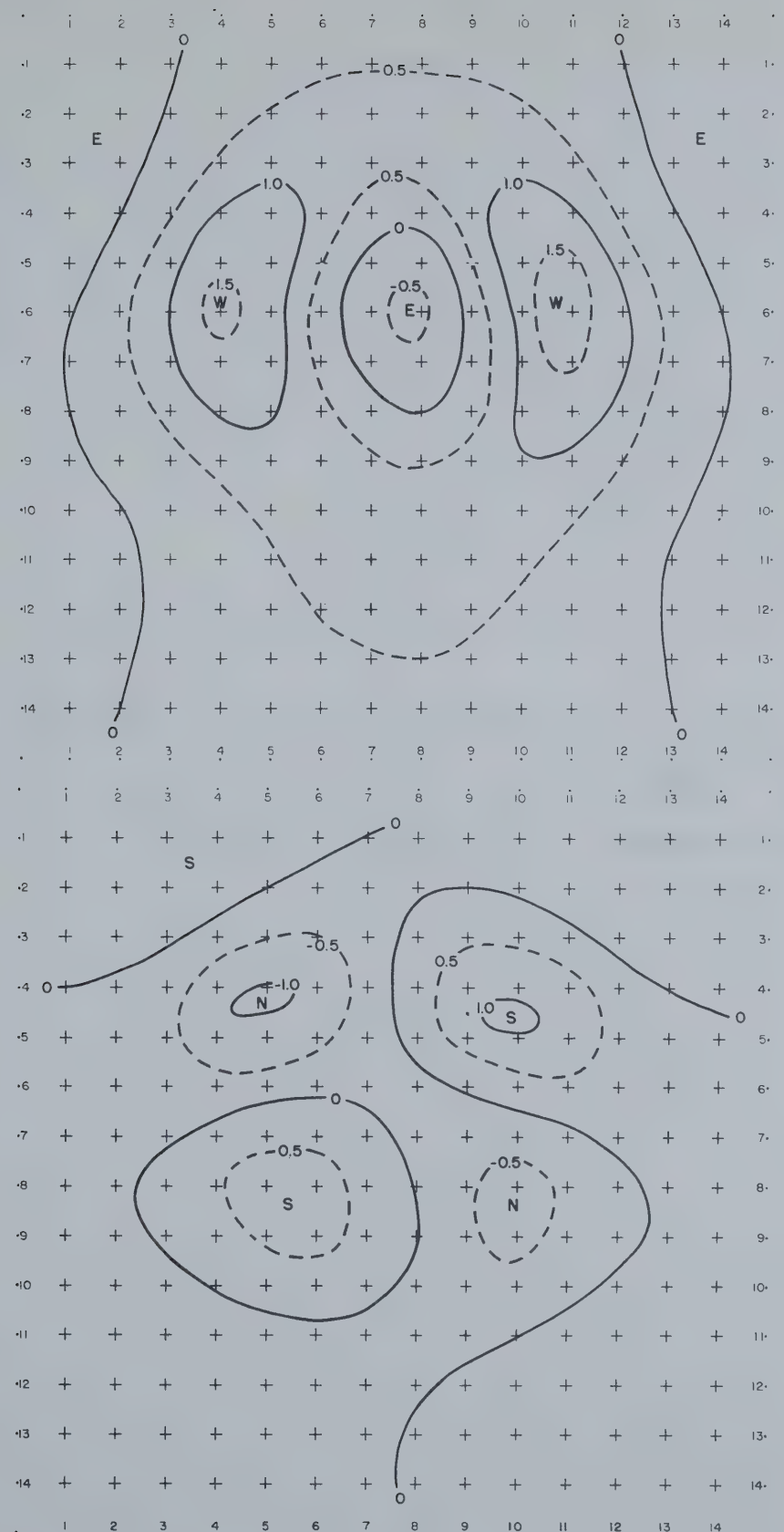

Fig. 40

Figure 41. Computed divergent wind at 50 centibars.

Top: component in grid system x direction.

Bottom: component in grid system y direction.

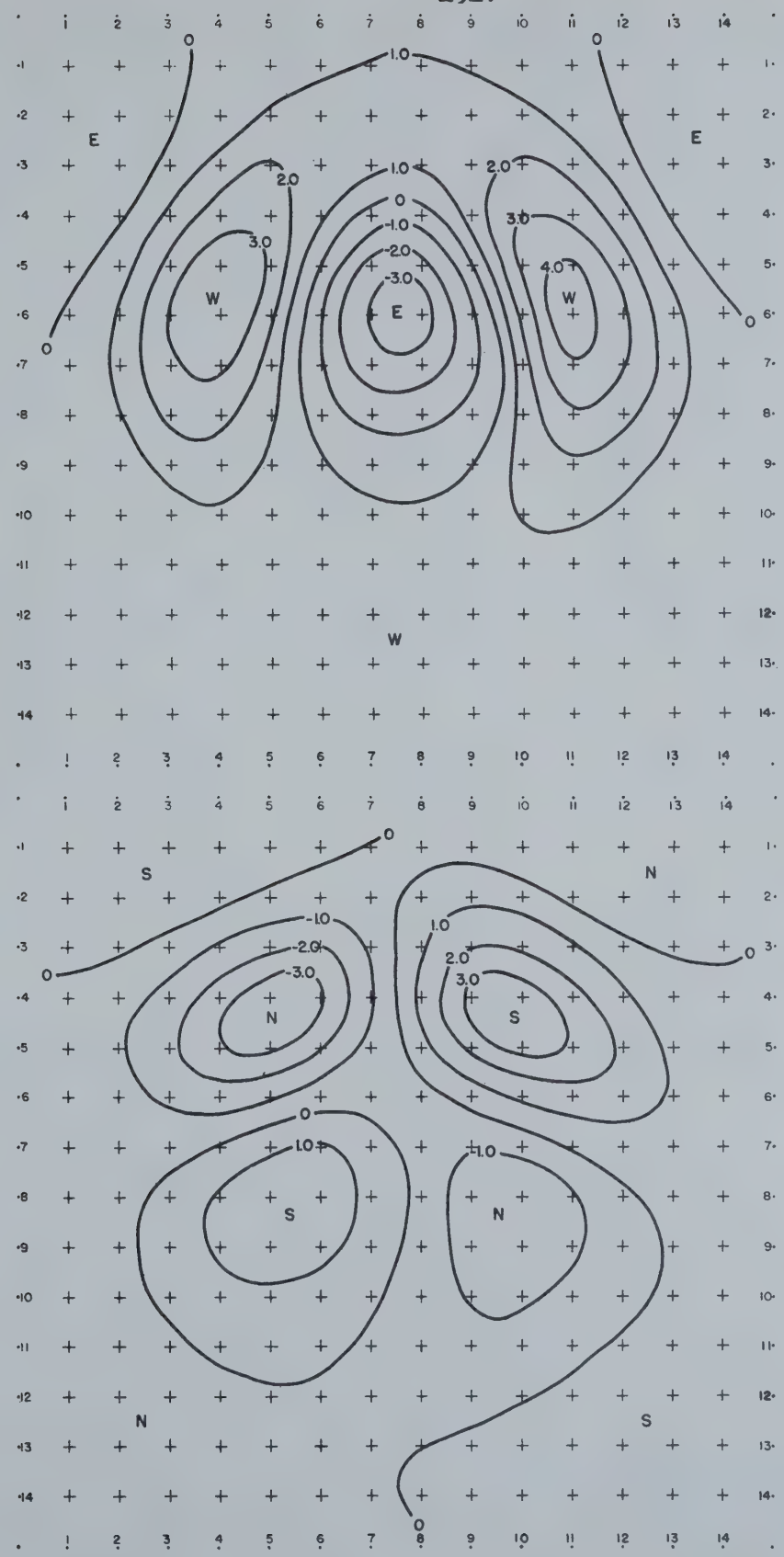

Fig. 41

degrees of azimuth, starting with southerly components in the first quadrant. There tend to be near-zero values along the north-south axis. The divergent wind over the vortex center has a very small northerly component at all levels. The centers of v in the northerly quadrants are about two times as strong as their counterparts to the south. The latter are barely south of the west-east axis, overlapping well into the southern halves of the u-component centers. The effects of the symmetry of the dominant $D^{(0)}$ disturbances are clear in both components.

Table 7 has been prepared to show the extent of the contribution of the divergent wind to the total wind of the system, and the comparison of the magnitudes of the rotational and divergent parts. Since the interest in this respect is largely with regard to occurrences of very large divergent components, we may note that at point 0511 on the 50 cb surface the divergent wind is almost 30 per cent of the nondivergent wind. The averages for the given selection of points are perhaps more significant. At 50 cb the average divergent wind for the sample is 2.6 m sec^{-1}. For the nondivergent component and the total wind the averages are 21.9 m sec^{-1} and 22.2 m sec^{-1}. The magnitude of $\underline{W}$ averages nearly 15 per cent of the magnitude of $\underline{V}_T$. At 70 cb the corresponding statistics are as follows: average $\underline{W}$, 0.9 m sec^{-1}; average $\underline{V}$, 14.7 m sec^{-1}; average $\underline{V}_T$, 14.7 m sec^{-1}; average percentage $|\underline{W}| / |\underline{V}_T|$, 7 per cent. It may be pointed out that the points used are chosen in a pattern favoring regions in which one or the other of the components of $\underline{W}$ is relatively large.

It is natural to wonder how the divergent wind affects the wind field of the total system. The best means for studying this is to

TABLE 7.-Comparison of divergent and nondivergent wind.

Grid Point	V_x	V_y	$\underline{V}$	u	v	$\underline{W}$	$\underline{V}_T$
	meters per second						
90 centibar pressure surface							
0404	+2.47	-4.13	4.81	+0.21	-0.01	0.21	4.81
0405	-0.08	-4.93	4.93	+0.38	-0.08	0.39	4.94
0406	-2.92	-4.23	5.14	+0.40	-0.10	0.41	5.16
0407	-4.83	-1.70	5.12	+0.33	-0.05	0.33	5.13
0408	-4.83	+1.70	5.12	+0.32	+0.06	0.33	5.13
0508	-9.51	+2.94	9.96	+0.27	0.00	0.27	9.96
0509	-7.02	+7.28	10.11	+0.38	+0.08	0.39	10.12
0510	-3.31	+8.30	8.94	+0.48	+0.11	0.49	8.95
0511	+0.04	+6.65	6.65	+0.34	+0.04	0.34	6.66
0604	-0.83	-9.42	9.46	+0.37	+0.09	0.38	9.47
0605	-3.82	-11.99	12.58	+0.58	+0.10	0.59	12.59
0606	-7.13	-10.61	12.78	+0.55	+0.03	0.55	12.79
0607	-9.37	-4.30	10.31	+0.37	-0.09	0.38	10.32
0608	-9.37	+4.30	10.31	+0.26	-0.13	0.29	10.32
0707	-2.99	-5.21	6.01	+0.53	+0.01	0.53	6.03
0708	-2.99	+5.21	6.01	+0.35	-0.12	0.37	6.02
0709	-2.10	+12.83	13.00	+0.35	-0.18	0.39	13.01
0710	-0.79	+14.44	14.46	+0.48	-0.17	0.51	14.47
0711	+0.38	+11.26	11.26	+0.40	-0.11	0.41	11.27
0804	+2.73	-11.15	11.48	+0.24	+0.14	0.28	11.49
0805	+4.08	-14.36	14.93	+0.64	+0.24	0.68	14.94
0806	+5.52	-12.79	13.93	+0.81	+0.25	0.85	13.95
0807	+6.48	-5.20	8.31	+0.68	+0.16	0.70	8.34
0808	+6.48	+5.20	8.31	+0.49	+0.02	0.49	8.32
0908	+13.44	+4.25	14.10	+0.66	+0.11	0.67	14.12
0909	+11.13	+10.46	15.28	+0.58	-0.03	0.58	15.29
0910	+7.69	+11.75	14.04	+0.49	-0.09	0.50	14.05
0911	+4.50	+9.11	10.15	+0.22	-0.02	0.22	10.16

TABLE 7.-Continued

Grid Point	V_x	V_y	$\underline{V}$	u	v	$\underline{W}$	$\underline{V}_T$
	meters per second						
70 centibar pressure surface							
0404	+7.26	-6.76	9.92	+1.03	-0.66	1.22	9.99
0405	+3.50	-7.85	8.59	+1.23	-1.01	1.59	8.74
0406	-0.73	-6.66	6.70	+0.81	-0.95	1.25	6.81
0407	-3.61	-2.65	4.48	+0.29	-0.40	0.50	4.51
0408	-3.61	+2.65	4.48	+0.28	+0.33	0.44	4.50
0508	-11.60	+4.53	12.44	-0.31	+0.19	0.37	12.45
0509	-7.84	+11.23	13.69	+0.49	+0.73	0.88	13.73
0510	-2.28	+12.88	13.08	+1.44	+0.98	1.74	13.20
0511	+2.70	+10.46	10.80	+1.55	+0.78	1.73	10.94
0604	+0.58	-14.56	14.57	+1.61	-0.37	1.65	14.66
0605	-3.88	-18.40	18.80	+1.34	-0.27	1.36	18.85
0606	-8.84	-16.24	18.48	+0.37	-0.13	0.40	18.49
0607	-12.22	-6.58	13.88	-0.44	-0.13	0.46	13.88
0608	-12.22	+6.58	13.88	-0.58	-0.13	0.59	13.89
0707	-3.23	-7.95	8.58	-0.19	+0.12	0.22	8.58
0708	-3.23	+7.95	8.58	-0.41	-0.22	0.46	8.59
0709	-1.89	+19.58	19.67	+0.08	-0.42	0.43	19.67
0710	+0.06	+22.05	22.05	+1.12	-0.34	1.17	22.08
0711	+1.76	+17.26	17.35	+1.63	-0.12	1.63	17.42
0804	+4.85	-17.04	17.72	+1.08	+0.46	1.18	17.75
0805	+6.95	-21.89	22.96	+1.07	+0.75	1.31	23.00
0806	+9.17	-19.47	21.52	+0.67	+0.69	0.96	21.55
0807	+10.65	-7.91	13.26	+0.21	+0.37	0.42	13.27
0808	+10.65	+7.91	13.26	-0.02	-0.07	0.07	13.26
0908	+20.87	+6.47	21.85	+0.43	+0.02	0.43	21.86
0909	+17.35	+15.92	23.55	+0.64	-0.43	0.77	23.56
0910	+12.10	+17.89	21.60	+0.99	-0.63	1.17	21.63
0911	+7.23	+13.88	15.65	+0.94	-0.40	1.02	15.68

TABLE 7.-Continued

Grid Point	V_x	V_y	$\underline{V}$	u	v	$\underline{W}$	$\underline{V}_T$
	meters per second						
50 centibar pressure surface							
0404	+13.78	-10.55	17.35	+2.70	-2.54	3.70	17.74
0405	+8.25	-12.07	14.63	+2.86	-3.52	4.53	15.31
0406	+1.96	-10.17	10.36	+1.14	-3.04	3.25	10.85
0407	-2.32	-4.04	4.66	-0.68	-1.18	1.36	4.85
0408	-2.32	+4.04	4.66	-0.68	+1.15	1.34	4.85
0508	-15.02	+6.83	16.50	-2.55	+0.65	2.63	16.71
0509	-9.42	+16.98	19.43	-0.12	+2.18	2.18	19.54
0510	-1.15	+19.54	19.58	+3.10	+3.26	4.50	20.08
0511	+6.24	+15.98	17.15	+4.04	+2.90	4.97	17.86
0604	+2.40	-22.04	22.17	+4.15	-1.63	4.46	22.61
0605	-4.22	-27.74	28.06	+2.32	-1.03	2.53	28.17
0606	-11.62	-24.44	27.06	-0.97	-0.26	1.00	27.08
0607	-16.65	-9.89	19.37	-3.00	-0.11	3.00	19.60
0608	-16.65	+9.89	19.37	-3.18	-0.17	3.19	19.63
0707	-3.75	-11.94	12.52	-2.42	+0.38	2.44	12.75
0708	-3.75	+11.94	12.52	-2.72	-0.46	2.75	12.81
0709	-1.77	+29.42	29.47	-1.41	-0.99	1.72	29.52
0710	+1.12	+33.17	33.19	+1.65	-0.80	1.84	33.24
0711	+3.62	+26.01	26.25	+3.85	-0.01	3.85	26.53
0804	+7.86	-25.62	26.80	+2.50	+1.10	2.73	26.94
0805	+11.04	-32.89	34.69	+1.22	+1.78	2.16	34.76
0806	+14.40	-29.24	32.60	-0.44	+1.55	1.62	32.64
0807	+16.62	-11.88	20.43	-1.48	+0.73	1.65	20.50
0808	+16.62	+11.88	20.43	-1.78	-0.29	1.80	20.51
0908	+31.67	+9.71	33.13	-0.73	-0.21	0.76	33.13
0909	+26.38	+23.90	35.60	-0.03	-1.24	1.24	35.62
0910	+18.49	+26.87	32.62	+1.28	-1.75	2.17	32.69
0911	+11.16	+20.86	23.66	+1.96	-1.22	2.31	23.77

construct streamline-isovel analyses for the divergent and nondivergent wind fields alone and in combination. It will also be of interest to determine the topography of constant pressure surfaces. These feedbacks into the synoptic considerations of the modeling stage are left as objects of later work.

8. GENERAL DISCUSSION OF RESULTS

The object of the foregoing sections has been to present a model of a cold-low wind field, and a procedure for deduction of implied properties of that model. The investigation defines the problems connected with making an explicit model of an atmospheric system, and develops a useful approach to deduction of the vertical structure of divergence in the system.

Evaluation of the meteorological significance of the results of the present experiment is not easy. There is not enough information for establishment of inter-relationships among data which have been obtained under varying circumstances. In the absence of direct observation of vertical motion, and of sufficiently detailed observations of other more accessible quantities, information can be gotten only by deduction. The premises can be chosen in many different ways. The present study differs from related lines of attack in that it is not directly based upon observation of a particular case. It is an approach to deduction of structure through mathematical modeling. As such, it has the advantage that the subject of investigation is in a clearly-defined category. However, the relationship of the entity studied to observed systems is difficult to define.

The results of this study are in prima facie disagreement with the generalization that to the east of a middle-latitude trough there is convergence in the lower levels and divergence in the upper levels of the troposphere, with upward motion reaching its maximum in the

middle troposphere. The situation in lower levels is modified by frictional convergence. The post-trough region is in general characterized by descending motion. In this investigation the computation of divergence required to maintain a steady state of vorticity in a model cold-low wind field has led to a very different picture. To be sure, the pattern of rising motions with south winds and descending motions with north winds is present to a limited extent. In terms of our treatment of the vorticity equation, its presence in these results is due to the advection of Coriolis parameter. This effect is not as important, however, as that of a relative westerly wind blowing through a ring-shaped maximum of absolute vorticity situated close in to the center of the vortex. The net result is that the strongest features of vertical motion are those of descent in the northeastern quadrant between 425 km and 1275 km from the center, and ascent at the center and in the northwestern quadrant to 1275 km from the center.

Conceivably this discrepancy (if such it is) might be reduced by adjustment of the geometry of the streamline-vorticity isopleth relationships. It is not conceivable that the essential nature of the disagreement can be altered within the existing kinematic framework, viz. that of a vortex imbedded in a relative westerly current. Any reasonable vortex-wind profile will lead to an annular-ring maximum in the vorticity field. It has been learned from this model that westerly zonal flow of a few meters per second combined with such a vortex-vorticity configuration gives a positive center of divergence in the northeast quadrant.

The study of nondivergent wind advection raises some interesting questions. The profile of vortex wind as such is simple and clearly realistic, yet the associated vorticity is not so simple, and may not be realistic. In particular, it would be quite interesting to investigate the existence of observational support for anticyclonic vortex vorticity a few hundred kilometers beyond the radius of maximum vortex wind. Speaking in terms of radial distributions of the form $c = c_o r^N$, the model vortex may be interpreted as a case in which the exponent N depends upon radial distance[1]. In these terms, negative vortex vorticity can be excluded by making N tend to -1 from above for large r. In the vortex wind of the present model, N goes from a value of more than 2 at the center to less than -1 at large r. It might be profitable to study cases of cold cyclones in terms of the presence or absence of negative relative vorticity at some moderately large radial distance (950 km in the model). Although the relative vorticities involved seem to be small, this aspect of structure could conceivably have appreciable significance.

A similar point arises in connection with the relative vorticity of the zonal component. This quantity is negative south of 41°N. The effect is again not a large one in the present model, but one cannot dismiss it as a factor. It also can be adjusted to modify the geometric relationships between the streamlines and vorticity isopleths.

---

[1] This interpretation of the vortex model as a generalization of the Rankine vortex was suggested by Professor Noel E. LaSeur.

Consideration of possibilities for modification of the pattern of vertical motion by provision of different frictional effects, within reason, indicates that such provision can produce an essential change in the mid-tropospheric results only by very selective reinforcement of the divergent-wind advection and vertical-motion effects. It is not known how great an effect can be achieved in this way. A related possibility is that subtle interactions of topographical effects may be a decisive factor in the determination of upper-level vertical motion. This would presuppose a necessary relationship between terrain and locations at which cold lows can be in the postulated steady state. The postulate of simultaneous achievement of zero local rate of change of relative vorticity in wind structures of the type under consideration is plausible, but nevertheless unverified. Since we cannot be certain that the concept has a counterpart in reality, we are not ready to consider what terrain has to do with the occurrence of cold lows with steady-state vorticity.

Directing attention toward the question of how the essentials of the $D^{(0)}$ patterns might be altered, it is recalled that the relationship between the zonal wind and the vortex vorticity gradient is a fundamental factor. It was noted earlier that an easterly relative zonal wind would produce the opposite of the distribution of $D^{(0)}$ which has been found for this model, as far as the important term $\underline{U} \cdot \nabla \zeta_c$ is concerned. The very same vorticity model could be regarded as a permanent-type vorticity system, that is, one in which the vorticity is steady state in a coordinate system moving toward the east at a constant velocity. In such a model, the zonal wind $\underline{U}$ would be easterly relative to the

vortex at lower levels. A large number of interesting variations are possible just using the zonal profile of fig. 1, not to mention the possibilities of other types of latitudinal variation. The results of the present model indicate very positively that a stationary system in westerly zonal flow does not have distinct reversals of sign of divergence along verticals within the troposphere. However, given propagation velocities such that the relative zonal wind is easterly in lower levels, a variety of vertical distributions can be achieved. There is obvious resemblance between these considerations and the Bjerknes-Holmboe deductions for trough-ridge systems in baroclinic westerlies [52].

Consideration of the bases for deduction of the distribution of divergence and vertical motion relative to trough in westerly flow, whether these be theoretical [52] or observational [53], points up the reasons why the present study should not necessarily be expected to conform to the generalizations suggested by such processes of deduction. There naturally are differences between open troughs and vortices, and between the structure of a developing vortex and an upper-tropospheric vortex which has reached maturity in the sense of time-changes of relative vorticity.

Valid standards of comparison for the system studied in this investigation may be sought among studies of maturing cold-core vortices. The comparisons should ideally be restricted to those real situations which most nearly conform to the conditions of the model. There is a dearth of case studies in the latter restricted category, especially insofar as the requirement of steady-state vorticity is concerned.

Further pursuit of the present line of numerical experimentation demands intensive study of observed cold lows. Such a study should investigate whether or not the local rate of change of vorticity can reasonably be neglected in any cold lows. If the concept of a class of cold lows with nearly steady-state vorticity has physical meaning, we can better define the characteristics of a model which represents this class.

The deduced structure of the present model has been considered in relation to a limited number of case-studies which may be pertinent prototypes. The conclusions drawn from such comparisons will now be discussed briefly. A thorough evaluation of the status of the present experiment as a meteorologically significant study is neither possible nor appropriate at this stage. More detailed consideration of the case studies upon which this discussion is based will be included in a later report.

Reed [16] and Palmén and Nagler [54] have used individual cold-low case studies to construct provisional schematics of structure. They seek to deduce vertical-motion and/or horizontal-divergence fields required for dynamic consistency in development and maintenance of the observed fields of mass and motion in selected cold lows. Reed, in particular, sought to reconcile increases of cyclonic vorticity at the tropopause level with the divergence required in the "centrifugal pump" model first proposed by V. Bjerknes [55]. Using wet-bulb potential temperature as a tracer, Reed deduced a scheme of three-dimensional motions relative to the trough line of a developing and moving vortex by construction of trajectories. The deduction of divergence distribution in the same coordinate system are further checked by use of the

trajectories in conjunction with the Ertel vorticity theorem [56]. The analysis is very convincing, and must be reconciled with the "centrifugal pump" model if the latter is to be applied to the development and maintenance of the full-fledged cold-low stage, as had been done by Hsieh [7]. The scheme obtained by Reed is generally similar to that found by Fleagle [53], discussed above. The part of the total period (1500 GCT 11 March to 0300 GCT 13 March 1951) for which the system was a deep closed system was only the last twelve hours. Hence comparison of the present model with these results is subject to reservations similar to those mentioned with respect to developing troughs.

Palmén and Nagler made a detailed synoptic analysis of the case of 3-7 February 1947. They consider the temperature field in cross-section along a contour line in the belt of strongest wind on the 200 mb surface to make a qualitative reconstruction of the three-dimensional air flow just above and below the tropopause. The vertical motions obtained were applicable at 0300 GCT 5 February 1947. The system considered was well-developed at this time, but never became a cut-off cold low. The scheme of circulation is derived under a number of assumptions. It is of interest in the present context in that it introduces a new element into the idealizations of vertical circulation available for consideration. As shown in schematic representation, there is cross-stream vertical circulation in the southern quadrants. This is to be superimposed upon general subsidence to the west of the trough line and ascent to the east of the trough line, since the considerations on which the deduction is based do not give an absolute picture.

The air under the frontal surface in the southwest quadrant has a component toward the northeast near the surface and upwards near the center. Above the front the cross-stream circulation in the troposphere is completed by a northeast component near 300 mb, and descent in the farther southwest. Above this circulation there is one of reverse sense, producing downward motion of the extra-tropical tropopause over the central region of the wind dome. A similar scheme of relative vertical motions is shown for the southeastern quadrant in a vertical cross-section running toward the southeast from the cold dome. Looking in the direction of the flow from a point south of the center on the trough line, one would see the sense of the cross-stream circulation to be counter-clockwise. This means downward motion below the frontal surface in the southeastern quadrant. In the same vertical plane, a stratospheric cross-stream circulation meshes with the tropospheric cell and straddles the extra-tropical tropopause. There is apparently no element of superimposed circulation in the central region of the cold dome.

There is some suggestion in the present results that this scheme is partially carried out in the absolute motion of a cut-off cold low at maturity. The Palmén-Nagler case is a better standard of comparison than those considered so far only in that the vertical circulation presented is for a system definitely classified as a deep high-level cyclone. It is not otherwise a member of the class represented by the present idealization since it is never cut off from the maximum westerlies, nor is it ever a permanent-type system.

The case of 0300 GCT January 1953 was used as a guide in precription of features of the model wind field. It can not be considered a prototype, but it is in many respects the closest of those cases for which independently derived information on structure is available. The whole month of January 1953 is a much-analyzed period. Published work of Arnason [41] deals with the period 1500 GCT 27 January to 0300 GCT 28 January. His study is on analysis of large-scale fields of vertical component of velocity and horizontal divergence by an adiabatic method of computing vertical motion from averaged contour patterns. The raison d'etre and objectives of his study are very much the same as those of this work. Both seek ultimately to provide what Palmén and Nagler [54, p. 236] may have had in mind in the following portion of their discussion of cross-stream vertical circulation:

> "The three-dimensional air flow between the ridge and the trough is evidently extremely complicated and a complete solution of the problem . . . would involve a discussion of the whole vorticity problem and its connection with the divergence field."

The results published by Arnason pertain to a synoptic situation which is in no way suited for comparison with a cold-low model. However, his published work was the pilot project for a similar treatment of twenty-five 12-hour periods of January 1953 on the MIT Whirlwind I electronic digital computer. The output for the period 0300 GCT 9 January - 0300 GCT 10 January was obtained by personal communication[1].

---

[1]Thanks are due J. M. Austin, Department of Meteorology, Massachusetts Institute of Technology, for his willingness to loan these unpublished results.

It has been studied closely in comparison with the results of the present research.

No detailed account of the conclusions drawn from comparison of the MIT data can be made meaningful without extensive presentation of their bases, and none will be attempted at the present time. Arnason's method is to compute the vertical motion by an adiabatic method. The horizontal divergence is obtained from the continuity equation. One salient point of this method is that when the terms of the vorticity equation are computed with the smoothed observations and computed quantities of the Arnason procedure, it is common to find that the vorticity equation does not balance. This suggests the question of whether or not the thermodynamic energy equation is satisfied by the results of the present study. This question is parallel to asking if the results of the Arnason procedure are consistent with the vorticity equation, which for it is an independent check as consistency of the field of temperature change is for our procedure.

The MIT-computed mean values of divergence and vertical motion in the 12-hour periods preceding and following 0300 GCT 10 January 1953, it may also be reported, differ from one another about as much as from those of our model. Only in a very generalized sense is the descent-from-ridge-to-trough, ascent-from-trough-to-ridge scheme carried out. Considering these points in connection with other suggestions of the vertical circulations in and surrounding a cut-off cold dome, one can only conclude that no one scheme can be considered to be established in perference to the others. The explanation for such a plethora of structures on the scale smaller than the

ridge-to-ridge distance in the basic current may be due to variations of the stage of life cycle to which the various sets of results apply. In this point of view, the reason that the present model has a more marked departure from Fleagle's deduction for developing troughs is that it, more than any of the others, is a deep high-level cyclonic vortex, mature in a very clearly-defined (and possibly unrealistic) sense.

There is another independent source of information on the 10 January 1953 case. The whole month of January was the subject of an experiment with the thermotropic and barotropic numerical forecasting models by the Numerical Prediction Project of the Geophysics Research Directorate and the Air Weather Service [57]. The thermotropic results are of some interest in the present context. The thermotropic procedure gave a mean value of vertical velocity for the 1000-500 mb layer at 1500 GCT on 9 January and on 10 January. The hour of interest is midway through this period. There was little change in the nature of the system in 24 hours, especially with regard to its mid-tropospheric part and the second twelve hours. Yet the layer-average instantaneous vertical motion on 10 January was virtually featureless in the region of the cold low, in marked contrast to 9 January. At the beginning of the period there was a 4 cm sec^{-1} center of upward motion at 2 o'clock from the center, with weak upward motion to a short distance behind the axis and weak downward motion elsewhere to the west for a long distance. Twenty-four hours later the system had moved about $3\frac{1}{2}$ latitude degrees to the east-northeast (eastward movement of 3 degrees in the first twelve hours and northeastward movement of 1 degree in the second twelve hours). The vertical

motion at the end of the period was less than 2 cm sec^{-1} everywhere in the region of the low. The zero line meandered in through the northwest quadrant, crossed the axis just north of the center, and bulged eastward to indicate weak downward motion to a distance of 4 latitude degrees eastward of the axis. This observation is further evidence that no single pattern of distribution of vertical motion is associated with the configuration of height fields that we choose to label "cold low".

It is of interest to note that the MIT results and the GRD results both indicate a definite change in the structure of the system at some time near 0300 GCT 10 January 1953. The choice of this system as a general guide to the model for the present study is loosely supported by these indications that some kind of turning point was passed at the time in question.

The computed structure of the model shows downward motion in the northeastern quadrant and upward motion over the center and to the northwest. Even though the model was not intended to be judged as a mathematical representation of the 10 January 1953 case, precipitation maps were prepared for the latter. Hourly precipitation data for the period 0200-0400 GCT give uncertain support to the vertical-motion distribution of the model. There was no rain for 450 km northeastward from the center. The rain area beginning at that distance to the northeast is over the foothills and mountains of North Carolina and Tennessee, and is therefore complicated by orographic factors. There is another rain area centered 450 km north of the 0300 GCT position of the low center, with no particular

orographic reason for its presence there. This region of rain occurrence is more or less connected to another just over the center of the low. The sizes, shapes and locations of the regions of rain and no rain correspond very roughly with the relatively regular and extensive regions of upward and downward motion in fig. 34, for example. There are elements of contradiction and elements of support to the degree of unsatisfactory indeterminacy usually found in comparisons of this sort. As a subjective judgement, the agreement between rainfall patterns and thermotropic layer-average vertical motions or the MIT-computed time-averaged vertical motions is no better than between rainfall and computed vertical motion for the steady-state vorticity model.

9. CONCLUSION

The meaning of "numerical experiment" as applied to this work is in essence the simplest of concepts. The method is to substitute numbers for some of the physical variables in a set of relationships whose properties are of interest. If the relationships are a complete set of constraints for the circumstances under consideration, they may then be solved for those members which have not been specified. The desired product is increased understanding of atmospheric processes.

Meteorological theory contains many examples of chains of reasoning based upon simplified and/or specialized forms of the basic equations. Although such deductive exercises sometimes provide valuable physical insight, their resolving power is limited. There is considerable dependence upon intuition, and sometimes there are disturbing elements of ad hoc assumption. Even though these may turn out to be valid, it is desirable that they be replaced by the drawing of rigorous implications for realistically complex circumstances. In order to do this, meteorologists have turned to the use of high-speed computing aids.

The experiment reported here undertook to follow through the implications of the constraints exercised by the hydrostatic, continuity and vorticity equations upon the structure of horizontal divergence and vertical motion. These constraints are placed upon a mathematically modeled distribution of vorticity in the steady state. As is to be expected in most experiments in numerical deduction, several

questions of the validity of numerical processes arise. One purpose of the study was to develop and show the efficacy of a certain numerical process for application of the vorticity method of computing vertical motion. As a meteorological research, questions of the design of the experiment from the point of view of realism of the assumed circumstances and results are not only present but mixed up together. This study had the corollary purpose of trying out a model whose properties are clearly defined and as realistic as practicable and desirable in an exploratory study. Lest the question of success or failure in this corollary purpose appear ambiguous, it may be pointed out again that "trying-out" of the model has meant observing why it behaves as it does and how this may be improved.

This numerical experimentation has accomplished what it set out to do. Its purposes have been achieved with certain limitations whose assessment depends upon further study. With respect to aspects of meteorological significance, a degree of limitation on the meaningfulness of the results is present, though difficult to evaluate. Above all, this undertaking is most satisfactory from the point of view of provision of clear signposts to directions of profitable further study.

As indicated by considerations presented in section 6, every available basis for evaluation of the mathematical aspects of procedure points toward their validity. There is work yet to be done in refinement of method and further evaluation of procedure. Rigorous analysis of the question of ultimate convergence to a solution is desirable.

Though effects of boundary value prescription are thought not likely to be the potential source of trouble which they are in the initial-value problems of the field of numerical prediction [58, 59], these effects should be included in any further study of the procedure. Boundary conditions undoubtedly have some bearing on existence of solutions, and may have importance in regard to choices of finite-difference approximations.

In regard to meteorological usefulness of the experiment in itself, it was perhaps to be expected that the analysis of this model would further muddy the waters to about the same extent as one more case study would have done. One is in no better position to assert that characteristic fields of vertical motion and horizontal divergence in a cut-off high-level cyclone are "thus, and so". Yet the effort has not been futile, in spite of the equivocal nature of some of the synoptic-meteorological aspects of the conclusions. The computed implications of the idealized model clearly show the following things:

1. The geometry of the vorticity isopleths and streamlines in a circular vortex imbedded in relative westerlies has important consequences in computation of vertical motions by the vorticity method. Note is made in section 8 of the many possibilities opened when eastward translation of the system is allowed. It should be of considerable value to go on from there to develop the picture of the cutting-off process and the cut-off state in terms of the configuration of the vorticity distribution and the relative westerly component of the basic flow. The present model is not too elementary a starting point for such a project.

2. The balance of the vorticity equation in a cold-low with zero local rate of vorticity change is not achieved by cancellation of nondivergent-wind advection against the "zeta-dee" term. Advection of vorticity by the irrotational component of the wind, vertical advection of vorticity and the tipping term are each big enough at times that only in a very crude way can they be disregarded. The average absolute value of the vertical-motion corrections at the points of Table 5 is thirty per cent of the initial divergence approximation. Divergent-wind advection averages more than one-third of the same basic comparison term. A rather systematic tendency to cancellation between these two divergence-linked effects is emphasized by the fact that the average absolute value of their algebraic sum $D^{(F)}-D^{(0)}$ has a value of one-fourth the sum of their individual average absolute values. A similar balancing within the vertical-motion increment itself has been explicitly considered in section 7. It is readily conceivable that in other models, with less symmetry and greater nondivergent-wind advection of vorticity, the divergence-linked terms could reinforce rather than cancel. There is no apparent reason to expect that inclusion of non-zero vorticity tendency should lessen the importance of these terms.

3. Further extension of the kind of mathematical modeling attempted in this research calls for development of additional case studies from which the essential common characteristic of such synoptic entities can be more completely determined. In any case, more elaborate provisions with regard to the lower layers of the model are required in order to realize the hoped-for reliable deductions of unobservable quantities. Since such provisions themselves concern unobservables, the

available means for carrying out this objective is extension of the governing system to include relationships which act as consistency checks upon modeling of case-study generalizations.

Integration to the 500 mb surface does not yet reveal any sign of a surface of "least divergence" [60]. Indeed, the integration did not have to be carried any further than 500 mb because the trend was so clear. This raises questions to be considered in connection with item 1, above, and the need for systematic case studies guided by the present results. What is the reason for the vertical orientation of the computed divergence isopleths? Can a level of maximum vertical motion be achieved within the troposphere, in any way other than by having relative easterly motion in the lower layers?

All of the above items are in one way or another connected with the hypothesis that zero local rate of change of vorticity is a key to characterization of the cut-off high-level cyclone. Its unknown degree of validity plagues attempts at interpretation of the results of this model on the basis of comparison with case studies. Possible ways of circumventing this difficulty are to make local rate of vorticity change a dependent variable in an extended set of governing equations, or to include its distribution as the object of case studies. Alternatively one may seek elsewhere for situations of practical interest in which it is clearly permissible to assume that vorticity is constant with time. For example, Mantis [61] has dealt with the mature tropical cyclone as an appropriate subject for such an assumption. Perhaps the wind field of a mature tropical cyclone is by this time known in depth with sufficient exactitude that a

modeling approach similar to that of this experiment can contribute to understanding of warm-core vortices. From the point of view of using relative vorticity distribution to characterize motion systems, the existence of vortex structure is a more fundamental characteristic than scale. It is interesting to note that detailed information on the structure of wind fields in hurricanes demonstrates the existence of an annular ring of maximum vorticity [62], though of course on a reduced scale and with greater complexity of detail than in the present cold-low model.

REFERENCES

1. Richardson, T. F., 1922: Weather prediction by numerical process. Cambridge, University Press, 236 pp.

2. Charney, J., 1951: Dynamic forecasting by numerical process. Compendium Meteor., Boston, Amer. meteor. Soc., 599-620.

3. Charney, J., and A. Eliassen, 1949: A numerical method for predicting perturbations of the middle latitude westerlies. Tellus, 1, 38-54.

4. Eliassen, A., 1949: The quasi-static equations of motion with pressure as independent variable. Geof. Publ., Vol. XVII, No. 3.

5. Haltiner, G. H., and F. L. Martin, 1957: Dynamical and physical meteorology. New York, McGraw-Hill, 470 pp.

6. Sherman, Leon, 1953: Estimate of the vertical velocity based on the vorticity equation. J. Meteor., 10, 399-400.

7. Hsieh, Yi-Ping, 1949: An investigation of a selected cold vortex over North America. J. Meteor., 6, 401-410.

8. Palmén, E., 1949: On the origin and structure of high-level cyclones south of the maximum westerlies. Tellus, 1, 22-31.

9. Phillips, H. B., 1933: Vector analysis. New York, John Wiley and Sons, 236 pp.

10. Sherman, Leon, 1952: On the scalar-vorticity and horizontal-divergence equations. J. Meteor., 9, 359-366.

11. Palmén, E., 1951: Aerology of extratropical disturbances. Compendium Meteor., Boston, Amer. meteor. Soc., 599-620.

12. Peterson, Roy, 1956: A comparison of relative vorticities computed from geostrophic and observed winds. Technical Paper No. 5, Project SCUD, Contract Nonr 285(09), N.Y.U., 45 pp.

13. Spar, Jerome, E. L. Fisher, E. Paroczay, and R. E. Peterson, 1955: Evaluation of terms in the vorticity equation. Progress Report No. 1, Project SCUD, Contract Nonr 285(09), N.Y.U., 34 pp.

14. Deardorff, J. W., 1957: The spatial distribution of vertical motion within a mature cyclonic vortex. Sci. Rept. No. 3, AF Contract 19(604)-314, Univ. of Wash., 46 pp.

15. Tojo, S., 1953: The dynamics of a vortex imbedded in a constant zonal current. J. Meteor., 10, 175-178.

16. Reed, Richard J., 1953: A synoptic study of the mechanics of cold-low formation. M.I.T. Tech. Rept. No. 13, ONR Contract N5ori-07804, 19 pp.

17. Headquarters, Air Weather Service, 1945-1948: Northern hemisphere historical weather maps, sea level and 500 millibar. Washington, D. C.

18. U. S. Weather Bureau, 1949-1953: Daily series synoptic weather maps, part 1, northern hemisphere sea level and 500 millibar charts. Washington, D. C.

19. Sumner, E. J., 1953: Coldpools: a statistical and synoptic study. Met. Mag., 83, 291-301.

20. Cressman, G. P., 1954: An approximate method of divergence measurement. J. Meteor., 11, 83-90.

21. Cressman, G. P., 1953: An application of constant vorticity charts. J. Meteor., 10, 17-24.

22. Petterssen, S., 1953: On the relationship between vorticity, deformation and the configuration of the pressure field. Tellus, 5, 231-237.

23. Kuo, Hsiao-Lan, 1955: On quasi-nondivergent prognostic equations and their integration. Sci. Rept. No. 2, General Circulation Project, M.I.T., 42 pp.

24. Bolin, B., 1955: Numerical forecasting with the baroclinic model. Tellus, 7, 27-49.

25. Charney, J., 1955: The use of the primitive equations of motion in numerical prediction. Tellus, 7, 22-26.

26. Holmboe, J., G. E. Forsythe and W. S. Gustin, 1945: Dynamic meteorology. New York, John Wiley and Sons, 378 pp.

27. James, R. W., 1950: On the theory of large-scale vortex motion in the atmosphere. Quart. J. R. meteor. Soc., 76, 255-276.

28. Knighting, E., 1950: Large scale vortex motion in the atmosphere. (Correspondence). Quart. J. R. meteor. Soc., 77, 136-137.

29. James. R. W., 1950: Reply. (Correspondence). Quart. J. R. meteor. Soc., 77, 137-138.

30. Goldie, A. H. R., 1939: Depressions as vortices. Geophys. Mem., No. 79, 18 pp.

31. Brunt, David, 1939: Physical and dynamical meteorology. Cambridge, University Press, 428 pp.

32. Sherman, Leon, 1952: A numerical forecasting investigation, part I: theory. Technical Report, Contract Nonr-158(00), Fla. State Univ., 20 pp.

33. Deetz, C. H., and O. S. Adams, 1944: Elements of map projection. C. and G. S. Spec. Pub. No. 68. Washington, D.C., Government Printing Office, 226 pp.

34. Petterssen, S., 1956: Weather analysis and forecasting, vol. 1, motion and motion systems. New York, McGraw-Hill, 428 pp.

35. Saucier, W. J., 1955: Principles of meteorological analysis. Chicago, Univ. of Chicago Press, 438 pp.

36. Adams, O. S., 1918: General theory of Lambert conformal conic projection. Washington, D.C., Government Printing Office, 38 pp.

37. Palmén, E., 1948: On the distribution of temperature and wind in the upper westerlies. J. Meteor., 5, 20-27.

38. Charney, J., and N. A. Phillips, 1953: Numerical integration of the quasi-geostrophic equations for barotropic and simple baroclinic flows. J. Meteor., 10, 71-99.

39. Southwell, R. V., 1949: Relaxation methods in theoretical physics. London, Oxford University Press, 248 pp.

40. Thompson, P. D., and W. L. Gates, 1956: A test of numerical prediction methods based upon the barotropic and two-parameter baroclinic models. J. Meteor., 13, 127-141.

41. Arnason, G., 1955: A case study of the field of large-scale vertical velocity and horizontal divergence. M.I.T., Tech Rept. No. 16, ONR Contrac N5ori-07804, 70 pp.

42. Hildebrand, F. B., 1952: Methods of applied mathematics. Englewood Cliffs, N. J., Prentice-Hall, 523 pp.

43. Fjørtoft, R., 1952: On a numerical method of integrating the barotropic vorticity equation. Tellus, 4, 179-194.

44. Thompson, P. D., 1955: An iterative method for solving an elliptic equation with variable coefficients and its convergence. Tech. Mem. No. 5, Joint Numer. Wea. Prediction Unit, Suitland Md., 10 pp.

45. Scarborough, J. B., 1955: Numerical mathematical analysis. Baltimore, The Johns Hopkins Press, 554 pp.

46. Kunz, K. S., 1957: Numerical analysis. New York, McGraw-Hill, 381 pp.

47. Comrie, L. J., 1949: Chamber's six-figure mathematical tables, vol. II, natural values. New York, Van Nostrand, 576 pp.

48 Hildebrand. F. B., 1956: Introduction to numerical analysis. New York, McGraw-Hill, 511 pp.

49. Milne, W. E., 1953: Numerical solutions of differential equations. New York, John Wiley and Sons, 275 pp.

50. Thompson, P. D., 1956: A theory of large-scale disturbances in nongeostrophic flow. J. Meteor., 13, 251-261.

51. Thompson, P. D., 1956: A two-parameter nongeostrophic model suitable for routine numerical weather forecasting. Tech. Mem. No. 11, Joint Numer. Wea. Prediction Unit, Suitland, Md., 15 pp.

52. Bjerknes, J., and J. Holmboe, 1944: On the theory of cyclones. J. Meteor., 1, 1-22.

53. Fleagle, R. G., 1947: The fields of temperature, pressure, and three-dimensional motion in selected weather situations. J. Meteor., 4, 165-185.

54. Palmén, E., and K. M. Nagler, 1949: The formation and structure of a large-scale disturbance in the westerlies. J. Meteor., 6, 227-242.

55. Bjerknes, V., 1923: Dynamics of the circular vortex. Geof. Publ., Vol. II, No. 4.

56. Ertel, H., 1942: Ein neuer hydrodynamischer wirbelsatz. Met. Zeit., 59, 277-281.

57. Gates, W. L., L. S. Pocinki and C. F. Jenkins, 1955: Results of numerical forecasting with the barotropic and thermotropic models. Geophysics Res. Papers, No. 46, 168 pp.

58. Platzman, G. W., 1954: The computational stability of boundary conditions in numerical integration of the vorticity equation. Archiv für Meteor., Geophys. und Bioklim., 7, 29-40.

59. Gates, W. L., 1957: Hemispheric numerical forecasting with the barotropic model, and some remarks on boundary-condition error. J. Meteor., 14, 332-342.

60. Landers, H., 1955: A three-dimensional study of the horizontal velocity divergence. J. Meteor., 12, 415-427.

61. Mantis, H. T., 1950: A model of a tropical cyclone in the steady state. Met. Papers, Vol. I, No. 3, N.Y.U., 39 pp.

62. Blumen, W., and N. E. LaSeur, 1958: Some details of the wind field in individual hurricanes. Sci. Rept. No. 7, AF Contract 19(604)-753, Fla. State Univ., 45 pp.

CONTRACT NO. Nonr 1600 (00)
NR NO. NR 082-071

DISTRIBUTION LIST FOR UNCLASSIFIED TECHNICAL REPORTS

Addressee	No. of Copies
Geophysics Branch, Code 416, Office of Naval Research, Washington 25, D. C.	2
Director, Naval Research Laboratory, Attention: Technical Information Officer, Washington 25, D. C.	6
Officer-in-Charge, Office of Naval Research London Branch Office, Navy No. 100, Fleet Post Office, New York, New York	2
Office of Naval Research Branch Office, 150 Causeway Street, Boston, Massachusetts	1
Office of Naval Research Branch Office, 346 Broadway, New York 13, New York	1
Office of Naval Research Branch Office, Tenth Floor, The John Crerar Library Building, 86 East Randolph Street, Chicago, Illinois	1
Office of Naval Research Contract Administrator, Southeastern Area, c/o George Washington University, 2110 G. Street, N. W., Washington 7, D. C.	1
Office of Naval Research Branch Office, 1030 East Green Street, Pasadena 1, California	1
Office of Naval Research Branch Office 1000 Geary Street, San Francisco, California	1
Office of Technical Services, Department of Commerce, Washington 25, D. C.	1
Armed Services Technical Information Agency, Arlington Hall Station, Arlington 12, Virginia	10
Assistant Secretary of Defense for Research and Development, Attention: Committee on Geophysics and Geography, Pentagon Building, Washington 25, D. C.	1
Department of Aerology, U. S. Naval Post Graduate School, Monterey, California	1
Bureau of Aeronautics (AY), Navy Department, Washington 25, D. C.	1

Mechanics Division, Naval Research Laboratory Anacostia Station, Washington 20, D. C., Attention: J. E. Dinger, Code 3820 1

Radio Division I, Code 3420, Naval Research Laboratory Anacostia Station, Washington 20, D. C. 1

Meteorology Section, Navy Electronics Laboratory, San Diego 52, California, Attention: L. J. Anderson 1

Library, Naval Ordinance Laboratory, White Oak, Silver Spring 19, Maryland 1

Bureau of Ships, Navy Department, Washington 25, D. C. Attention: Code 327 (Technical Library) 2

Chief of Naval Operations, Navy Department, Washington 25, D. C., Attention: Op-533D 2

Oceanographic Division, U. S. Navy Hydrographic Office, Suitland, Maryland 2

Library, Naval Ordnance Test Station, Inyokern, China Lake, California 1

Project AROWA, U. S. Naval Air Station, Building R-48, Norfolk, Virginia 2

The Chief, Armed Forces Special Weapons Project, P. O. Box 2610, Washington,D. C. 1

Office of the Chief Signal Officer, Engineering and Technical Service, Washington 25, D. C., Attention: SIGGGM 1

Meteorological Branch, Evans Signal Laboratory, Belmar, New Jersey 1

Office of the Quartermaster General, 2nd and T Sts., Washington 25, D. C., Attention: Environmental Protection Section 1

Office of the Chief, Chemical Corps, Research and Engineering Division, Research Branch, Army Chemical Center, Maryland 2

Commanding Officer, Air Force Cambridge Research Center, 230 Albany Street, Cambridge, Massachusetts, Attention: ERHS-1 1

Headquarters, Air Weather Service, Scott Air Force Base, Illinois, Attention: Director, Scientific Services 2

Commanding General, Air Material Command, Wright Field, Dayton, Ohio, Attention: MCREEO 1

Commanding General, Air Force Cambridge Research Center, 230 Albany Street, Cambrdige, Massachusetts, Attention: CRHSL 1

Commanding General, Air Research and Development Command, Andrews Air Force Base, Washington 25, D. C., Attention: RDDG 1

Department of Meteorology, Massachusetts Institute of Technology, Cambridge, Massachusetts 1

Department of Meteorology, University of Chicago, Chicago 37, Illinois 1

Institute for Advanced Study, Princeton, New Jersey 1

Scripps Institute of Oceanography, La Jolla, California 1

General Electric Research Laboratory, Schenectady, N. Y. 1

St. Louis University, 3621 Olive Street, St. Louis 8, Mo. 1

Department of Meteorology, University of California at Los Angeles, Los Angeles 24, California 1

Department of Engineering, University of California at Los Angeles, Los Angeles 24, California 1

Woods Hole Oceanographic Institution, Woods Hole, Massachusetts 1

The Johns Hopkins University, Department of Civil Engineering, Baltimore, Maryland 1

The Johns Hopkins University, Department of Physics, Homewood Campus, Baltimore, Maryland 1

New Mexico Institute of Mining and Technology, Research and Development Division, Socorro, New Mexico 1

Geophysical Institute, University of Alaska, College, Alaska, Attention: C. T. Elvey 1

Blue Hill Meteorological Observatory, Harvard University, Milton 86, Massachusetts 1

Laboratory of Climatology, Johns Hopkins University, Seabrook, New Jersy 1

Department of Meteorology, New York University, New York 53, New York 1

Texas A and M, Department of Oceanography, College Station, Texas 1

Rutgers University, College of Agriculture, Department of Meteorology, New Brunswick, New Jersey 1

National Advisory Committee of Aeronautics, 1500 New Hampshire Avenue, N. W., Washington 25, D. C. 2

U. S. Weather Bureau, 24th and M Sts., N. W., Washington 25, D. C., Attention: Scientific Services Division 2

Air Coordinating Committee, Subcommittee on Aviation Meteorology, Room 2D889-A Pentagon, Washington 25, D. C. 1

American Meteorological Society, 3 Joy Street, Boston 8, Massachusetts, Attention: The Executive Secretary 1

Research Professor of Aerological Engineering, College of Engineering, Department of Electrical Engineering, University of Florida, Gainesville, Florida 1

University of Pennsylvania, Department of Meteorology, Philadelphia, Pennsylvania 1

Director of Research, Munitalp Foundation, Inc., 36th Floor, 570 Lexington Avenue, New York 22, New York 1

Chief Scientist, U. S. Navy Sofar Station 8, APO 856, c/o Postmaster, New York, New York 1

Commanding General, Quartermaster Research and Development Command, Quartermaster Research and Development Center, Natick, Mass., Attn: Environmental Protection Division 1

Commanding Officer, Headquarters, Chemical Research and Engineering Command, Army Chemical Center, Maryland 2

Mr. Arthur Belmont, McGill University, Montreal, Canada 1

Miss Shelia Coon, Librarian, Willow Run Research Center, University of Michigan, Willow Run Airport, Ypsilanti, Michigan 1

Illinois Water Resources Board, Urbana, Illinois, Attn: Mr. Glenn Stout 1

A. D. Little, Inc., 30 Memorial Drive, Cambridge 42, Mass., Attn. Dr. Bernard Vonnegut 1

Commanding General, Army Electronic Proving Ground, Fort Huachuca, Arizona, Attn: Chief, Aviation and Meteorological Department 1

Commander, 3rd Weather Wing, Offut Air Force Base, Nebraska, Attn: Weather Central 1

Commander, 5th Weather Group, Westover AFB, Massachusetts, Attn: Weather Central 1

Commander, 2nd Weather Group, Langley Air Force Base, Attn: Weather Central, Virginia 1

Commander, 4th Weather Group, Andrews Air Force Base, Washington 25, D. C., 1

Commander, 8th Weather Group, Randolph AFB, Texas 1

Commander, Detachment No. 28-40, APO 241, c/o Postmaster Attn: Weather Central, New York, New York, 1

Commander, 1st Weather Wing, APO 925, c/o Postmaster, Attn: Weather Central, San Francisco, California 1

Commander, 3rd Weather Group, Ent Air Force Base, Attn: Weather Central, Colorado 1

Commander, 9th Weather Group, Scott Air Force Base, Illinois 1

Commander, Detachment No. 21-5, APO No. 117, c/o Postmaster Attn: Weather Central, New York, New York 1

Dr. E. C. Bowen, Division of Radio Physics, CSIRO, University Grounds, Sydney, N. S. W., Australia 1

Institute of Atmospheric Physics, University of Arizona, Tucson, Arizona 1

University of California at Los Angeles, Department of Meteorology, Los Angeles, California 1

President's Advisory Committee on Weather Control, Headquarters, 1128 General Services Administration Bldg.,Washington 25,D.C. 1

Chief, Technical Support Branch, 2d Weather Wing (MATS), APO No. 57, New York, New York 1

Commander, 2nd Weather Wing, Attn: Technical Services Division, APO No. 132, New York, New York 1

UNIVERSITY OF ILLINOIS-URBANA
3 0112 112997959